ALPHA FOUNDATION FOR THE IMPROVEMENT OF MINE SAFETY AND HEALTH

Final Technical Report

Project Title: Analysis of Coal Mine Seal Integrity from Explosively Driven Projectiles
Grant Number: AFC719-31
Organization: Missouri University of Science and Technology
Principal Investigator: Dr. Kyle Perry
Contact Information: 226 McNutt Hall, Rolla, MO 65409 kperry@mst.edu 573-341-4549
Period of Performance: 8/1/2018 – 9/30/2020

Acknowledgement/Disclaimer:

This study was sponsored by the Alpha Foundation for the Improvement of Mine Safety and Health, Inc. (ALPHA FOUNDATION). The views, opinions and recommendations expressed herein are solely those of the authors and do not imply any endorsement by the ALPHA FOUNDATION, its Directors and staff.

Table of Contents

1.0 Executive Summary

This project's purpose was to assess the performance and integrity of select seal designs when impacted by objects typically found in an underground coal mine that have become improvised projectiles when subjected to an explosion. Though MSHA has set standards for pressure rating coal mine seals, there are currently no standards for impact resistance. To accomplish this goal, researchers at Missouri S&T prepared a test site at S&T's experimental mine, designed and built a projectile generator, and conducted impact testing on three different seal types currently used in the industry which are MSHA approved. Impact tests were conducted using a wide variety of wood, concrete, and steel objects and materials commonly found in underground mines. Projectiles were propelled by a charge of black powder with a wooden wad and were held in place by foam sabots in the bore. The velocity of each projectile was measured by an infrared chronometer which was used to determine its impact energy. Impact effects on the seals were measured using strain gauges, LIDAR scans before and after impact, high speed cameras, and visual inspection (Steward, 2020).

Researchers tested three MSHA approved seals: 50M-01.1 – Strata Mine Services Plug Seal (50 PSI), 50M-02.2 – Minova Main Line Tekseal® (50 PSI), and 120M-18.0 Strata Mine Services Reinforced Concrete Seal (120 PSI). Each seal was poured by their respective manufacturer at the thickness required for a 6-feet tall, 10-feet wide seal. Each seal was run through a series of tests using multiple projectile types including items such as wooden timbers, roof bolts, hand tools, cast concrete slugs, and steel slugs. Projectile types were selected based upon the likelihood of them remaining in the sealed-off area and becoming improvised projectiles. For example, the wooden timber is similar to crib block. Projectiles attained impact velocities up to 500 ft/s and energies up to 88,000 ft-lbs. Seals experienced damage ranging from cratering to cracking to significant cracking depending on the seal and projectile type. The pumpable cementitious seal seemed to be more vulnerable to projectile damage showing that the strength of the material used to construct the seal plays an important role on the seals ability to resist penetration from a projectile. However, only two different types of seal materials were tested.

This research will help regulators and designers recognize the potential for projectile damage on seals and account for it in the future to ensure miners are safe in the event of an explosion inby the seals. From this research, a preliminary recommendation of extending the clean-up area to 300 feet inby the seals is suggested if no other measures are taken. The currently used 50-feet as stated in both manufacturers' approved installation guidelines may be inadequate, but further research is necessary to properly quantify an appropriate distance a projectile can fly when exposed to the MSHA prescribed pressure versus time design curve.

2.0 Problem Statement and Objective

This project specifically addresses topic area #4 of Alpha Solicitation and Call for Proposals AFC719; "Evaluation of Current Seal Design Criteria." This research addressed the third area within this topic: "There are no criteria associated with projectile damage to a seal. Is this a concern for current 50 and 120 PSI seal designs?" Previous research in structural and nuclear engineering has been conducted on projectile impact damage on various types of concrete and concrete composites. This project assessed the performance and integrity of select seal designs when impacted by objects typically found in an underground coal mine that may become improvised projectiles when subjected to an explosion.

The Mine Health and Safety Administration (MSHA) classifies any mining accident that claims five or more lives as a mining disaster. On January 2, 2006, an explosion occurred at the Sago mine. Root cause analysis of this disaster revealed that lightning was the most likely ignition source of an explosive methane/air atmosphere behind a sealed off, unmonitored section of the mine. The energy of the lightning transferred to an abandoned pump cable and provided the ignition source for the explosion. The explosion generated estimated pressures in excess of 93 PSI which destroyed the ventilation seals in these sections. This explosion claimed the lives of thirteen miners due to carbon monoxide poisoning. As a result of this and other mining related disasters, Congress passed the Mine Improvement and New Emergency Response Act (MINER), which was signed into law on June 15, 2006.

The MINER Act provided new regulations for both unmonitored and monitored seals. Under Title 30 of the Code of Federal Regulations (30CFR) section 75.335; monitored seals are now required to withstand a 50 PSI overpressure for a four second duration. Unmonitored seals are required to withstand a 120 PSI overpressure for the same four second duration [30CFR, 2018]. Several seals have been approved by MSHA to withstand these overpressures. However, no criteria have been published on the effect of projectile damage to these seal designs.

The primary objective of this research was to determine the effects that different types of projectiles have on mine seals. Through the use of various tools and instrumentation, the objective was achieved on three currently approved seals which implement two different types of seal material.

3.0 Research Approach

Projectile Generator Design and Construction

Design

Mine seals may be subject to a wide variety of impacts from different objects commonly found in a mine during an underground explosion. To test the mine seals, researchers sought to design and build a projectile generator capable of firing many different types of projectiles and materials, including wood beams, hand tools, roof bolts and roof bolt plates, personal protective equipment, and concrete and steel cylinders. Researchers determined that the projectile generator needed a large bore (the inside diameter of the barrel), of approximately 12 inches, and decided on a simple steel tube design. This design was plugged at one end, loaded from the muzzle, and was deemed the best choice as manufacturing and fitting a breech plug was within the capabilities of S&T machine shops and personnel. Cannon grade black powder was used as the propellant due to its low maximum pressure and availability (Steward, 2020).

Finding a length of steel tube large enough to become the barrel proved difficult. Eventually a 12-inch inner diameter, 20-inch outer diameter seamless 4140 steel pipe was found in the US; a cutoff of a piece imported from Germany. This piece became the barrel of the projectile generator, weighing roughly 5,800 pounds and having a length of 8.5 feet (Steward, 2020).

Before the proposed barrel could be purchased, it first had to be evaluated to determine if it could safely contain the pressure of firing multiple shots without yielding or failing. To ensure safety and simplify the calculations, the barrel was evaluated in the worst-case scenario for a gun: a completely obstructed bore under pressure from the largest charge of powder. The barrel pressure calculations proceeded with the assumption that the barrel would have to withstand the residual pressure of three pounds of cannon grade black powder burning completely and only expanding into the volume of the "chamber" behind the projectile (Steward, 2020).

According to the provided mill report, the barrel steel has a yield tensile strength of 61,000 PSI and an ultimate tensile strength of 112,000 PSI. Both the internal yield pressure and ultimate burst pressure of the pipe were calculated and compared to the maximum pressure the propellant can produce (Steward 2020). Researchers used the following interior ballistics equations (Carlucci, Jacobson, 2013) to calculate the yield and burst pressures:

$$P_i = \frac{\varsigma^2 - 1}{\sqrt{3 * \varsigma^4 + 1}} * S \tag{1}$$

$$P_i = \frac{\left(\frac{20}{12}\right)^2 - 1}{\sqrt{3 * \left(\frac{20}{12}\right)^4 + 1}} * 61{,}000 \tag{2}$$

$$P_i = \frac{\left(\frac{20}{12}\right)^2 - 1}{\sqrt{3*\left(\frac{20}{12}\right)^4 + 1}} * 112{,}000 \quad (3)$$

In these formulas, P_i is internal pressure (PSI), ς is the ratio of the outer diameter to the inner diameter (OD/ID) (unitless), and S is the yield or tensile strength (PSI). Equation 2 yields 22,000 PSI as the maximum pressure that the barrel can contain before yielding. Therefore, the gas pressure from firing must be kept below that value (Steward, 2020).

The next design step after determining the max barrel pressure was to determine how much pressure the cannon grade black powder produces per unit of weight and what chamber volume would keep that pressure below the yield strength of the barrel. Every combustible or explosive substance has a maximum static pressure it is capable of producing (in a given volume) based on the amount (moles) of gas produced per unit of volume for a given initial density and constant reaction temperature. Maximum static pressure can be found with a combination of stoichiometry, a modified Nobel-Able equation of state given by Cooper (2010), and several assumptions. The authors could find no stoichiometric formula in previously published research that accurately represented the reaction, likely because black powder was largely supplanted by smokeless powder in the early 20th century (Sasse, 1985) and only occasional research has been published since (Steward 2020).

An analysis of black powder's combustion products, performed by the chemists Noble and Abel (recorded by Davis, 1941), was used to develop Table 3.1. The moles per kilogram of black powder (moles/kg in Table 3.1) were found by using values provided by Noble and Abel and a re-arranging of a simplified Noble-Abel equation of state provided by Cooper (2010), solving for the moles of gas per kilogram n_{kg}, and accounting for the volume percentage of each individual gas (Steward, 2020):

$$n_{kg} = \frac{P * (V * \%v)}{T * \left(0.0821 + \frac{0.025}{T}\right)} * 1000 \quad (4)$$

Table 3.1. Noble Abel Analysis

	KNO3	C9H5O1	S	-->	K2CO3	K2SO4	K2S	S	CO2	CO	N2	H2	H2S	CH4
grams/mol:	101.1	129.1	32.1		138.2	174.3	110.3	32.1	44.0	28.0	28.0	2.0	34.0	16.0
% mass:	74.8%	14.7%	10.5%		61.2%	15.3%	14.5%	9.0%						
% vol:									49%	12%	33%	1%	3%	4%
moles/kg:									5.43	1.37	3.62	0.12	0.29	0.47
% mass:	74.8%	14.7%	10.5%		35%	9%	8%	5%	23.89%	3.85%	10.14%	0.02%	0.99%	0.76%
												Σ Moles Gas/kg:		11.31

With the addition of the percentage volume (%v) and multiplying by 1,000 to arrive at the moles of gas per kilogram of black powder (n_{kg}).

For example, solving for the moles/kg of CO_2: (equation uses SI so also included in this section)

$$n_{kg} = \frac{1 * (0.2472 * 0.49)}{273.15°K * (0.0821 + \frac{0.025}{273.15°K})} * 1000 \quad (5)$$

(0.2472 liters is the volume given by Noble and Abel) yields 5.43 moles of CO_2 per kg of black powder. Using this equation for all gasses in Table 1, the total gas production of black powder was found to be 11.31 moles/kg (5.1 moles/lb.). Some slight errors were introduced using this method. Several of the trace quantities of solid products were eliminated from the calculations, and moisture content was also ignored. This, combined with the approximate nature of the calculations, resulted in about a 3% loss of mass from the original given weight. The error is small and was deemed to be within an acceptable margin. Finally, the maximum pressure produced in the worst-case scenario for the projectile generator could be computed. Using Cooper's equation modified equation of state for pressure (Cooper, 2010) (Steward, 2020):

$$P = \frac{0.0821 * 15.4 \text{ mol} * 1623 °K}{3.71 \text{ liters} - 0.025 * 15.4 \text{ mol}} \quad (6)$$

when 3 lb. (1.4 kg) of black powder produces 15.4 moles of gas in the projectile generator's 226 in^3 (3.71-liter) chamber, the equation yields a pressure of 617 atm or 9,074 PSI. The projectile generator barrel has a calculated yield pressure of 22,000 PSI, therefore the yield factor of safety in the worst-case scenario is 2.4. Using the burst pressure of 41,000 PSI, the projectile generator has an absolute factor of safety of 4.5. In this manner the projectile generator's barrel was proven safe for use, provided a ratio of 3 lb. of black powder per 226 in^3 chamber volume (or 2 inch chamber length) is not exceeded while using a disintegrating powder container such as insulation foam. See Steward (2020) for a more detailed explanation of the projectile generator barrel design process.

Once the projectile generator's barrel was proven to be safe for use and the maximum charge weight determined, researchers designed the rest of the device. The calculations for the barrel assumed a solid breech plug (the closed end of the barrel) with a factor of safety at least as high as the barrel. Using a CAD program, researchers drew the breech plug shown in Figure 3.1.

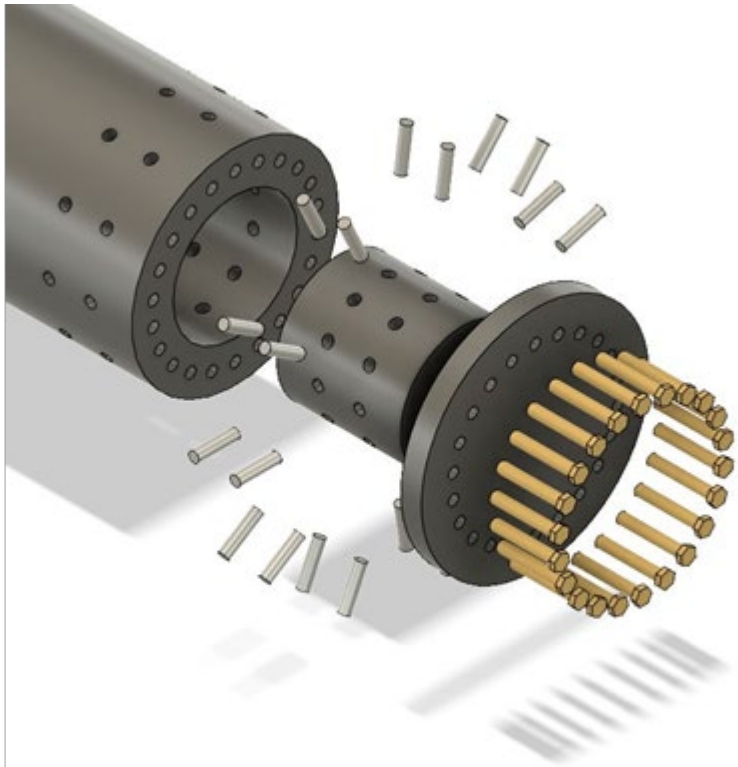

Figure 3.1. Breech Plug and Plate

The largest possible force on the breech face can be calculated by taking the max static pressure of 9,074 PSI and multiplying it by the area of the bore (113 in^2), resulting in a force of 1,026,000 lbs. Researchers chose a 12-inch diameter by 12-inch-long cast steel cylinder as a breech plug to be pinned in place with pull-out steel dowels and then capped with a steel breech plate. Removing the breech plate and the plug in particular would be difficult but not impossible if the need arose. Forty-four pins and bolts (twenty-two each) were used to hold the breech plug and plate in place. The dowel pins were arranged in a series of two rows of eleven pins each, with holes drilled through the barrel and two inches into the breech plug and the four-inch-long dowel pins inserted through the barrel wall and into the plug (Steward, 2020).

Having a shear strength of 102,000 lbs., the pull-out dowel pins have a combined strength of 2,244,000 lbs. An additional 22 holes were drilled around the circumference of the breech plate and two inches into the rear of the projectile generator parallel to its axis. Researchers tapped these holes for the threads on the bolts and attached the breech plate to the rear of the projectile generator with the bolts. With a tensile strength of 117,810 lbs., twenty-two bolts have a combined strength of 2,591,820 lbs. In total, the breech design can support a force of 4,835,820 lbs. This design gave the projectile generator breech a factor of safety of 4.7. The barrel and breech plug were shown to be safe using these methods, and the actual factor of safety is much higher as the barrel is not entirely sealed due to the touch hole (Steward, 2020).

Construction

Construction of the projectile generator was carried out at S&T's Rock Mechanics building. Researchers assembled and welded the frame, shown in Figure 3.2. Outriggers were attached to provide stability during firing, and angled roll-stops (seen on the top right portion of the frame) were added for increased safety (Steward, 2020).

Figure 3.2. Frame During Construction

Other parts for the projectile generator were manufactured concurrently. The breech plug is shown in Figure 3.3, just after machining, and in Figure 3.4 it has been fitted to the projectile generator and spot-welded in place. Figure 3.4 also shows the drilling and tapping of the holes for the bolts and pins that hold the plug and plate in place. Figure 3.5 is a picture of the completed projectile generator barrel, and Figure 3.6 shows the complete projectile generator, unpainted. Also visible in Figure 3.6 are four additional steel straps, which were heated and hammered into place around the barrel then welded to the frame. These straps ensured that the barrel could not break loose from the frame during transport or firing (Steward, 2020).

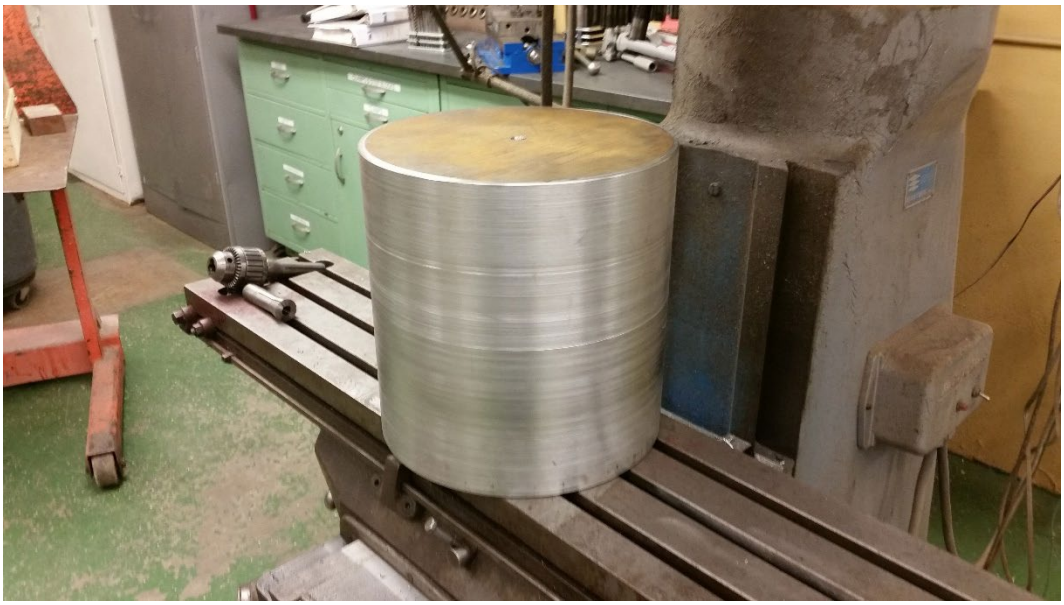

Figure 3.3. Breech Plug

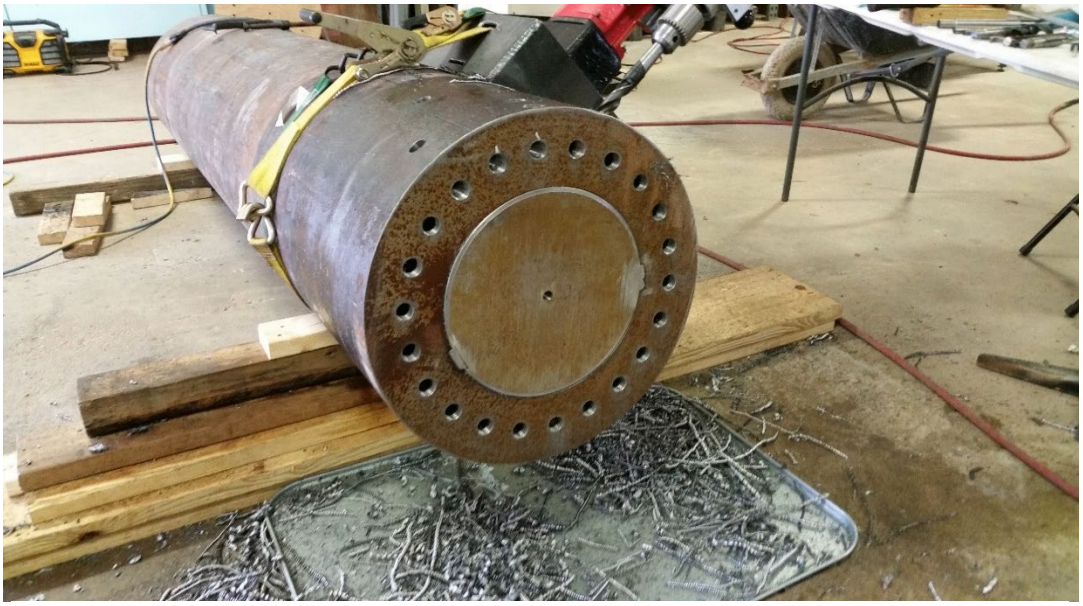

Figure 3.4. Drilling

Figure 3.5. Completed Barrel


Figure 3.6. Completed Projectile Generator

Finally, the projectile generator was placed in position at the test site as shown in Figure 3.7. The projectile generator was specifically designed to fire almost any projectile that fits within a 12-inch diameter circle. To that end, researchers decided on a design very similar to a shotgun wad system in which a wooden "wad" or disk is used to seal the bore during firing and propel projectiles down the barrel. Wads were originally disks cut off from a wood utility pole and lathe turned to the bore diameter, but they were often too cracked along their axis to create an effective gas seal and weighed up to 10 lbs. by themselves. Researchers then used a water jet cutting CNC machine and a CNC router to cut plywood disks which were stacked together and glued to create the wad. This method worked well, obturating the bore and holding together during firing; it also cut the wad weight significantly, allowing higher velocities for the same weight projectile. However, plywood wads shattered in the bore when fired with more than two pounds of black powder due to the increased pressure. Testing determined that charges over two pounds became cost inefficient (due to only moderate velocity gains for additional powder), so researchers used plywood wads and only 1 lb. of powder for all subsequent testing (Steward, 2020).

Figure 3.7. Projectile Generator at Test Site

Cannon grade black powder was used as the propellant due to the properties discussed in Section 2. Researchers made the powder charges by double wrapping the desired weight of powder into a squat aluminum foil cylinder, then taping that cylinder into the center of a two-inch-thick piece of foam insulation cut to fit the bore. While protecting the black powder from sparks or electrical shock during loading, the foil could also easily be pierced with a brass rod through the projectile generator's touch hole. After piercing the powder charge, researchers then inserted an electric match through the touch hole and into the powder. The projectile generator was fired from a safe location with an electric blasting machine (Steward, 2019). Foam insulation disintegrates

rapidly under high temperature and pressure, and researchers realized that it provided an additional measure of safety to the projectile generator by increasing the chamber volume. When the projectile generator is loaded, the powder charge, contained in a thick foam disk, is pressed to the rear of the projectile generator. The wad is then rammed down the bore until it contacts the foam disk, and the projectile pushed down on top of the wad (Steward, 2020).

To keep projectiles from damaging the bore, researchers cut foam sabots to fit around each projectile. This allowed the use of many different types of projectiles: wood beams, roof bolts, roof bolt plates, concrete and steel cylinders, hand tools, etc. Foam added very little to the overall weight of the shot and did not damage the seals or equipment as plastic or metal sabots might have (Steward, 2020).

Projectiles

Researchers constructed and fired a wide variety of objects and materials at the three mine seals. These tests included the firing of the following: 5x5 inch five-foot-long wood beams, 30 lb. concrete slugs, four roof bolts plates in a sabot, four roof bolts in a sabot, various hand tools, a section of narrow gauge mine rail, and ten-, twenty- and thirty-pound steel penetrators (Steward, 2020). Figures 3.8 through 3.15 display these projectiles. Projectiles that experienced only surface level damage on impact (all steel penetrators, roof bolts, and the mine rail replaced once) were re-used during testing, all other tests were shot with previously unfired projectiles.

Figure 3.8. Wood Beam

Figure 3.9. Hand Tools

Figure 3.10. Roof Bolt Plates

Figure 3.11. Roof Bolts

Figure 3.12. Steel Rail

Figure 3.13. 30 lb. Concrete

Figure 3.14. 10 lb. Steel

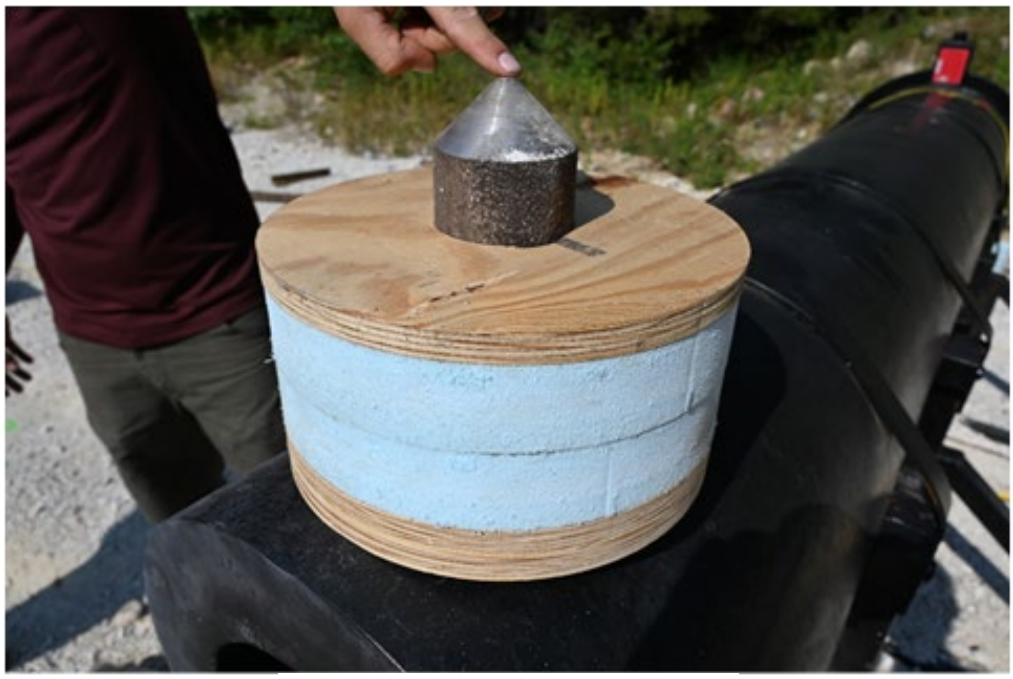

Figure 3.15. 20 lb. Steel

Figure 3.16. 30 lb. Steel

Test Setup and Methodology

The projectile generator was positioned on a gravel pad approximately twenty-five feet from the face of the seals, which were poured or placed on a concrete pad for support. Both the unreinforced concrete plug seal and the reinforced seal were poured together on the same pad. Once testing of both was complete, the unreinforced concrete seal was demolished, and the unreinforced pumpable cementitious seal was placed in the same location.

Several systems were used for data collection and analysis. Two sets of IR laser emitters/receivers and a data acquisition system recorded the time of the projectiles as they broke the IR beams, data which researchers then used to find the average impact velocity of the projectiles based on the known distance between the IR sensors. Six strain gauges measured the strain on the rear face of the seals; three gauges were arranged in a strain rosette centered on the seal, two were placed along the vertical centerline at the bottom and top edges, and one was placed along the horizontal centerline at the left-most edge when viewed from the front. The strain gauges fed data to the data acquisition system through a signal conditioner. Researchers used a LIDAR scanner to measure the volume lost (if any) after each shot for the reinforced and unreinforced concrete seals; personnel trained in the scanner's use were unavailable during testing of the unreinforced pumpable cementitious seal due to COVID-19 exposure. High definition video cameras recorded the projectile impacts and were also used to document results after each test. Finally, all seals were visually inspected and extensively photographed before and after each shot.

Figure 3.17 displays the general test setup. Figure 3.18 shows the unreinforced pumpable cementitious seal in place for testing, still on its wood shipping frame. Figure 3.19 displays the layout of the strain gauges on the back of the seals. Figure 3.20 is a video still of a calibration shot fired through the chronograph.

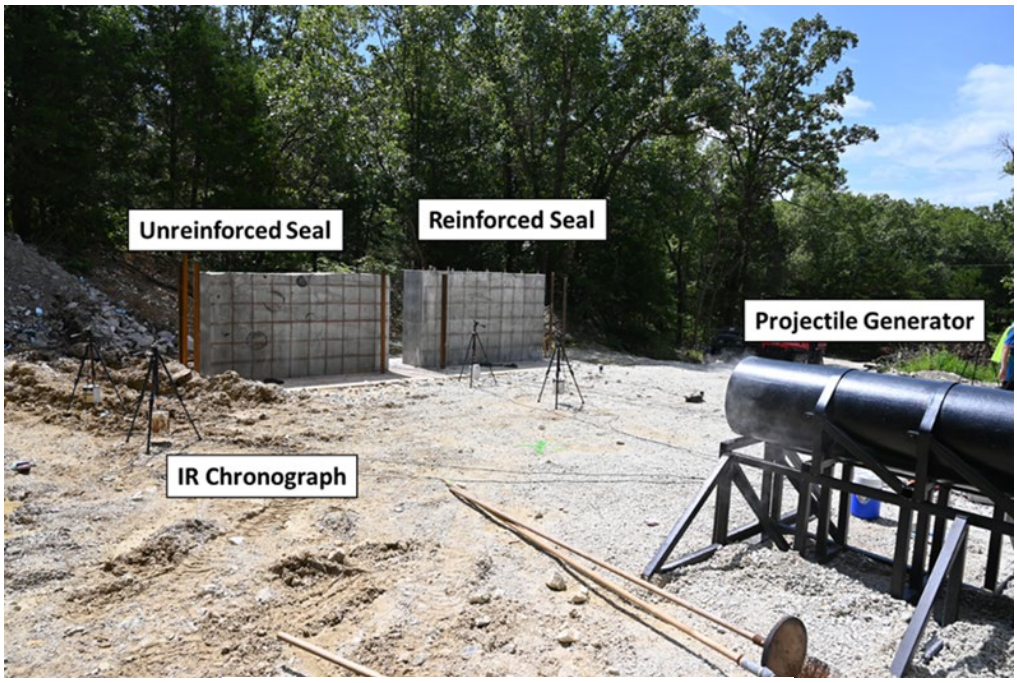

Figure 3.17. Test Setup and Concrete

Figure 3.18. Unreinforced Pumpable Cementitious Seal

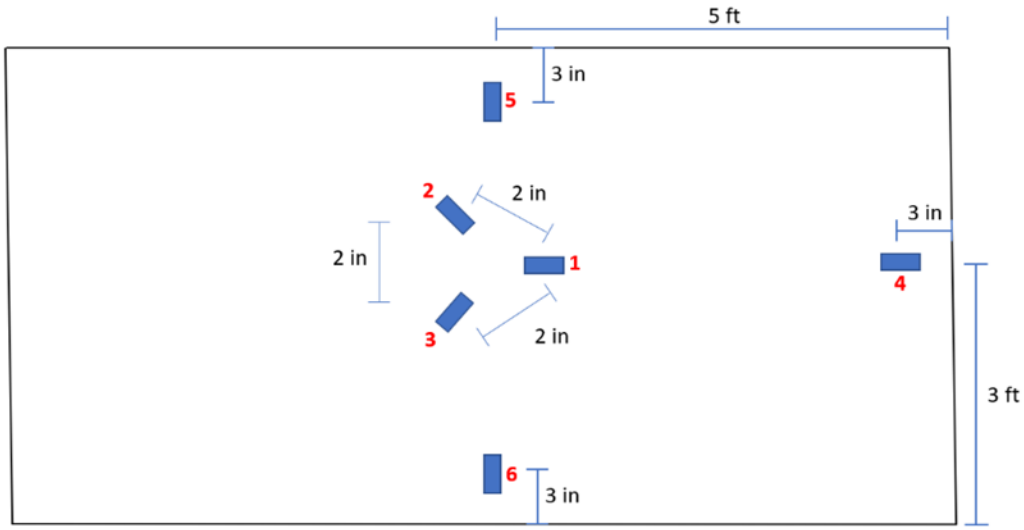

Figure 3.19. Strain Gauge Locations (Rear Face), not to scale

Figure 3.20. Test Shot Through Chronograph

Each seal was poured by their respective manufacturer to the specifications required by their MSHA-Approved Installation Manual. Table 3.2 shows the general dimensions and strengths for the seals tested in this research.

Table 3.2. Seal Dimensions and Strengths

Seal Type	Height (ft)	Width (ft)	Thickness (ft)	Minimum Compressive Strength (PSI)
Strata 50 PSI Plug	6	10	3.25	3,000
Strata 120 RC	6	10	2	4,000
Minova 50 PSI Plug	6	10	5	400

The strain gauges used in this research were Model 740B02 from PCB Piezotronics. These were selected for their very fast response rate which allows for a high sampling rate which is necessary in a dynamic system like projectile impact. The sensors are only 0.6 inches long, 0.2 inches wide, and 0.07 inches thick. The rear face seal surface was checked for material integrity and any loose material was removed. The gauges were applied using a high strength epoxy provided with the gauges. A sample of the strain gauge installation is shown in Figure 3.21. The strain gauges are designed to be reusable upon removal and relocation. However, a couple strain gauges were damaged (cable detachment) when removing them from the seals and were replaced. Each gauge comes with a unique serial number and calibration sheet which was used to convert from recorded voltage to microstrain.

Figure 3.21. Strain Gauge on Rear Face of a Seal

The data from the strain gauge rosette in the middle of the rear face of the seal was used to calculate the principal stresses. These principal stresses are the maximum stresses the seal experiences on the rear face at any point in time from a projectile impact and are not related to the pressure design specifications (50 PSI or 120 PSI seal approvals). A program was written to utilize these data and convert the rosette strain into principal strain which was then converted to stress. The rosette data (strains a, b, & c along with known angles, theta, between them) are analyzed using Equations 7 to determine the strain in X and Y and shear in the XY plane. An example of a strain gauge measurement is found in Figure 3.22.

$$\begin{aligned} \epsilon_a &= \epsilon_x * cos^2\theta_a + \epsilon_y * sin^2\theta_a + \Upsilon_{xy} * sin\theta_a * cos\theta_a \\ \epsilon_b &= \epsilon_x * cos^2\theta_b + \epsilon_y * sin^2\theta_b + \Upsilon_{xy} * sin\theta_b * cos\theta_b \\ \epsilon_c &= \epsilon_x * cos^2\theta_c + \epsilon_y * sin^2\theta_c + \Upsilon_{xy} * sin\theta_c * cos\theta_c \end{aligned} \tag{7}$$

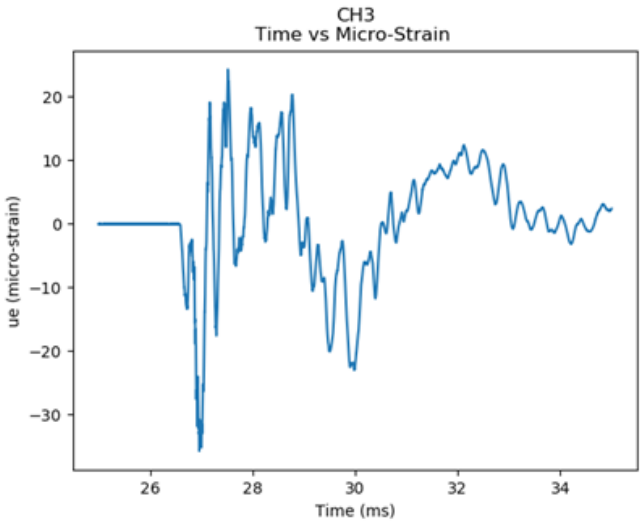

Figure 3.22. Sample Strain Gauge Waveform

For each timestep of approximately 1 microsecond over the time period in which the maximums occur, the ε_x, ε_y, and γ_{xy} were solved from the equations listed in (7) and taken to Equation 8 to determine the principal strains, ε_1 and ε_2.

$$\epsilon_1, \epsilon_2 = \frac{\epsilon_x + \epsilon_y}{2} \; +/- \; \sqrt{(\frac{\epsilon_x - \epsilon_y}{2})^2 + (\frac{\Upsilon_{xy}}{2})^2} \tag{8}$$

Figure 3.23 shows an example (30lb concrete on Reinforced Concrete seal) of the principal stress graph produced from the calculations and implementation of Hooke's law to covert strain to stress using the modulus of elasticity. The blue line (positive) indicates tension while the orange line (negative) is compression. Of most interest from this graph is the maximum tensile principal stress since concrete is weakest in tension. Therefore, the principal stresses were tabulated at the time where the tensile principal stress was at its maximum along with corresponding compression at the same time (shown as the red vertical line in Figure 3.23). Additional information and raw data can be found in the Appendices of this report.

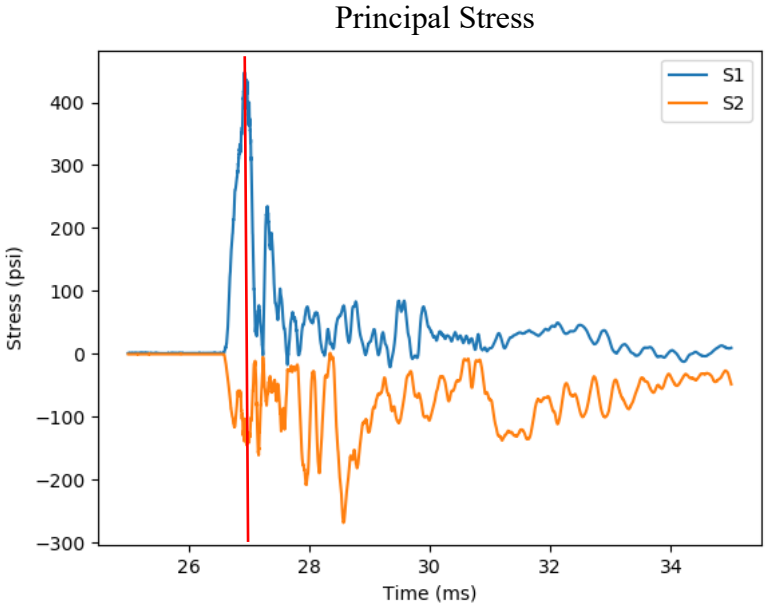

Figure 1.23. Principal Stress Derived from Strain Rosette.

Elastic response was assumed in the calculations since damage was minimal or non-existent on the rear face where the strain gauges were installed, and recordings of each gauge returned to their approximate initial values (within the noise level) after the seals returned to equilibrium after impact.

Initial testing with various weights of cast concrete slugs was performed to create a calibration chart for velocity. The concrete slugs were shot into an earth berm which allowed for the chronograph to be positioned a little further away from the projectile generator to reduce contamination interference as shown in Figure 3.20. Four data points with weight ranges from 10-

30 pounds using a one-pound black powder charge were collected which showed an as-expected trend. The velocity decreased as projectile weight increased as shown in Table 3.3.

Table 3.3. Projectile Speed versus Weight for Calibration Shots

Weight (lbs)	Velocity (ft/s)
10	630
20	515
25	507
30	470

There were issues initially with collecting quality velocity data with the chronograph when firing at the seals. Space limitations at the test site forced the IR chronograph to be located fairly close (~10-12 feet) from the muzzle of the projectile generator subjecting it to contaminants (blow by smoke, broken wadding/sabot, etc.). If the chronograph was moved further away from the muzzle, it would become too close to the seal and likely receive more ricochet damage than it already did (a tripod was destroyed). It was not possible, and potentially unsafe, to move the projectile generator further away from the seal. For many of the shots for the first seal tested (Strata 50 PSI Plug), inadequate wadding/sabots broke-up in the bore and were ejected at high velocities prior to the actual projectile leading to inaccurate velocity recordings. The odd-shaped projectiles required unique sabots or holding fixtures that were insufficient to hold the pressures and often broke. The designs of the sabots and wadding were strengthened and adjusted as further testing was conducted which achieved better results and more accurate numbers for the second and third seal tested. Therefore, the velocity data for the 50 PSI Strata Mine Services seal is suspect. However, greater confidence is held in the measured velocity values for the Strata 120 PSI RC and Minova 50 PSI Plug.

4.0 Research Findings and Accomplishments

Unreinforced 50 PSI Concrete Seal – Strata Mine Services

Both concrete seals were tested using the identical projectiles, but researchers fired more projectiles at the unreinforced seal during the wadding/sabot development process. Initial testing revealed that the first designs for projectile sabots did not stabilize the projectiles during flight; most projectiles impacted side-on or at angles to the seal and often at fairly low velocities. The extra tests allowed improvements to sabot design, flight characteristics, and velocity. Once the development phase was complete and the best design for a sabot determined, most projectiles fired from the projectile generator achieved stable trajectories (without tumbling or turning) from the muzzle to the target. In total, sixteen projectiles were fired at the unreinforced concrete seal, as compared to nine at the reinforced concrete seal and four at the unreinforced pumpable cementitious seal (nine were planned, but the seal was heavily damaged after four).

Table 4.1 presents the measured velocity (from the chronograph) and the volume lost due to impact (from the LIDAR scanner). The velocity data from this test set is suspect as discussed at the end of Section 3. Therefore, the estimated velocity from calibration testing is also included in the table. Future researchers should not use the velocity data from this specific seal as accurate, but it is included for completeness. Toward the end of the test series, one can see that measured velocities were starting to correlate with the calibration values better once the wadding and sabot designs were adjusted. Figure 4.1 displays the total damage to the unreinforced concrete seal after all sixteen tests. In Figure 4.1, the initial 20- and 30-pound steel penetrator tests which had wads that failed resulting in lower velocities are included in squares as well as the steel penetrator tests with adequate wads in circles. Figure 4.2 displays a LIDAR scan of the final impact on the seal. To easily compare the stresses generated by the projectiles, Figure 4.3 (from von Niederhausern, 2019) shows the relative stress (compared to the 10 lb. concrete projectile) caused by the impacts on the seal.

Table 4.1. Unreinforced Concrete Seal Velocity, Volume, and Energy Data

Projectile	**Projectile Weight Including Sabot (lb)**	**Measured Velocity (ft/s)**	**Calibration Velocity (ft/s)**	**Volume Loss (in^3)**	***Kinetic Energy (ft-lb)**	**Max Principal Stress (PSI)**
Hard Hat	1	145	734	0	324	565.6
Hand Tools	9	54	642	10.37	402	29.0
Roof Bolt Plates	17.5	191	560	3.6	9,924	58.0
Water Jug	1	169	734	0	443	58.0
5"x5" Wood	30	159	470	0	11,762	29.0
Roof Bolts	17	N/A	550	0.67	N/A	87.0
Concrete	10	122	630	0	2,315	0.0
Concrete	20	97	515	0	2,898	72.5
Concrete	30	168	470	0	13,179	217.6
Steel Penetrator	10	333	630	40.8	17,260	145.0
Steel Rail	25	334	506	1.1	43,228	304.6
Steel Penetrator	22	812	512	10.19	225,075	72.5
Steel Penetrator	32	405	455	24.7	81,302	101.5
Steel Rail	34.5	N/A	438	3.2	N/A	87.0
Steel Penetrator	22	N/A	511	10.2	N/A	174.0
Steel Penetrator	32	N/A	456	4351.1	N/A	72.5

* The measured velocity data was unreliable for this seal type as described at the end of Section 3. The measured velocity was used for the Kinetic Energy Calculation, but it too should be considered unreliable. It is included for completeness.

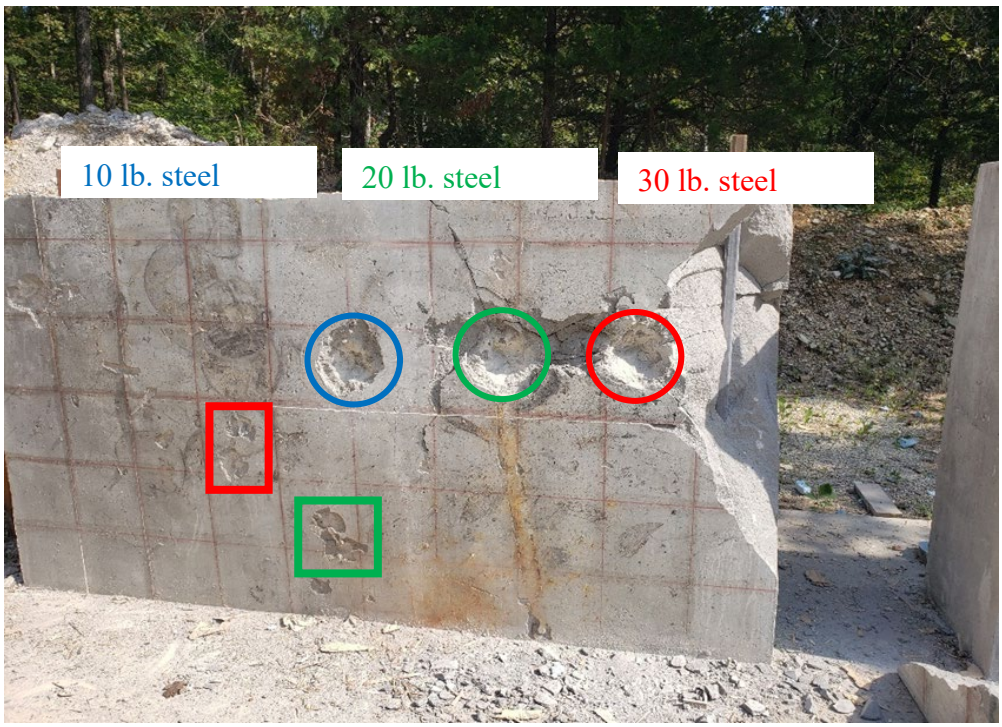

Figure 4.1. Unreinforced Concrete Seal, Post-Test. Circles Had Adequate Wadding While Squares Did Not

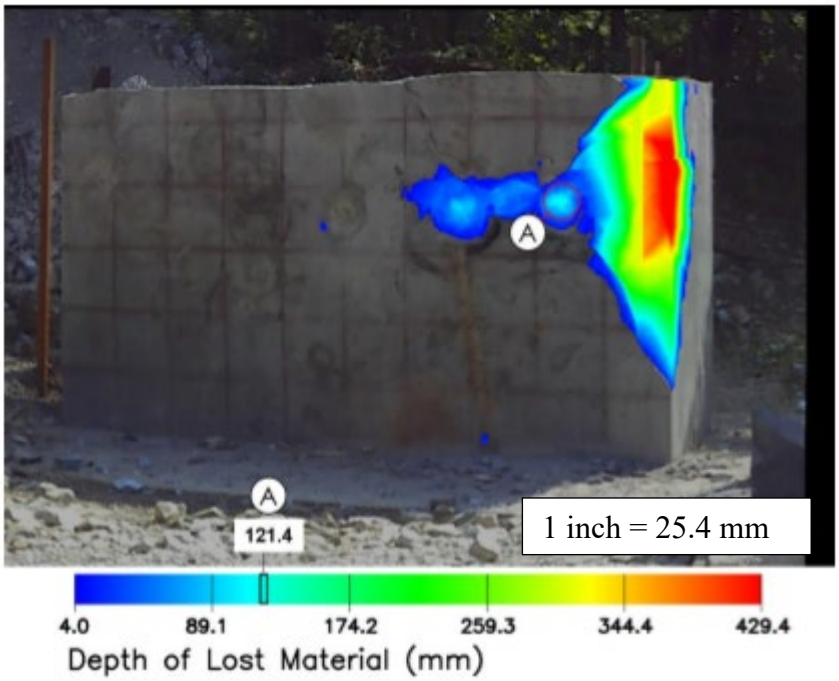

Figure 4.2. Depth of Lost Material, 30 lb. Steel (von Niederhausern, 2019)

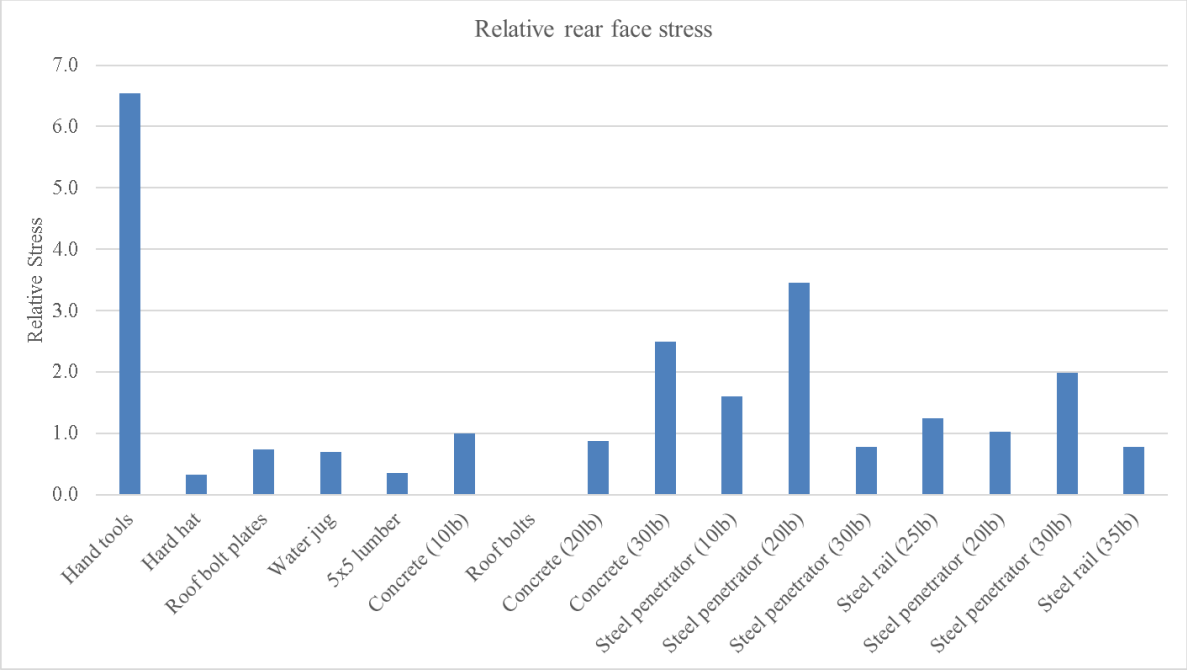

Figure 4.3. Graph of Unreinforced Concrete Seal Relative Stress Normalized to the 10-pound Concrete Slug (von Niederhausern, 2019)

As shown in Figure 4.3, the hand tools caused the most stress by about double the next projectile but did very little surface damage. This is believed to be an anomaly and not realistic since the tools impacted near the upper corner of the seal. Since the seal was unconstrained on the top and sides, reflections from the free surfaces occurred quickly and seemed to stack upon each other giving high values. If the seal were surrounded by host material in a mine, this phenomenon would be reduced by allowing the waves to travel into rock material. The 30 lb. concrete projectile caused the third most stress but did no surface damage. The steel penetrators, which are the worst-case scenario for an impact in a mine, did damage to the seal and induced significant stress when the impacted point-on (the two lowest-stress impacts of the 30 lb. and 20 lb. penetrators impacted side-on or obliquely). In particular, the 30 lb. steel penetrator (the second impact of that projectile, second from the right in Figure 4.3) removed the entire corner of the seal when it impacted location A in Figure 4.1. The other penetrator impacts caused cratering and extensive cracking in all directions around and between the impact sites. Tensile cracking was observed on the top and rear faces of the seal during the steel impacts as shown in Figure 4.4; see von Neiderhausern (2019) for further analysis of the stress waves and relief due to tensile failure in the unreinforced concrete seal.

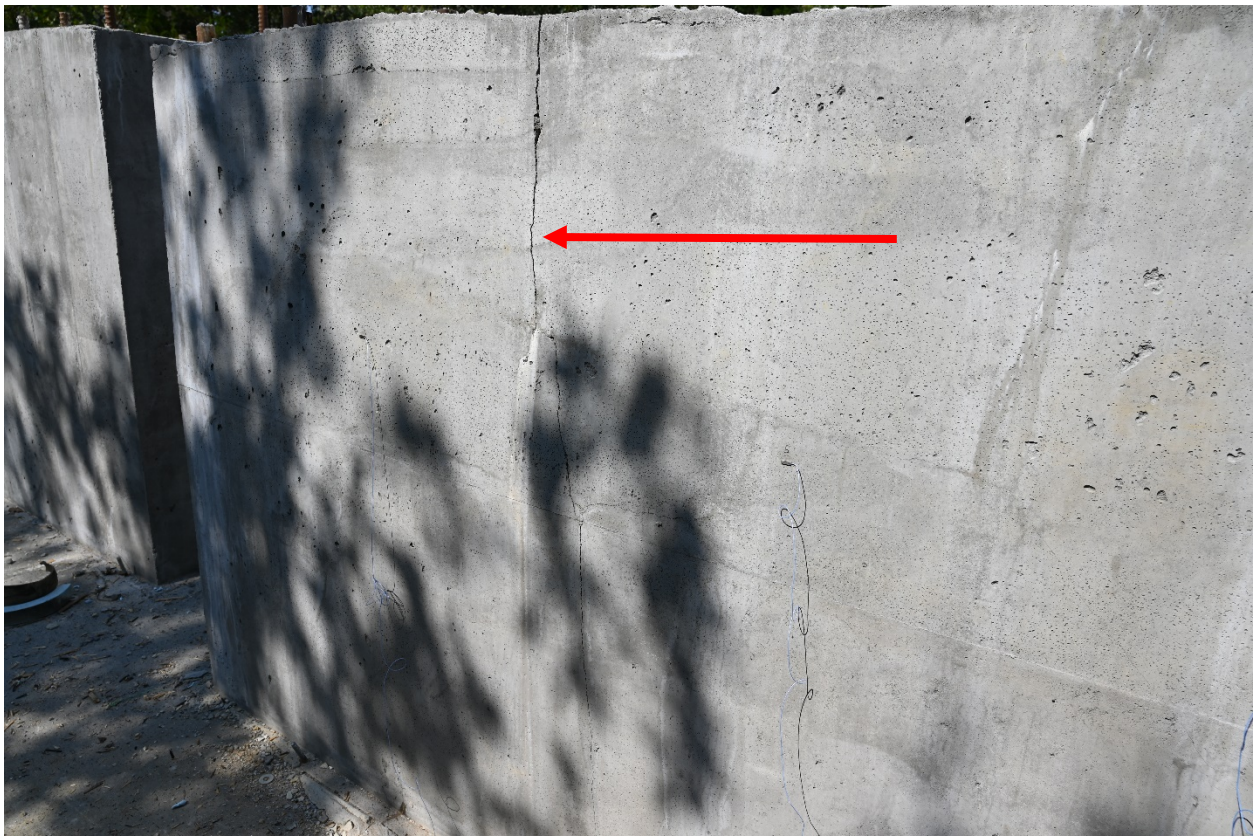

Figure 4.4. Crack on Rear Surface Extending Down from the Top

Figure 4.5 is a graph displaying the relative impact energy (x axis) vs rear face stress in PSI (y axis). The stress was derived from the strain gauge rosette at the center of the seal. The modified Weber number (x axis) is a dimensionless parameter used to compare impact parameters across projectile types which incorporates projectile and target properties. The original Weber number is typically used in fluid mechanics and is a ratio of the internal penetrating force to surface tension force. When boiled down, the modified Weber number is a ratio of the kinetic energy of the projectile and the surface energy of the target with a larger number indicating more likelihood of penetration (von Neiderhausern 2019). An interesting result of this analysis is that the concrete 30 lb. projectile had lower relative impact energy and did no surface damage but caused more rear-face stress than the 30 lb. steel penetrator, which removed a large portion of the seal entirely. This significant result will be compared to similar findings in the reinforced concrete seal and is discussed in greater depth by von Niederhausern (2019).

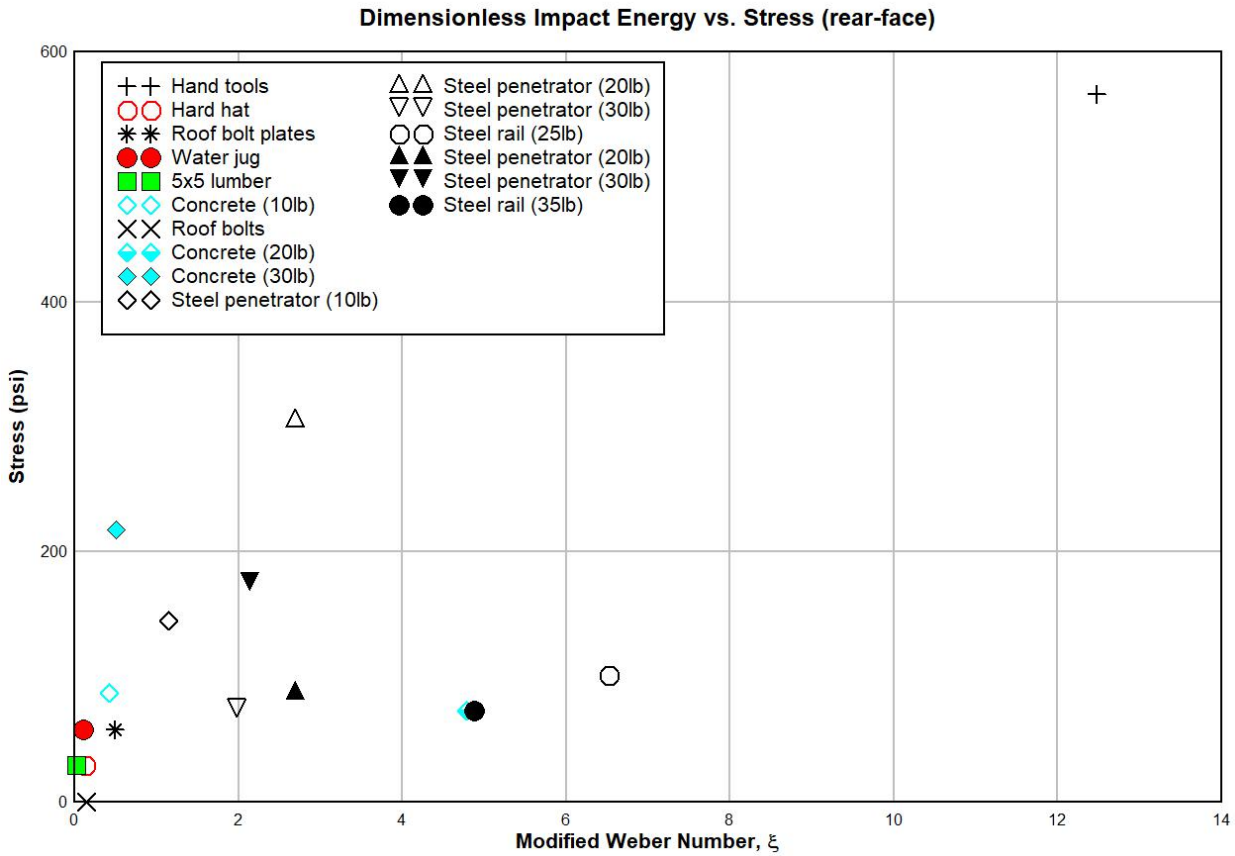

Figure 4.5. Graph of Unreinforced Concrete Seal Stress vs Impact Energy (adapted from von Niederhausern, 2019)

The concrete projectile was constructed of 4,000 PSI UCS concrete which is nearly the same concrete strength of the two Strata seals. Since the projectile and target are nearly identical in properties, the impedance match allows for a large percentage of the energy to be transmitted to the seal with little lost. Therefore, it becomes a matter of a small projectile mass versus a large seal mass which caused the projectile to completely shatter upon impact while transferring its kinetic energy into the seal resulting in higher stresses on the rear face. When considering the steel projectile of the same mass, the rounded point along with stronger mechanical properties of the steel caused energy to be used to pulverize the impact zone and create fractures in the concrete.

Due to this type of experimental testing, there are several considerations when evaluating Figure 4.5. Strain gauge location (Figure 3.19) was consistent throughout testing of the seal but impact location varied for each projectile in an attempt to impact a "clean/fresh" face. Therefore, some impacts may have been directly opposite of a gauge or the rosette while others were not. Progressive damage is also likely to effect true measured values. For example, the 30-pound steel penetrator which completely removed a corner of the seal (Figure 4.1) shows a lower stress than the first 20 pound steel penetrator test. Not only was the final 30-pound projectile fired toward the end where there were no strain gauges directly on the opposite side, but there were three additional

tests between those two which had heavy steel projectile impacting the seal. Progressive damage generating and extending cracks may have created an energy sink not allowing a direct path toward the strain gauges near the middle of the rear face of the seal. Additionally, energy going into complete separation and movement of the detached seal material reduced the amount available to get to the strain gauges.

Reinforced 120 PSI Concrete Seal – Strata Mine Services

The reinforced concrete seal included both vertical and horizontal rebar within the concrete. The vertical rebar had 18 inches of center to center spacing on both the inby and outby sides of the seal (two rows) and was Grade 60 #9 rebar. The horizontal rebar was spaced at 10 inches on the inby and outby side and was Grade 60 #6 rebar. All rebar had a least 2.5 inches of concrete cover from the surface of the rebar. With its high tensile strength when compared to concrete, the steel rebar provides additional reinforcement by accepting the tensile stresses developed during loading of the seal.

The reinforced seal withstood a similar battery of tests with far less obvious damage; likely due to the impact locations of the steel slugs being closer to the center of the seal (away from edges) and further from each other, as well as the reinforcement providing support. As with the unreinforced seal, projectiles other than the steel slugs did only slight surface damage. There was greater consistency with velocities due to improved sabot designs (compared to the unreinforced seal) leading to greater confidence when comparing projectile damage and stresses generated for this seal type.

Table 4.2 presents the projectile data. Figure 4.6 shows the final state of the reinforced seal after all testing was complete. The 10 lb. steel slug impacted on the left, the 30 lb. in the center, and the 20 lb. on the right. The 10 lb. slug impact site exhibited slightly less damage than the others, its penetration and crush zone were significantly less. Both the 30 and 20 lb. slugs penetrated deeper and had wider crushed and cracked zones, with the 20 lb. slug leaving a slightly deeper cavity (Steward 2020).

Impact locations are shown in Figure 4.8 (locations are approximate for the tools, roof bolts, and roof bolt plates). The 30 lb. impact site is the middle crater in Figure 4.6 and Figure 4.7; all sites exhibited similar characteristics with a crush zone, a heavily cracked and partially ejected zone, and some small but long cracks going towards free faces. Most of the material in the crushed zone was ejected during impact. The heavily cracked zone extended about an inch outside the crush zone and was also missing some material that was ejected or fell off the seal after impact. Though far less cracking occurred outside of these zones as compared to the unreinforced seal, researchers observed some small cracks traveling between the impact sites and from the impact sites to the edges of the seal. Some very slight cracking was also observed at the rear of the seal. No major failures or large cracks were observed during any of the tests and the reinforced seal did not fail as the unreinforced seal did (Steward 2020).

Table 4.2. Reinforced Seal Projectile Data

	Weight		Velocity	Kinetic Energy	
Projectile	**lbs. (Projectile)**	**lbs. (Projectile + Sabot)**	**ft/s**	**ft-lbs.**	**Joules**
Concrete	30.5	38.0	431	87,931	119,234
5x5 wood	31.5	38.0	423	87,595	118,779
10 lb. steel slug	10.0	18.5	507	40,000	54,240
20 lb. steel slug	21.0	31.0	477	74,313	100,769
30 lb. steel slug	31.0	42.5	379	69,143	93,758
Bolts	18.0	24.0	430	51,680	70,076
Plates	10.0	15.0	X	X	X
Rail	27.0	34.0	X	X	X
Tools	5.0	12.0	X	X	X

Figure 4.6. Reinforced Concrete Seal, Post-Test

Figure 4.7. 30 lb. Steel Slug Impact Site

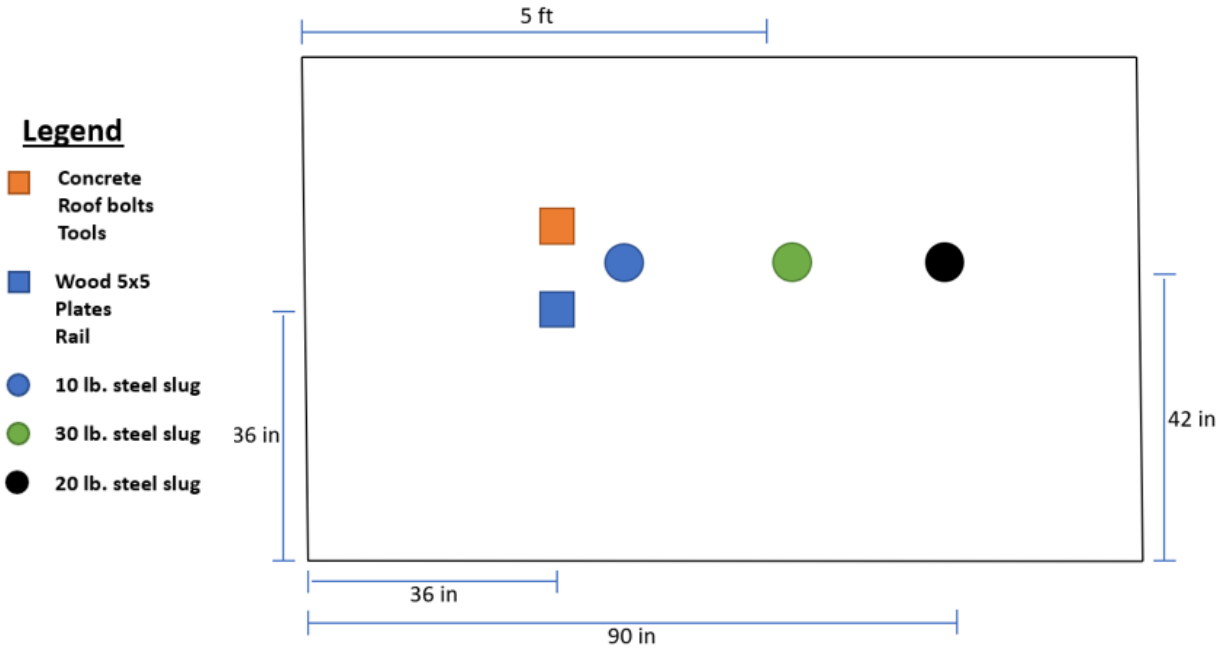

Figure 4.8. Impact Locations

LIDAR scans of the face were conducted after every shot and the final scan is shown in Figure 4.9. Table 4.3 displays the amount of volume lost from the reinforced seal. All projectiles other than the steel slugs did little visible damage to the face. Both the 20 and 30 lb. steel projectiles penetrated to a depth of about 3.15 inches and removed significant amounts of material, but the 10 lb. projectile only removed a small fraction and penetrated to about 2.4 inches. This result corresponds with their different impact energies (Steward 2020).

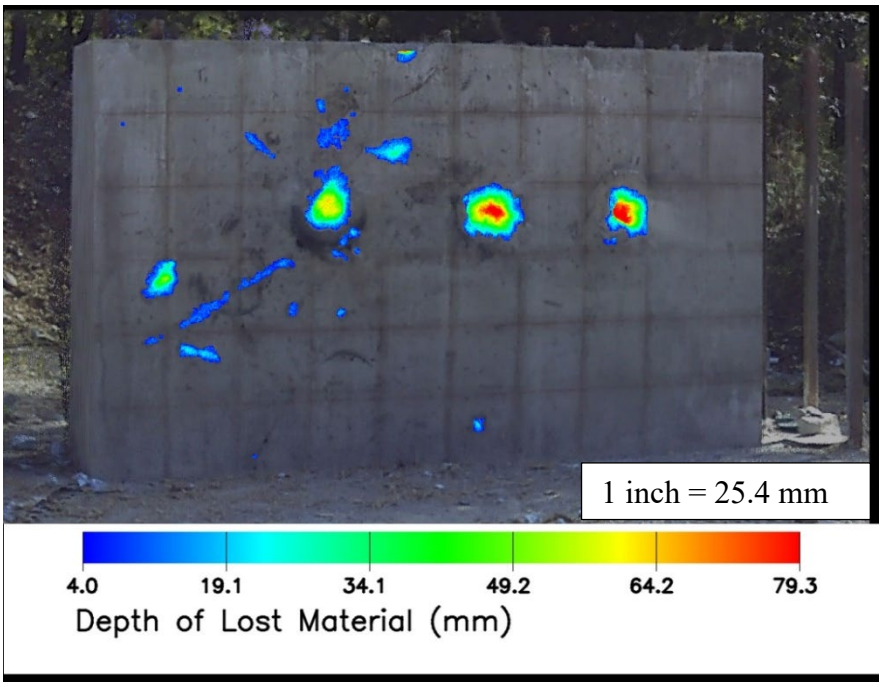

Figure 4.9. Depth of Lost Material

Table 4.3. Volume Lost

	Volume Lost
Projectile	**in^3**
10 lb. steel slug:	12.8
20 lb. steel slug:	84.3
30 lb. steel slug:	77.0
All other projectiles:	24.8
Total Vol Lost:	198.9

Calculated principal stresses and the calculated maximum tensile stress from measured strain from each impact are shown in Table 4.4. The impacts are in order of greatest to least and the sensor that registered the max value is also listed. Strain was converted to stress using a

modulus of elasticity of $4*10^6$ PSI, which is average for concrete. The maximum stress column in Table 4.4 shows the maximum calculated stress (from the maximum strain) by any individual sensor. Principal stresses were calculated using the maximum strain from the rosette, denoted as σ_1 and σ_2; positive numbers represent tension. Graphs of each individual sensor's data are available in Appendix B of Steward's thesis (2020). The calculated principal stresses denote the maximum possible stress that can be experienced on that plane, in this case the vertical rear surface of the seal. The principal stresses are oriented in a way that there is no shear stress. The rosette is designed to be able to determine the principal stresses. For example, the concrete projectile produced a maximum stress of 238.5 PSI (tension) at one of the rosette gauge locations. When accounting for all three gauges and their orientation, the maximum tensile stress in that area was determined to be 447.0 PSI. This value is important to determine because it is creeping up on the ultimate tensile strength of the concrete material. When that threshold is met, cracks begin to develop. While this rosette was measuring the plane strain on the back surface of the seal, strain and stress was also being developed axial (direction parallel to projectile path). The impact would send compression waves through the seal and when reaching the seal/air interface on the rear surface would reflect back in tension. Although not measured, this could lead to slabbing or spalling on the back surface with a large enough impact (which was not observed for this testing).

Table 4.4. Stress Data

Stress (PSI)				
Projectile	**Max Tensile**	**Sensor**	**σ1**	**σ2**
Concrete	238.5	2	447.0	-138.8
5x5 wood	197.0	3	287.8	17.6
10 lb. steel slug	167.3	2	256.0	-67.3
Roof Bolts	113.8	4	232.9	-136.7
Tools	101.4	5	133.1	-31.2
30 lb. steel slug	100.1	1	101.0	-238.5
20 lb. steel slug	87.1	3	156.3	-21.1
Plates	70.6	4	60.1	-30.4

Analysis of the data revealed surprising results. The projectiles with the highest kinetic energy did not necessarily cause the greatest stress on the rear face of the seal. Though the wood 5x5 and concrete projectiles had the most kinetic energy and caused the most stress, the 20 lb. and 30 lb. steel slugs had only slightly less and caused, on average, about 125 PSI less stress. All projectiles except the steel slugs caused no visible damage or only very slight surface damage, the steel projectiles did cause cratering. This may explain why they caused less rear face stress; some of their kinetic energy was absorbed in crushing the concrete at the impact area; and that crush period also resulted in a lower pressure impulse into the seal. Note that the 10 lb. steel slug created a smaller impact crater and caused significantly more rear face stress than the 20 or 30 lb. slugs (~70 PSI), while attaining only just over half their kinetic energy. As shown in Table 4, the 10 lb. slug also only crushed and removed a small fraction of concrete compared to the 20 and 30 lb. slugs (Steward, 2020).

Concrete has a tensile strength generally ranging from 400 to 700 PSI. As shown in Table 4.4, the lower end of that range was only exceeded once by the principal stress caused by the concrete projectile. Most induced stresses were at least within 25% of the 400 PSI tensile strength. Due to the location of the impacts and sensors, stresses high enough to cause cracking on the rear face may not have been recorded. The strain rosette was centrally located on the reinforced seal (Figure 3.19) during all shots; principal stresses at other locations may have reached the failure point. Stresses within the seal likely reached levels above the concrete's tensile strength between the impact points and the rear face, especially for steel slugs. The data recorded by the strain gauges was, in most cases, too noisy to draw solid conclusions about wave reflections, other than that there were many. Also important in consideration of the data is the types of pressure waves created in the rear of the seal (Steward, 2020).

Due to the placement of the strain gauges on the rear of the seals, they will experience both transverse and longitudinal waves and, as those waves reflect off the various surfaces and bottom of the seal, they will also experience wave superposition and interference. This greatly complicates analysis, especially when trying to determine strains and stresses other than those directly measured by the strain gauges. Axial stress (in this case, through the seal perpendicular to the rear face and the strain gauges) is an important component of concrete failure and causes scabbing when high pressure waves in a solid material meet a low impedance zone such as air (Cooper, 2010). Several attempts were made to solve for axial stress, but due to the complex nature of the waves and the single strain rosette for data, these attempts did not result in axial stress values that the researchers deemed legitimate (they varied from 550 PSI to 1,700 PSI) because no scabbing was observed on the rear face. Therefore, conclusions about the stress state of the concrete were only drawn from the strain gauge readings and the principal strains and stresses derived from them (Steward, 2020).

Unreinforced 50 PSI Pumpable Cementitious Seal - Minova

The unreinforced pumpable cementitious seal experienced catastrophic failure, extensive cracking, ejection and destruction of a large amount of seal material, and a penetration equal to about 66% of its thickness. Only four projectiles were fired at this seal before it was deemed too damaged to yield any more meaningful results from further tests: a wood 5x5 inch beam, hand tools, a 30 lb. concrete slug, and a 20 lb. steel penetrator. Figure 4.10 displays the damage to the seal after the four tests. Figure 4.11 shows the projectile impact locations. Velocity data is presented in Table 4.5.

As was typical of the other seals, cracks radiated from impact locations to free faces. Like the unreinforced concrete seal, the impact closest to the edge (30 lb. steel in the unreinforced concrete seal test, 30 lb. concrete projectile in the pumpable cementitious seal test) caused two cracks at a roughly right angle to each other to form towards the right side of the seal. In both cases, these traveled along the right side of the seal to the rear face. Judging from the exterior, the entire corner of the pumpable cementitious seal was likely separated from the rest of the seal with only friction keeping it from falling off as happened with the unreinforced concrete seal.

Table 4.5. Pumpable Cementitious Seal Projectile Data

	Weight		Velocity	Kinetic Energy	
Projectile	**lbs. (Projectile)**	**lbs. (Projectile + Sabot)**	**ft/s**	**ft-lbs.**	**Joules**
5x5 wood	30.0	34.5	188.0	16,465	22,326
Tools	5.0	8.0	560.0	24,348	33,016
Concrete	30.0	34.3	387.0	69,768	94,606
20 lb. Steel	21.0	29.0	387.0	48,838	66,224

Figure 4.10. Unreinforced Cementitious Seal, Post-Test

Unfortunately, personnel trained on the LIDAR scanner were unavailable due to COVID-19 exposure. The total volume lost was not measured for this seal. However, researchers did measure the dimensions of the craters. The wood 5x5 embedded in the seal, creating an exactly five inch by five inch hole about eight inches deep at a slight downward angle. The hand tools caused two craters on the left side of the seal, roughly twelve inches in diameter and about three inches deep. Causing the most extensive damage, the concrete projectile created a crater fourteen by seventeen inches wide and 12 inches deep. It also caused cracking almost identical to the unreinforced concrete seal, driving cracks through along the right side of the seal towards the rear face. The final shot, the 20 lb. steel projectile, caused less surface cracking than the other projectiles but penetrated 31 inches into the seal, which was 48 inches thick. Cracking opposite

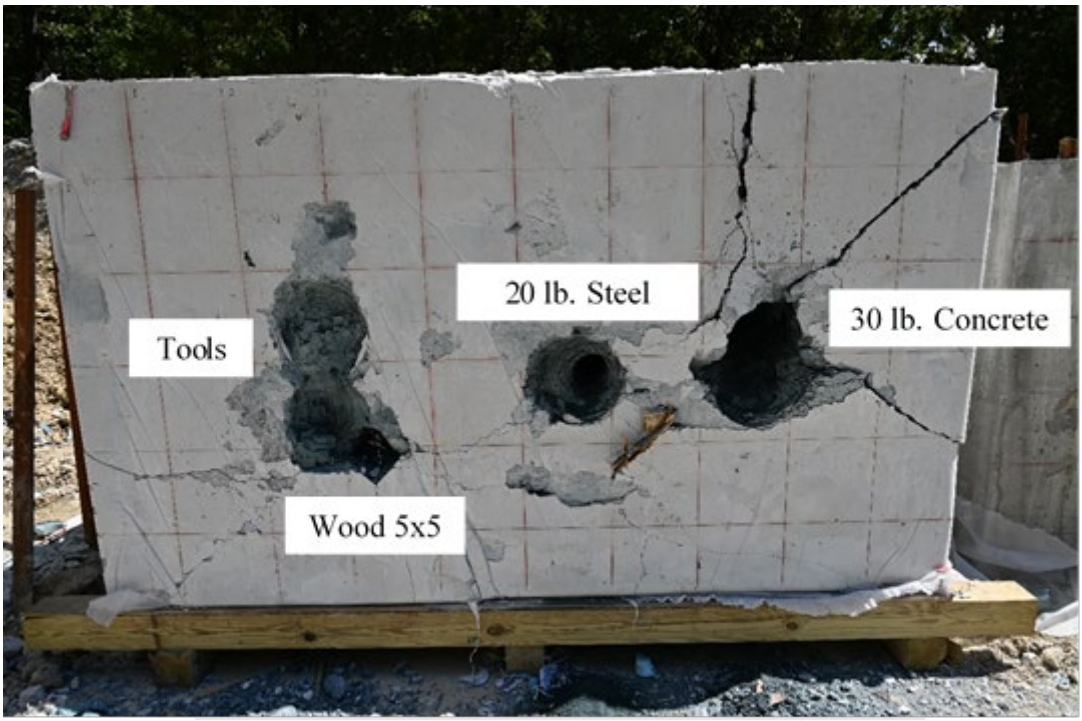

Figure 4.11. Unreinforced Cementitious Seal Impact Locations

the impact was observed but no major spalling or bulging occurred. Figure 4.12 is a picture of the rear face and right side of the seal, displaying the widespread cracking and fracturing of the seal. Both the concrete and steel projectiles caused several pounds (estimate) of seal material to be ejected on impact.

Strain gauge data from this seal did not conform to data from the other two seals; data shows that stress was very low. Considering that the seal experienced widespread crack formation in the rear face, this data is likely erroneous, but has been provided in the appendix for reference. Due to the nature of the pumpable cementitious seal's material (it was soft enough to be scratched with a fingernail) the surface was very easy to deform. The strain gauges were glued to the rear face and the seal material was simply too soft to transmit any significant strains into harder materials like the sensors.

Figure 4.12. Unreinforced Pumpable Cementitious Seal, Rear

Seal Comparisons

The two Strata seals performed similarly but the Minova seal was notably different. The strength of the material used to construct a mine seal has a significant effect on its ability to resist projectile penetration which can lead to damage. Since the Minova material was relatively soft, strain was not able to be measured on the rear face thereby only allowing comparison of projectile penetration. Table 4.6 shows a comparison of penetration between two different projectile types for the Strata Reinforced Concrete seal which uses 4,000 PSI (minimum) concrete and the Minova Plug seal which uses a 400 PSI (minimum) cementitious material. The performance difference is noticeable as shown in Figure 4.13.

Table 4.6. Penetration Comparison between Material Types

	Penetration (inches)	
	Strata RC Seal	Minova Plug
30lb Concrete	0	12
20lb Steel	3.15	31

Figure 4.13. 30-lb. Concrete impact comparison between seal material types. Left is harder seal material where concrete projectile is pulverized resulting in no penetration. Right is softer seal material with significant penetration with concrete slug still inside seal.

It must be noted that seals are designed for overpressure design (among other things), not projectiles. Both seals in Table 4.6 and Figure 4.13 are approved by MSHA for overpressure design and there is no current design standard for projectiles.

5.0 Publication Record and Dissemination Efforts

At the time of this final report, two M.S. theses and one conference publication have been produced. The final round of testing on the third seal recently concluded and the data is necessary to make comparisons for future publications. Several journal publications are in the initial phases of development. One publication will cover the testing of the first manufacturer's seals while another will cover the other manufacturer. Another publication on the projectile generator and instrumentation suite is planned as well.
The publications thus far are:

- von Niederhausern, B.A. (2019) *Projectile Impact Effects on a 50 psi Plug Type Coal Mine Seal* (Master's thesis, Missouri University of Science and Technology, 2019). MO.

- Steward, E. A. (2020). *Projectile Generator Design for Underground Coal Mine Seal Testing* (Master's thesis, Missouri University of Science and Technology, 2020). MO.

- Steward, Ethan and K. Perry, 2020, "Projectile Generator Design for Underground Coal Mine Seal Testing," Proceedings of the 46th Annual Conference on Explosives and Blasting Technique International Society of Explosives Engineering, Denver, CO.

6.0 Conclusions and Impact Assessment

Researchers conducted impact testing on three different mine seal designs using a projectile generator to propel objects and materials commonly found in underground mines to high velocities. Sensors measured the strain responses of an unreinforced 50 PSI and steel reinforced 120 PSI concrete seal from projectile impact but were unable to measure anything on the softer unreinforced 50 PSI pumpable cementitious seal. Seals were also evaluated with LIDAR scans (when available) and visual inspections. From these tests, the following conclusions were drawn:

- Mine seals can be damaged by materials commonly found in mines when propelled to velocities possible during an underground explosion (Steward, 2020)
- Hard, dense, non-deforming projectiles can cause cratering, cracking, and catastrophic failure of mine seals (Steward, 2020)
- Soft, deforming, or disintegrating projectiles of high mass can cause stress greater than the tensile strength of concrete while not causing immediately visible damage to mine seals (Steward, 2020)
- Small, dispersed objects (hand tools, roof bolt plates, roof bolts) may cause high stress but do very little surface damage to concrete seals
- The strength of the seal material is critically important. Soft pumpable cementitious-based seals are extremely susceptible to penetration from projectiles.
- Visual inspection of the non-impact face of a seal may not be sufficient to identify potentially critical damage in the structure as damage, including cracking, may not be visually discernable. As a result, impact damage could go undetected (von Niederhausern, 2019)

The data shows that dense, hard objects of sufficient mass (the steel slugs) cause significant surface damage by cratering and spalling the impact face but cause less stress in the rear face of the reinforced seal. Common steel objects found in a mine may include drill steel, I-beams, and equipment parts. Projectiles that deform or disintegrate upon impact (concrete, wood) cause little to no visible surface damage on higher strength concrete seals but may still generate rear-face stress over the tensile yield strength of concrete. Common frangible objects found in a mine may include large rocks and boulders, concrete chunks, and wood beams. Significant stress, cracking, cratering, or ejection of material at the impact face was observed in both concrete seals when struck with both deforming and non-deforming projectiles. Catastrophic failure resulting in fracturing and separation of large portions of material was observed in both the unreinforced concrete and pumpable cementitious seals. Surface damage and stresses equal to the tensile strength of concrete were observed in the reinforced concrete seal. Consequently, this study has shown that the materials found in an underground coal mine can cause significant structural damage to coal mine seals when propelled to velocities possible in a methane-coal dust explosion (Steward, 2020).

7.0 Recommendations for Future Work

This research has shown that projectiles can cause damage to coal mine seals in varying intensity depending on the projectile type. It takes a massive projectile traveling fast, but it is possible. The simplest way to reduce potential damage from projectiles is to eliminate the possibility of generating one. Although explosions inby seals in a rare occurrence, measures should be taken remove items that may be turned into projectiles prior to sealing the area. MSHA approved seal design installation guidelines from the two manufacturers whose seals were tested in this research state to clear debris 50 feet inby and outby the seal location. This may not be sufficient. Further research needs to be conducted to determine the length at which potential projectiles need to be removed. Once a matrix of projectile sizes and possible speeds can be determined from methane explosions, that research can be tied to this research to develop an appropriate guideline. Whether that is 100 feet, 500 feet, 1000+ feet, research needs to be done to determine the size of explosion necessary to lift and move varying types of potential projectiles certain distances. Until that research is concluded to determine the optimal length, these researchers would suggest 300 feet.

The projectile's mass, velocity, and shape are the driving factors in determining stress and penetration on a seal (depending on seal material). With an increased clean area distance, there is a lower likelihood of the projectile reaching the seal face at full theoretical velocity if it reaches it at all. There is more chance of tumbling, ricochets off ribs/roof/floor, impacting a crosscut rib, etc. that was not examined in this 'worst-case scenario' research. Therefore, the easiest solution will be the elimination of potential projectiles. A thorough study to understand how items are lifted from rest and accelerate during a methane/coal-dust explosion needs to be performed to determine travel distances and velocities. There will be a variety of variables to investigate including shape form of the projectile, mass, shock clearing and reflections, ricochets, gravitational effects, initial distance from the seal, mine design, etc. Once that research is performed, a select group of shapes and masses at certain distances will likely emerge as the most likely possible projectiles that could travel far enough to impact a seal. Those velocities, tied with their mass and shape, could then be compared to the experimental testing described in this report to estimate damage. A certain "acceptable" damage threshold will then need to be determined by the manufacturers in order to correlate the acceptable clean area distance inby and outby.

In the event of an explosion inby seals, a qualified individual should visually inspect the seals at a minimum. However, this is likely not sufficient as there is potential for internal cracks which may affect the structural integrity of the seal that are not evident on the visual outby side of the seals. Instrumentation and tools to identify the presence of internal fractures is optimal, but with the massive thickness of concrete seals, may still not be feasible or accurate.

8.0 References

1. Steward, E. A. (2020). *Projectile Generator Design for Underground Coal Mine Seal Testing* (Master's thesis, Missouri University of Science and Technology, 2020). MO.

2. Perry, K. A. (2010). *Development of Modern Sealing Techniques for Underground Coal Mining* (Doctoral dissertation, University of Kentucky, 2010). KY.

3. Perry, K. A. (2018) *Analysis of Coal Mine Seal Integrity from Explosively Driven Projectiles.* Rolla, MO: Missouri University of Science and Technology.

4. von Niederhausern, B.A. (2019) *Projectile Impact Effects on a 50 psi Plug Type Coal Mine Seal* (Master's thesis, Missouri University of Science and Technology, 2019). MO.

5. Jacobson, S. S., & Carlucci, D. E. (2013). *Ballistics - Theory and Design of Guns and Ammunition* (2nd ed.). Taylor & Francis.

6. Cooper, P. W. (2010). *Explosives Engineering*. Wiley-VCH Inc.

7. Sassé, R. A. (1985). A Comprehensive Review of Black Powder. Aberdeen Proving Ground, MD: US Army Ballistic Research Laboratory.

8. Davis, T. L. ((1941) (2016)). The Chemistry of Powder and Explosives. Pickle Partners Publishing.

9.0 Appendices

Appendix A - Unreinforced Concrete Seal

DATA

The collected and output data from testing is provided below for all tests performed.
For figures in this appendix referencing strain sensor serial numbers, the positions and associated serial numbers are given in Figure A.1 and Table A.1.

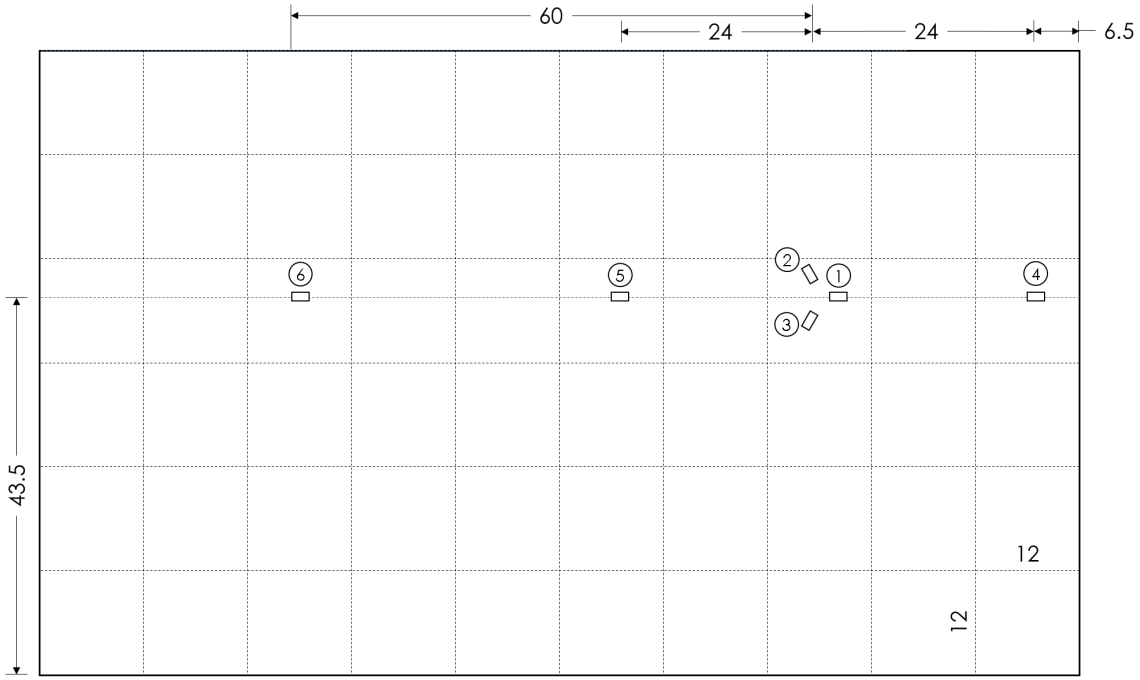

Figure A.1 Strain sensor installation

Table A.1 Sensor ID, data channel, and serial number matrix

Sensor ID (ref. Figure 0.1)	Data channel	Serial number (for testing on 31 Jul 19)	Serial number (for all other tests)
1	CH3	8268	8229
2	CH4	8269	8268
3	CH5	8267	8267
4	CH6	8229	8269
5	CH7	8229	8228
6	CH8	8266	8266

Test dates and the sequence of testing is given in Table A.2, with the impact locations projected onto the rear face in Figure A.2.

Table A.2 Test dates, sequence, and total projectile weights

ID	Testing date	Test case	Total projectile weight (lb)
A	31 July 2019	Hard hat	1
B		Water jug	1
C		Hand tools	9
D		Roof bolt plates	17.5
E	13 August 2019	5 x 5 lumber	30
F		Roof bolts	17
G		Concrete (10 lb)	10
H	27 August 2019	Concrete (20 lb)	20
I		Concrete (30 lb)	30
J		Steel penetrator (10 lb)	10
K	6 September 2019	Steel rail (25 lb)	25
L		Steel penetrator (20 lb)	22
M		Steel penetrator (30 lb)	32
N	19 September 2019	Steel rail (35 lb)	34.5
O		Steel penetrator (20 lb)	22
P		Steel penetrator (30 lb)	32

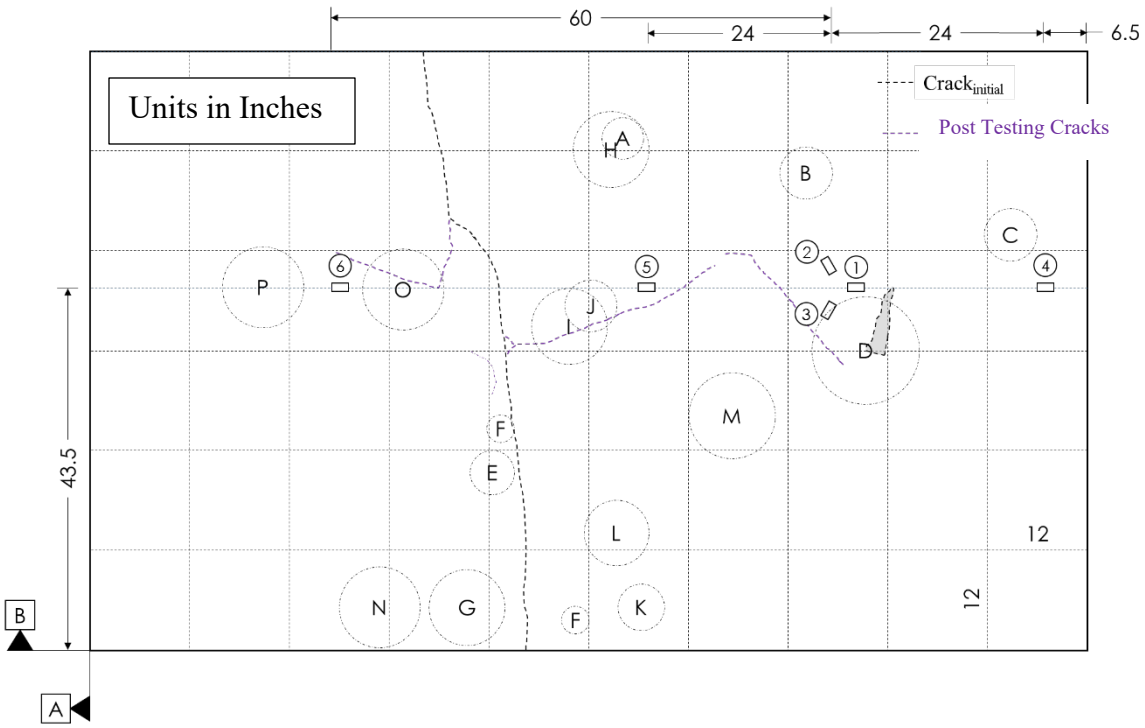

Figure A.2 Impact locations viewed from rear face as if seal were transparent along with rear face initial (pre-test) and post-test cracking

A, Hard hat, 31 July 2019

Figure A.3 Hard hat

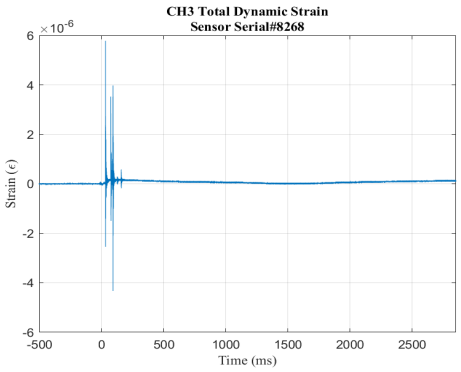

a.

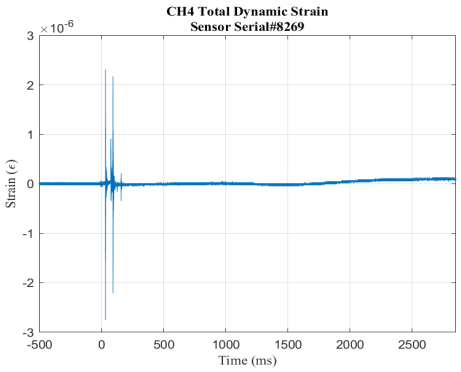

b.

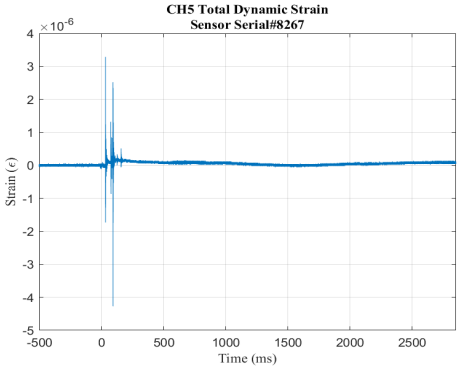

c.

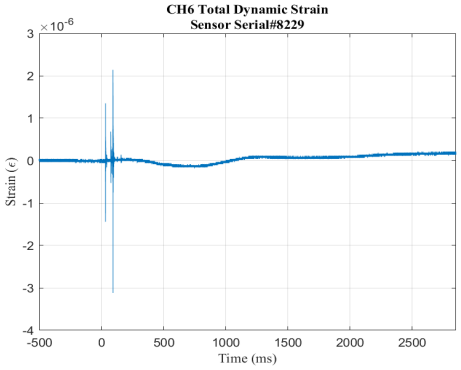

d.

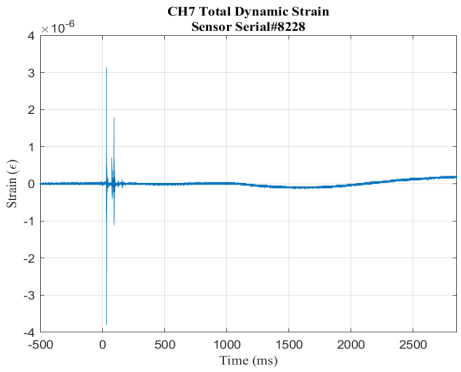

e.

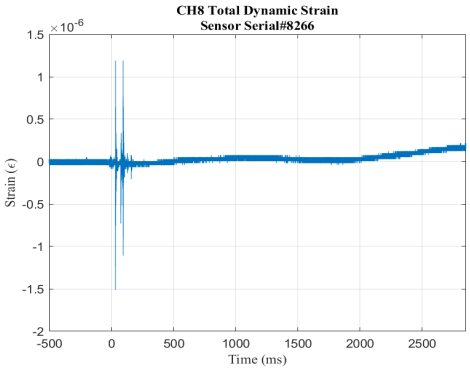

f.

Figure A.4 Strain response, hard hat, test date: 31 Jul 19

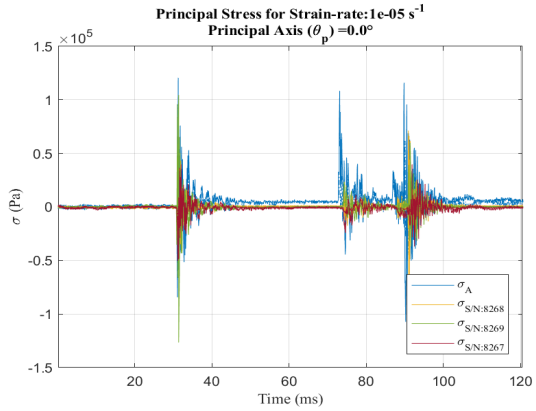

a.

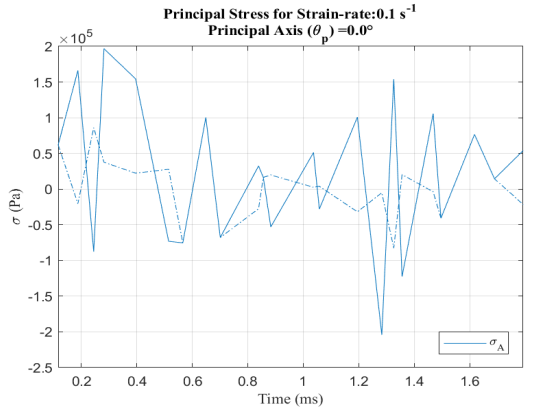

b.

Figure A.5 Principal stress at strain-rate, hard hat, test date: 31 Jul 19

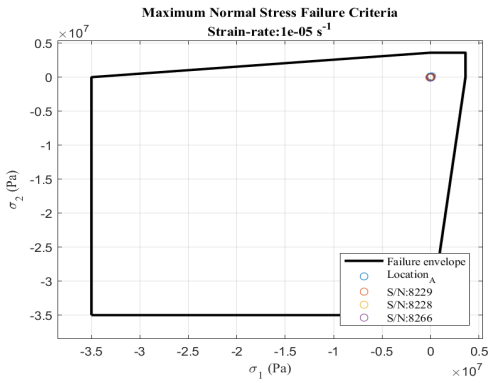

a.

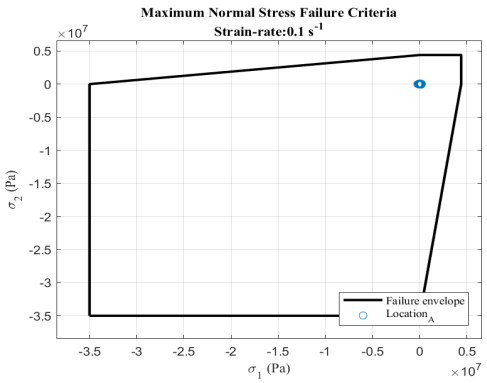

b.

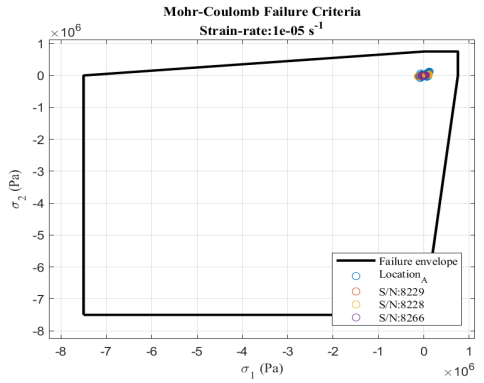

c.

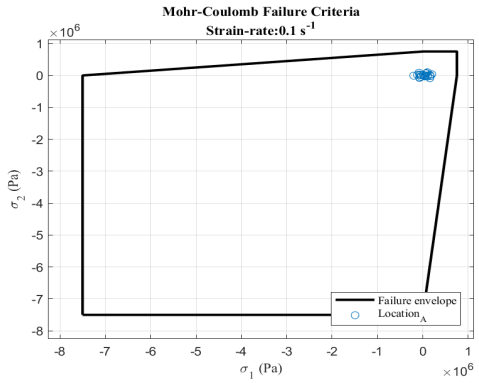

d.

Figure A.6 Failure criterion envelopes, hard hat, test date: 31 Jul 19

For all failure envelopes, any data point which falls above or to the right of the envelope would constitute failure. Any data point below or to the left (or inside the envelope) is sustainable by the seal.

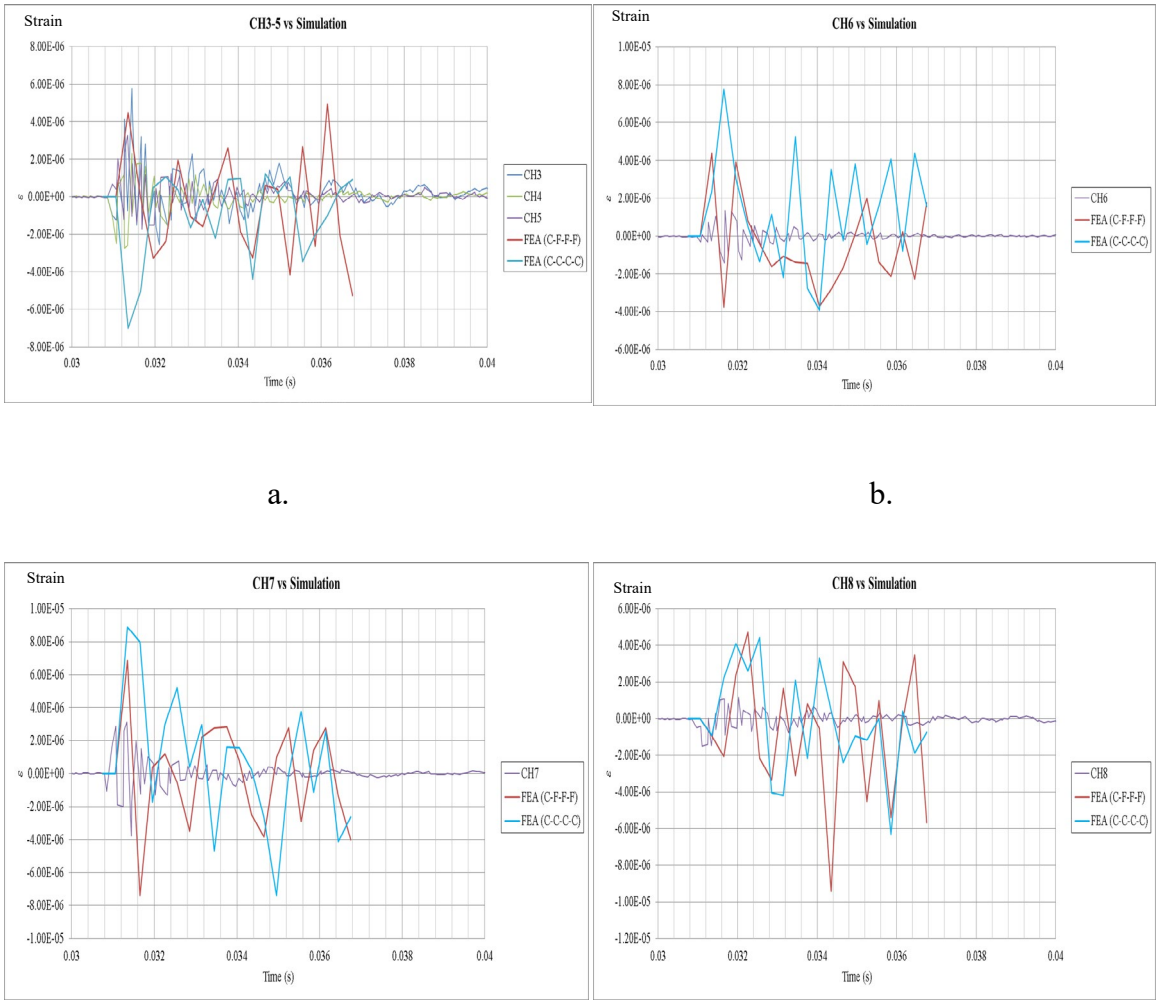

Figure A.7 Strain response and FEA comparison, hard hat, test date: 31 July 19

Though not part of the research objectives, one of the graduate students (Bruce von Niederhausern) decided to do some Finite Element Analysis (FEA) for his Thesis. "A finite element simulation was developed for each impact case to estimate the stress state in the seal. For each test case, the impact was modeled using simplified geometries of the projectile with projectile mass as the driving parameter of the simulated projectile. Each test simulated a normal, planar impact. The seal was modeled as both a fixed-free-free-free plate and a fixed-fixed-fixed-fixed plate in order to compare empirical data with the test configuration (fixed-free-free-free) and then to use the model to extrapolate the response to an operational configuration (fixed-fixed-fixed-fixed)." Fixed is denoted as "C" while Free is denoted as "F" in the legend on all these types of figures. Further information can be found in his Thesis which is listed in the references. In summary, the FEA simulations tend to overestimate the strain likely due to modeling simplifications.

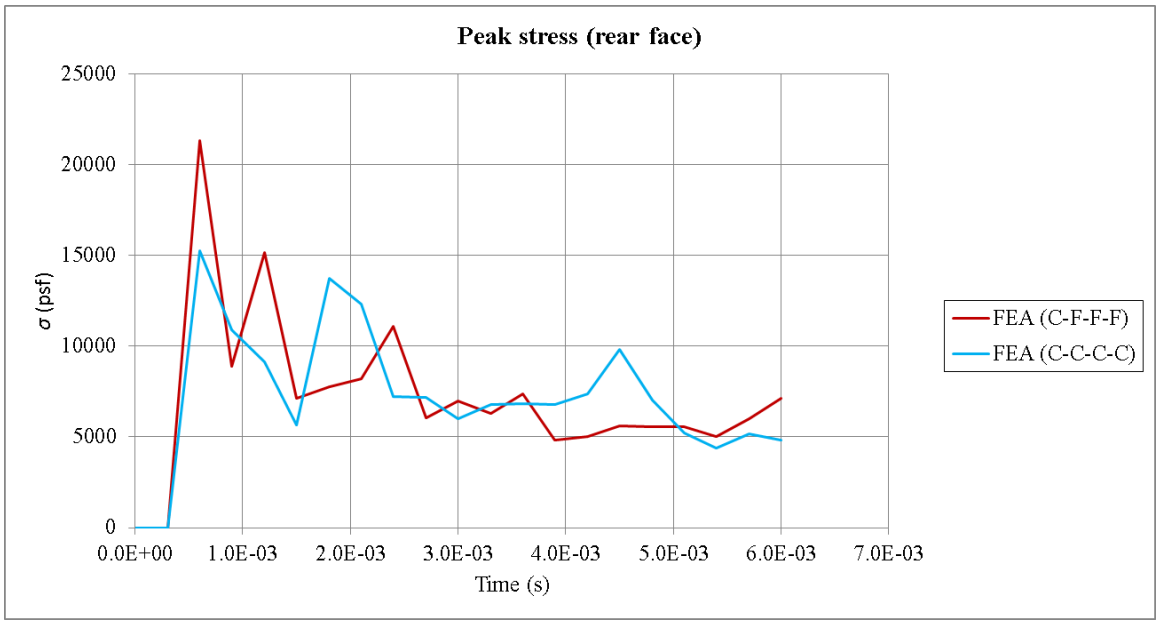

Figure A.8 FEA peak rear face stress, hard hat, test date: 31 Jul 19

B, Water jug, 31 July 2019

Figure A.9 Water jug

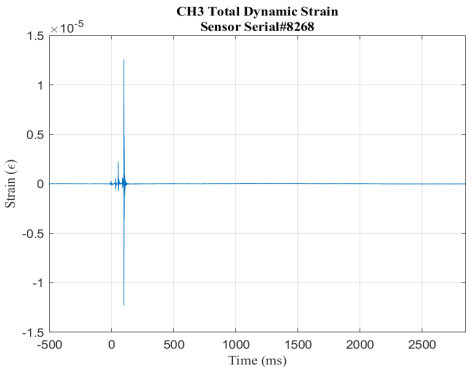

a.

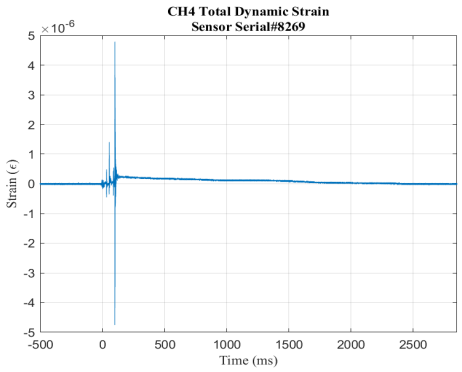

b.

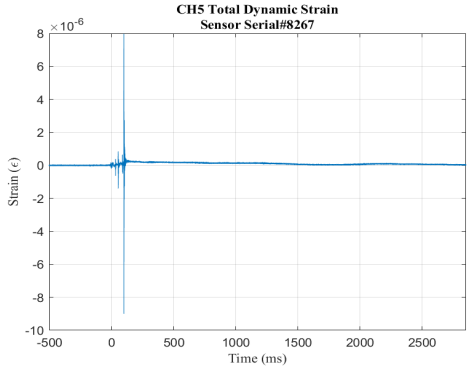

c.

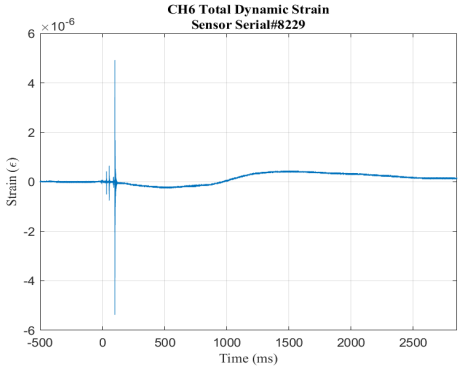

d.

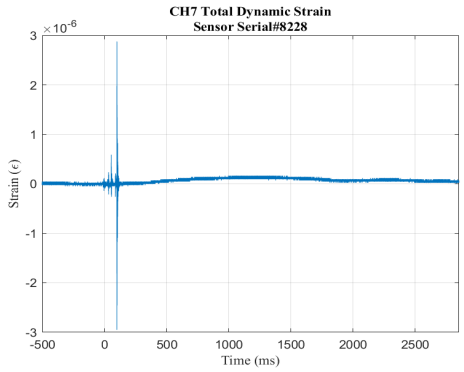

e.

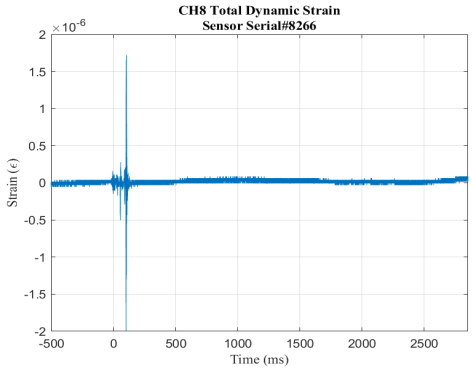

f.

Figure A.10 Strain response, water jug, test date: 31 Jul 19

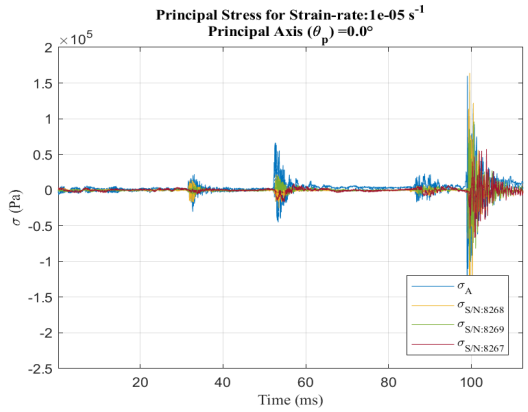

a.

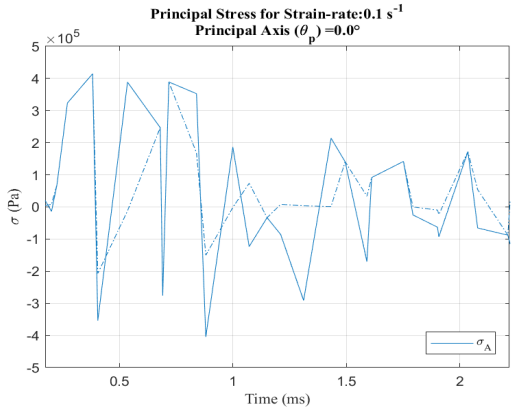

b.

Figure A.11 Principal stress at strain rate, water jug, test date: 31 Jul 19

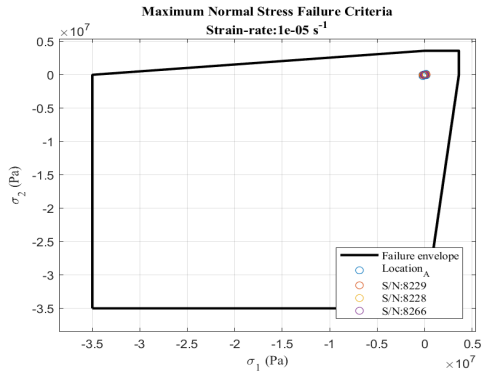

a.

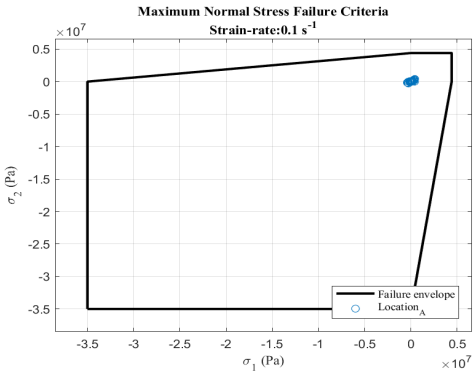

b.

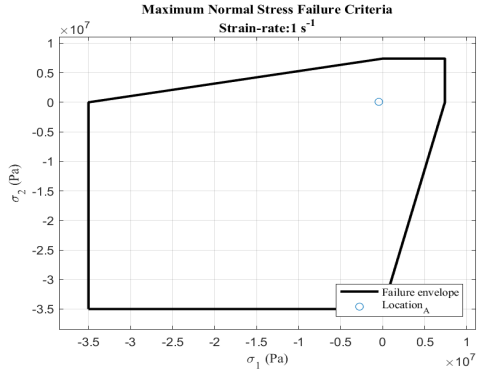

c.

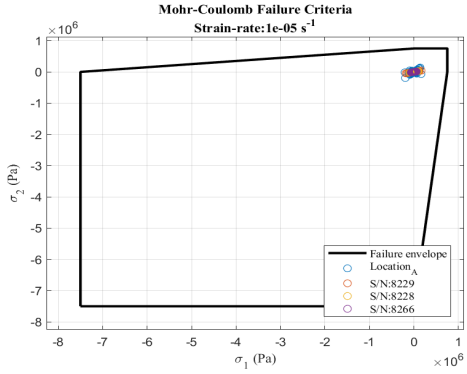

d.

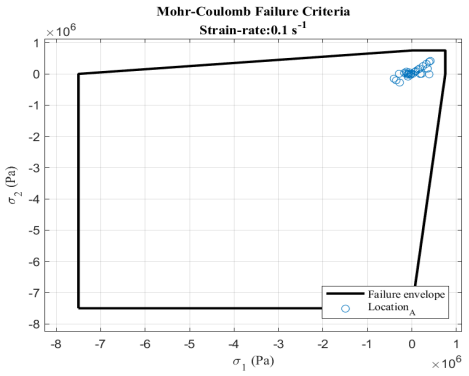

e.

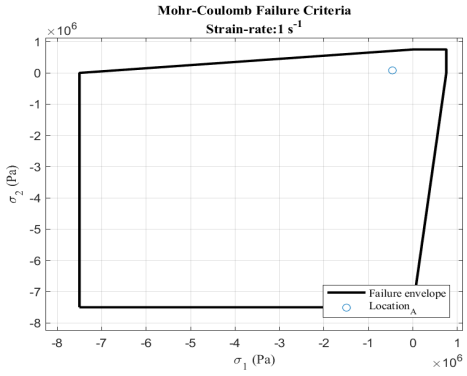

f.

Figure A.12 Failure criterion envelopes, water jug, test date: 31 Jul 19

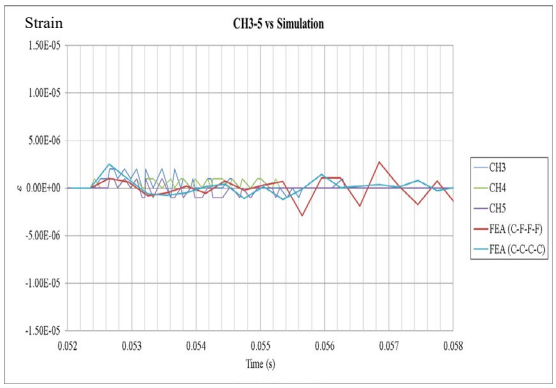

a.

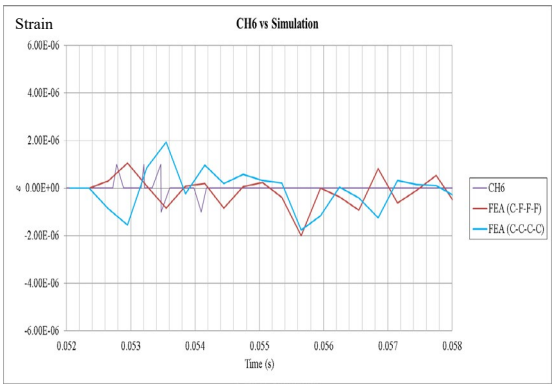

b.

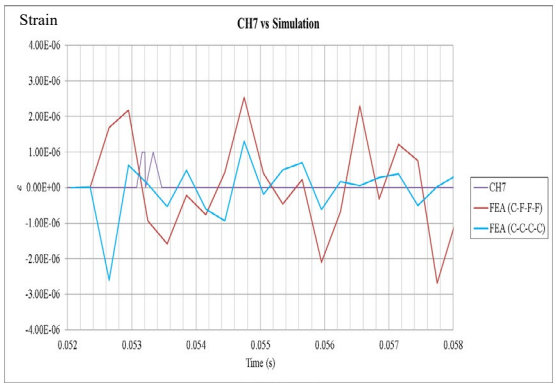

c.

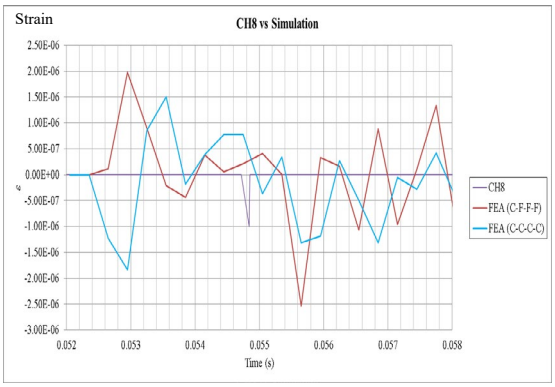

d.

Figure A.13 Strain response and FEA comparison, water jug, test date: 31 Jul 19

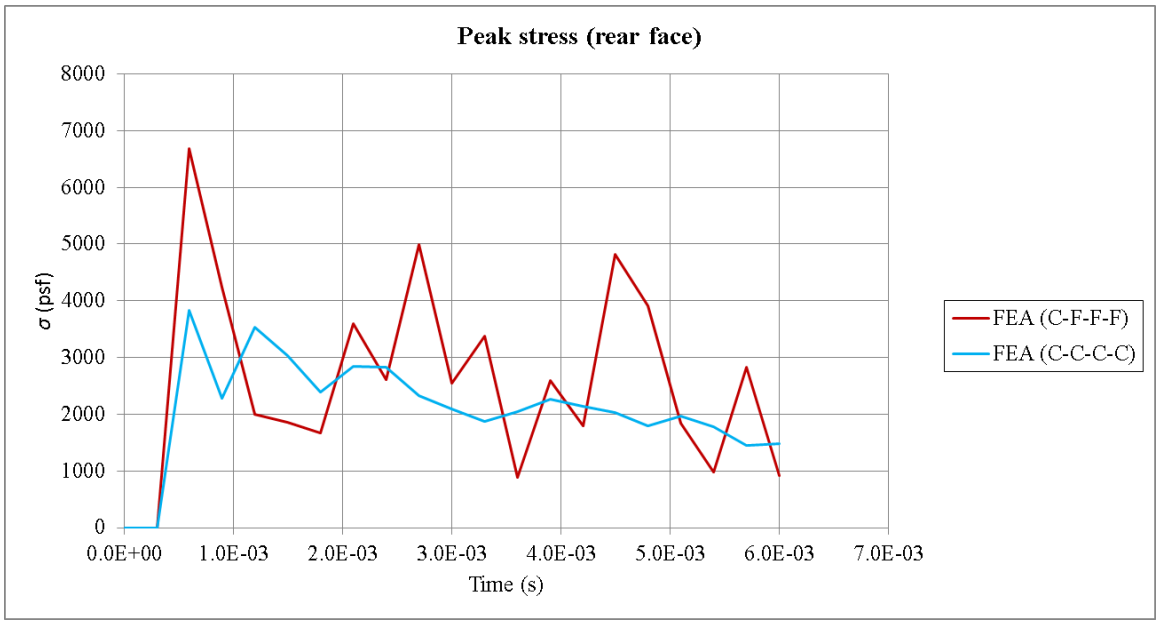

Figure A.14 FEA peak rear face stress, water jug, test date: 31 Jul 19

C, Hand tools, 31 July 2019

Figure A.15 Hand tools

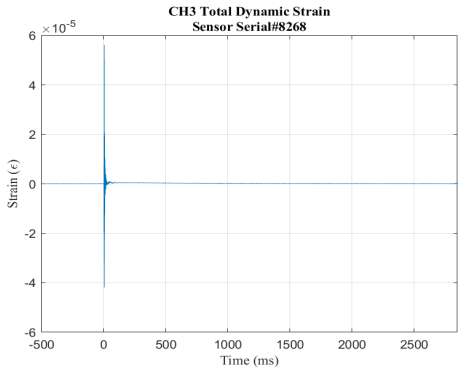

a.

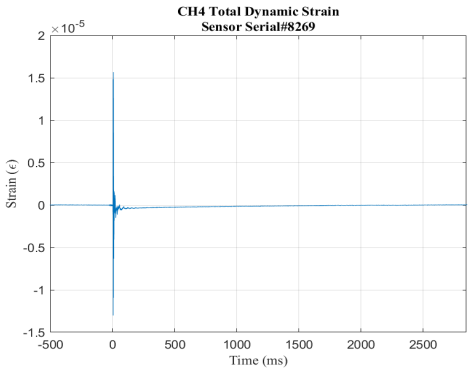

b.

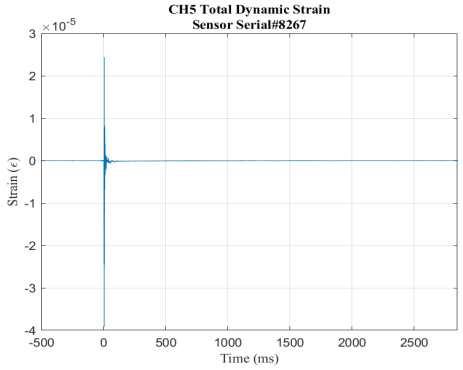

c.

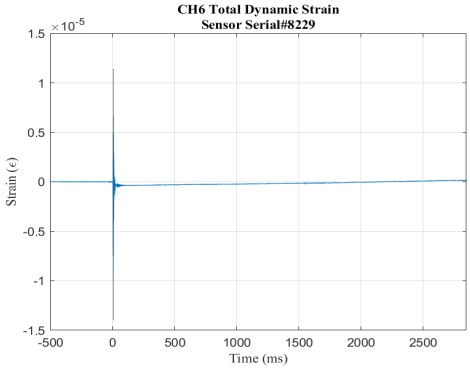

d.

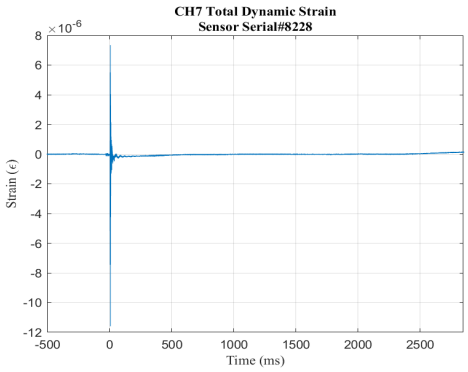

e

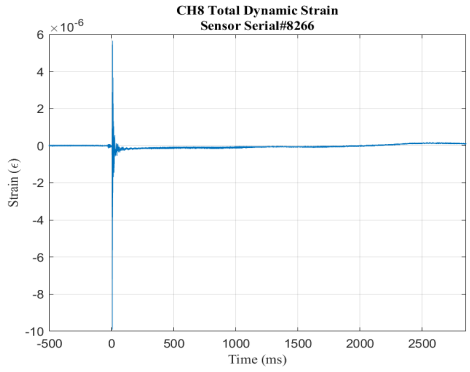

f

Figure A.16 Strain response, hand tools, test date: 31 Jul 19

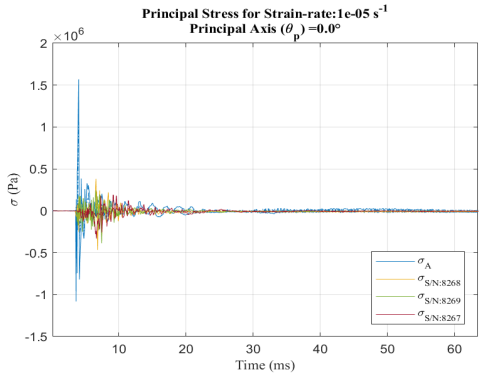

a.

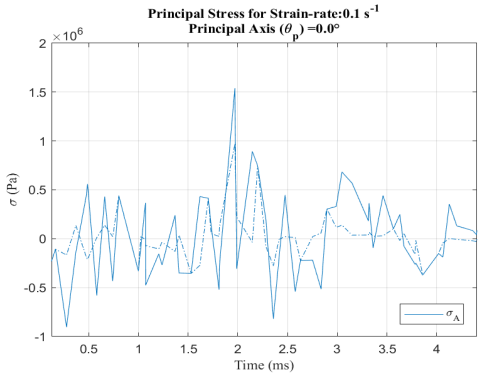

b.

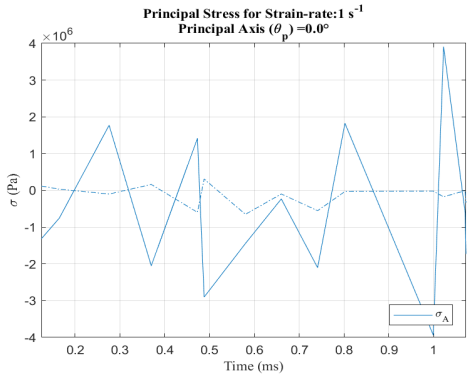

c.

Figure A.17 Principal stress at strain rate, hand tools, test date: 31 Jul 19

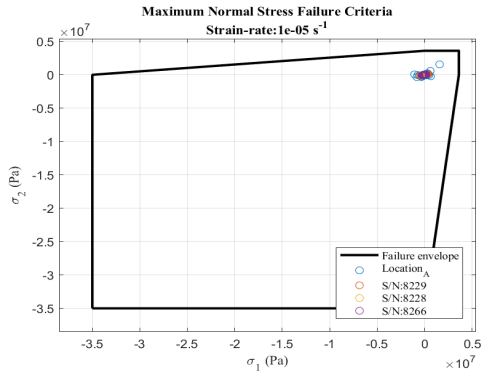

a.

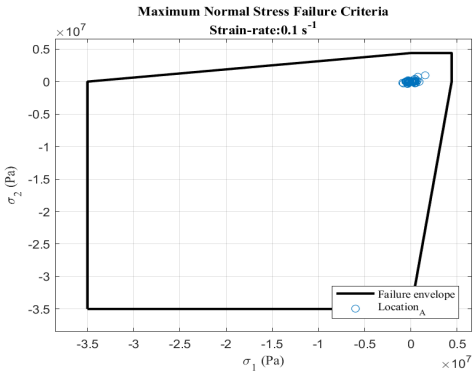

b.

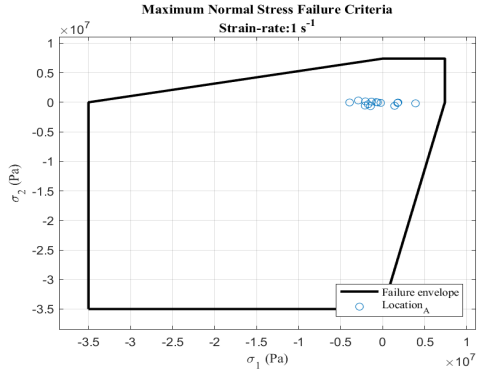

c.

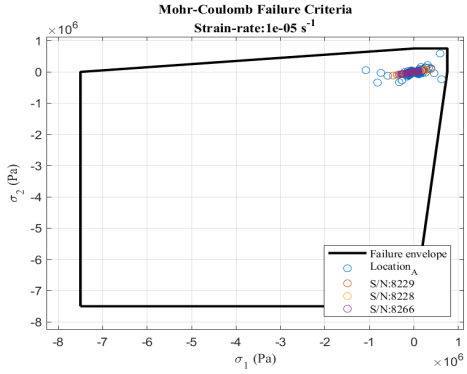

d.

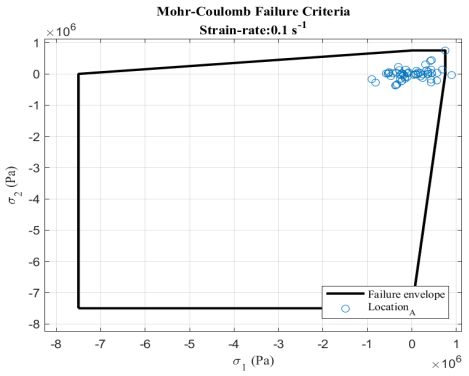

e.

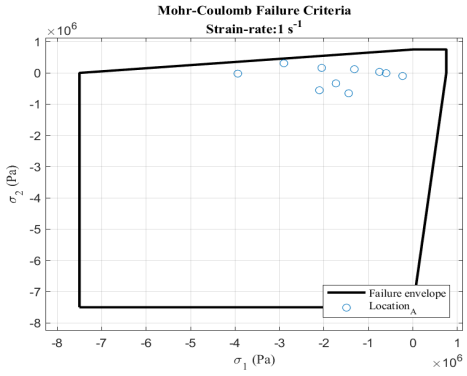

f.

Figure A.18 Failure criterion envelopes, hand tools, test date: 31 Jul 19

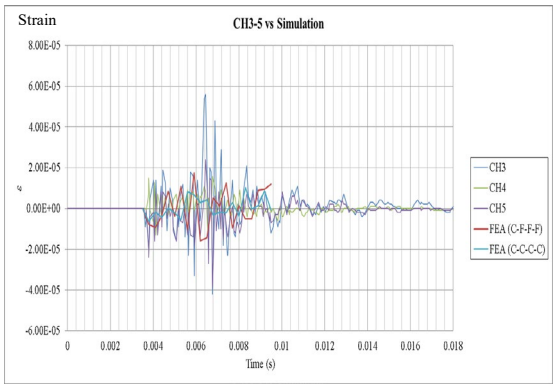

a.

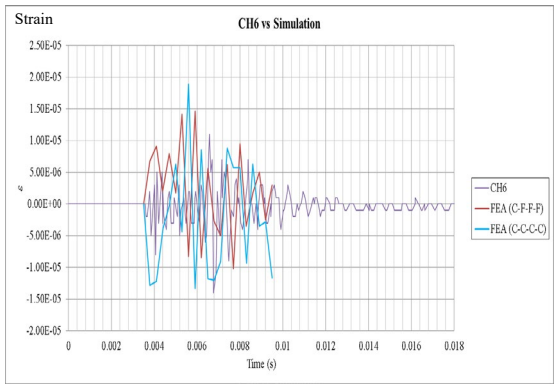

b.

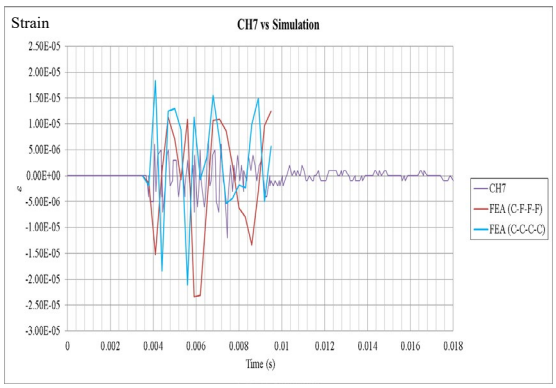

c.

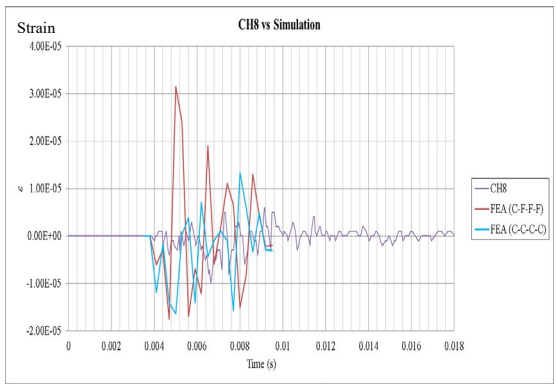

d.

Figure A.19 Strain response and FEA comparison, hand tools, test date: 31 Jul 19

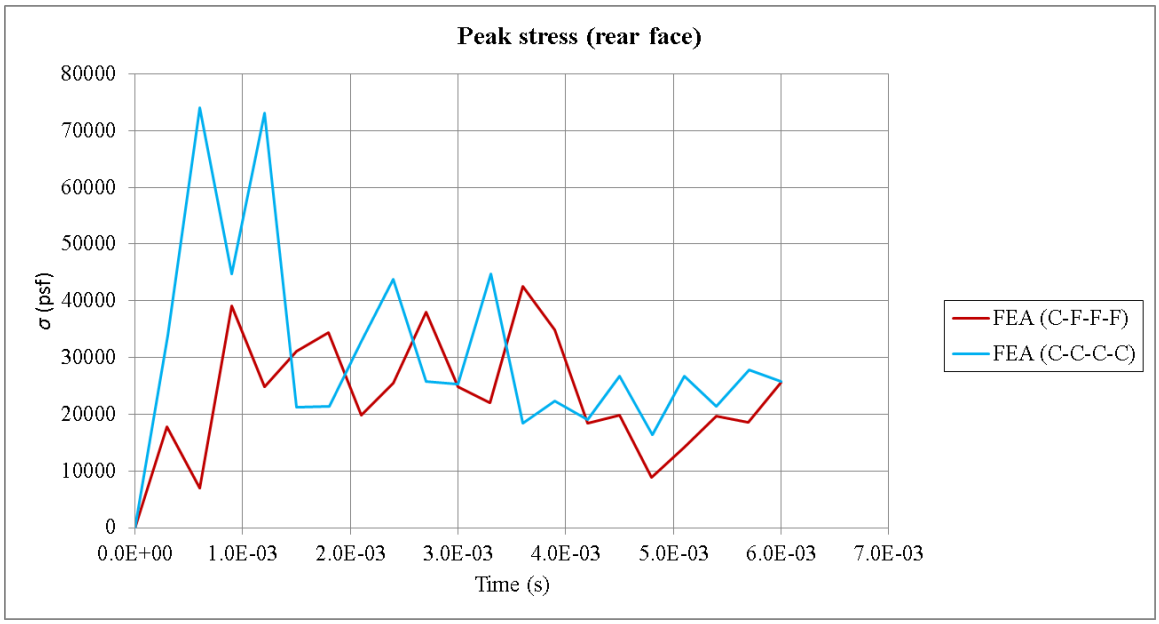

Figure A.20 FEA peak rear face stress, hand tools, test date: 31 Jul 19

D, Roof bolt plates, 31 July 2019

Figure A.21 Roof bolt plates

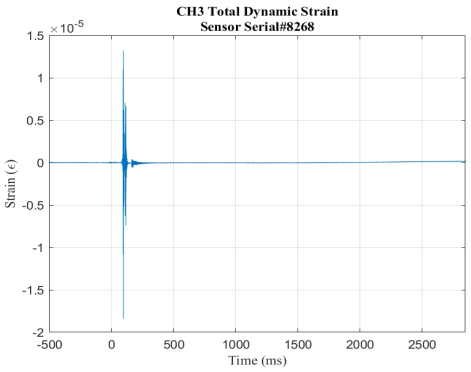

a.

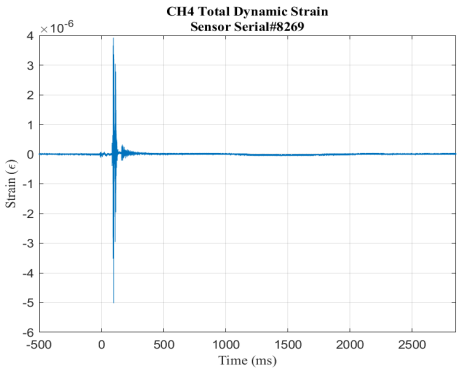

b.

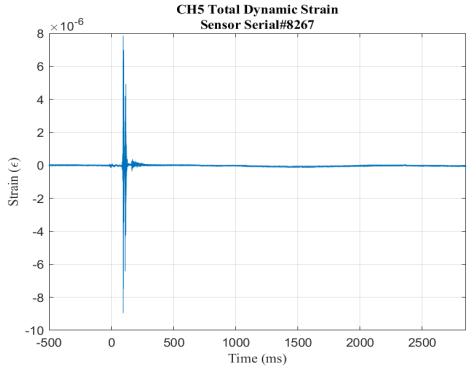

c.

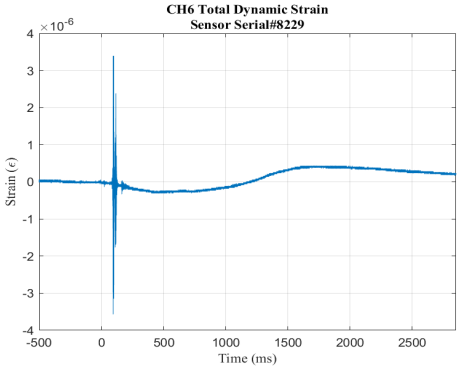

d.

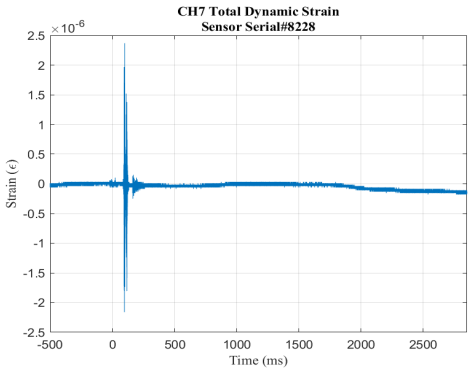

e

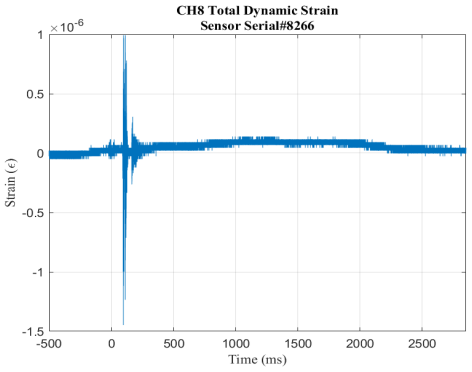

f

Figure A.22 Strain response, roof bolt plates, test date: 31 Jul 19

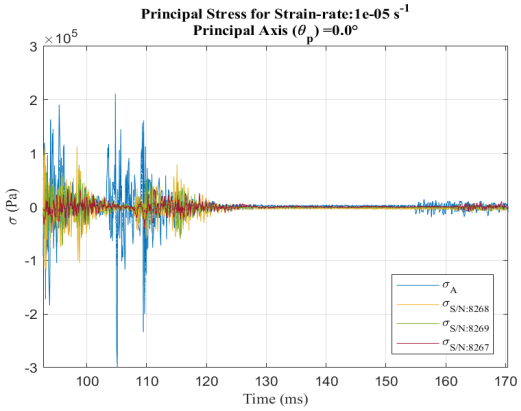

a.

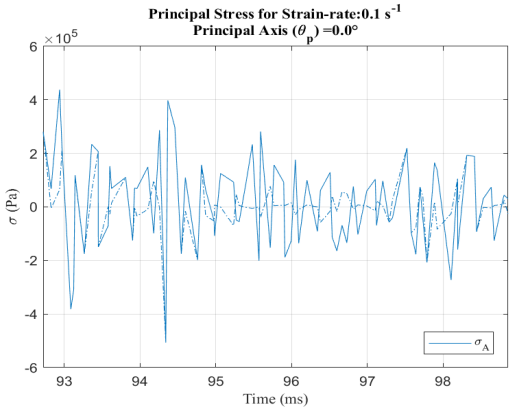

b.

Figure A.23 Principal stress at strain rate, roof bolt plates, test date: 31 Jul 19

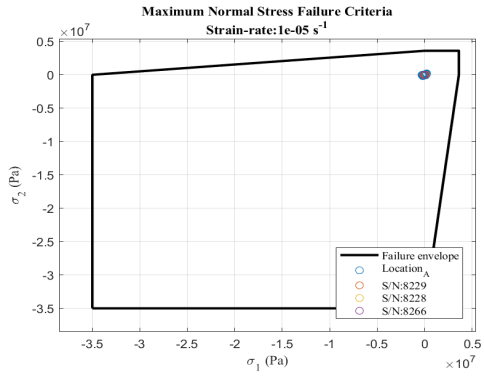

a.

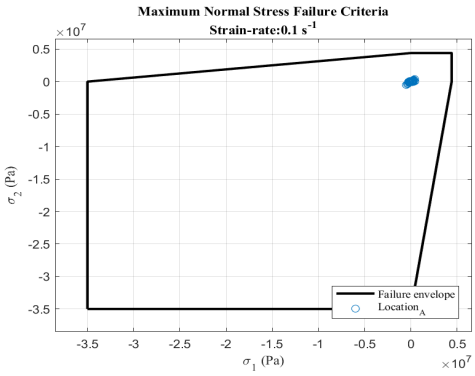

b.

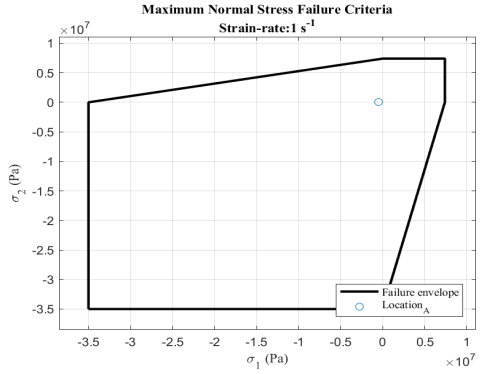

c.

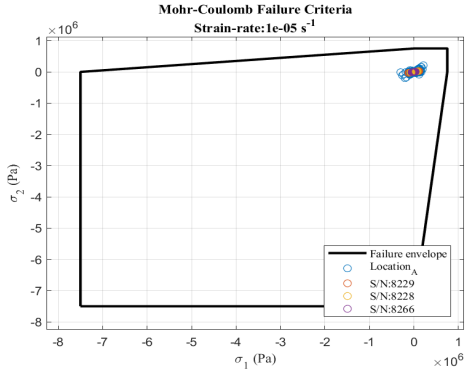

d.

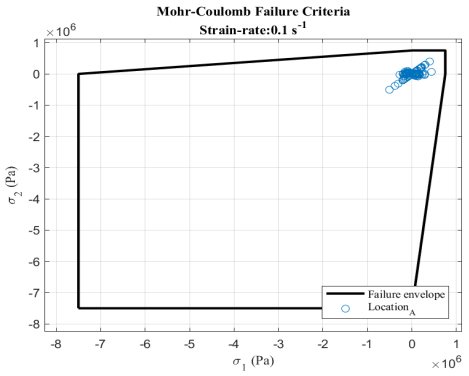

e.

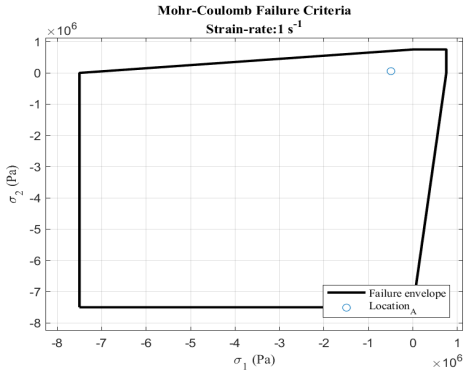

f.

Figure A.24 Failure criterion envelopes, roof bolt plates, test date: 31 Jul 19

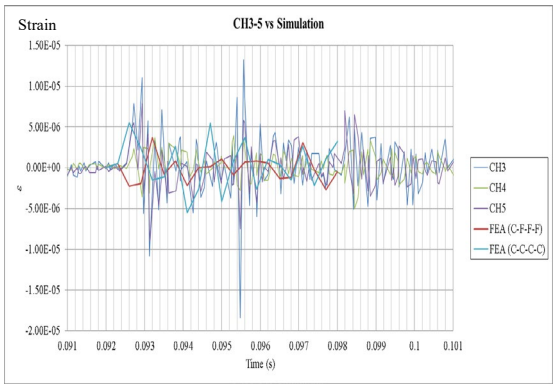

a.

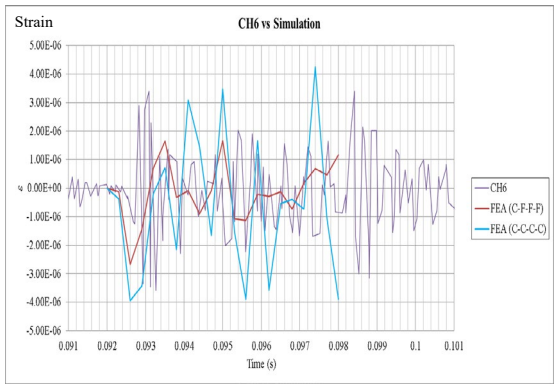

b.

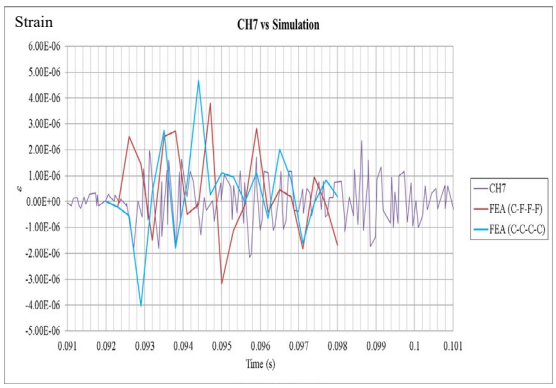

c.

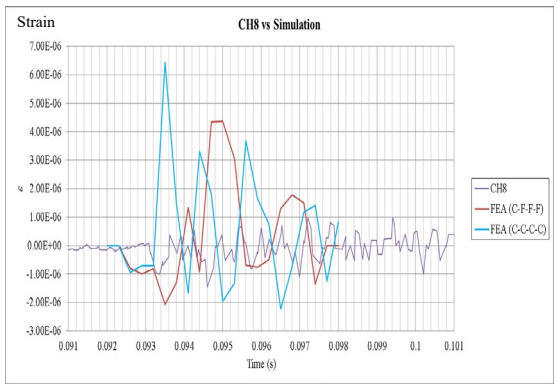

d.

Figure A.25 Strain response and FEA comparison, roof bolt plates, test date: 13 Aug 19

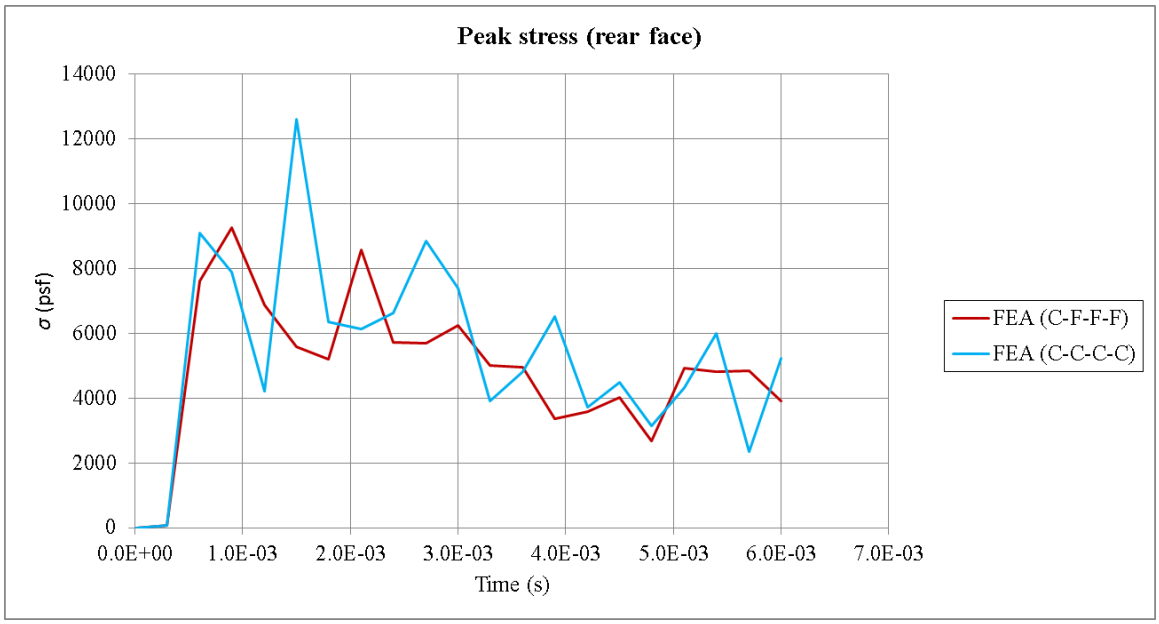

Figure A.26 FEA peak rear face stress, roof bolt plates, test date: 13 Aug 19

E, 5 x 5 lumber, 13 August 2019

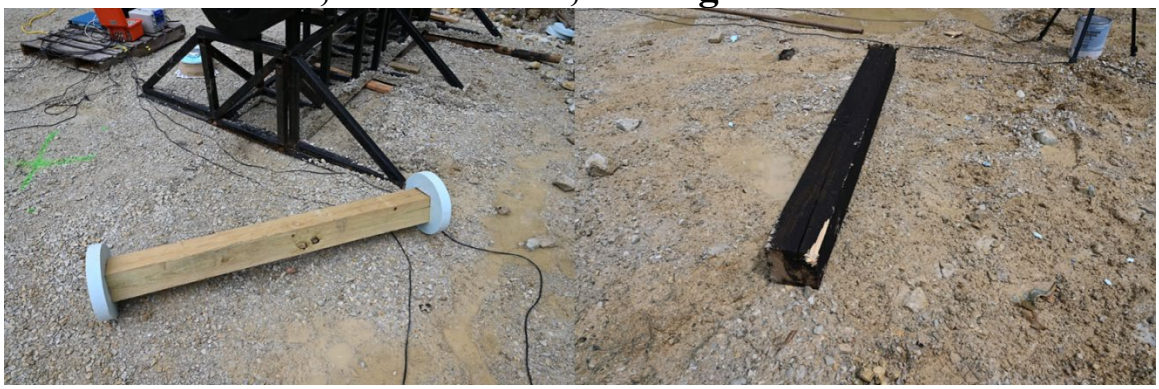

Figure A.27 5 x 5 lumber

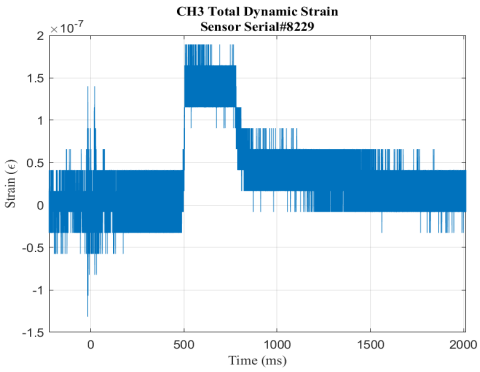

a.

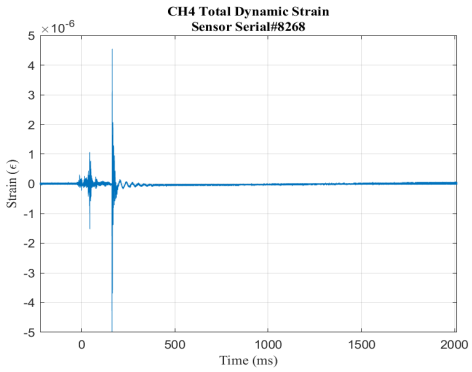

b.

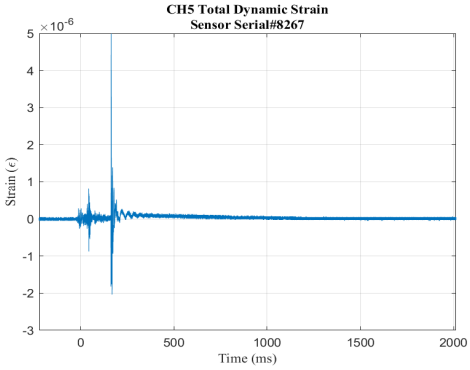

c.

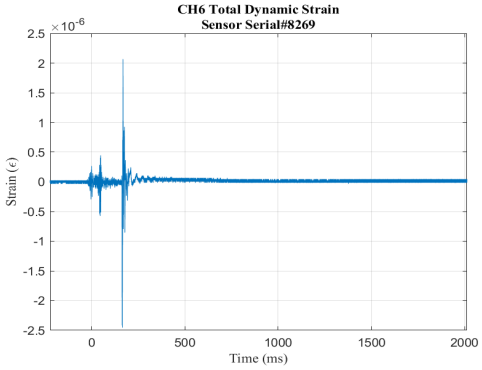

d.

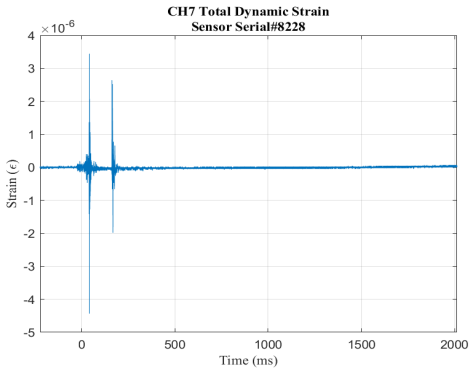

e.

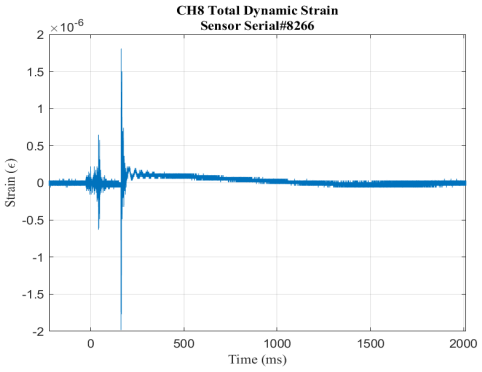

f.

Figure A.28 Strain response, 5 x 5 lumber, test date: 13 Aug 19

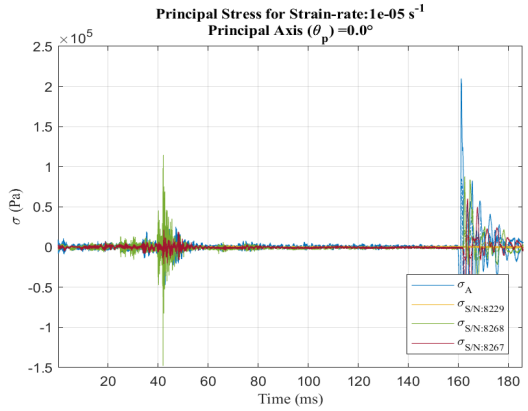

a.

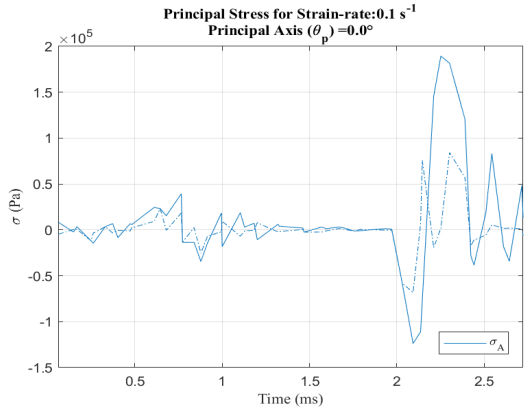

b.

Figure A.29 Principal stress at strain rate, 5 x 5 lumber, test date: 13 Aug 19

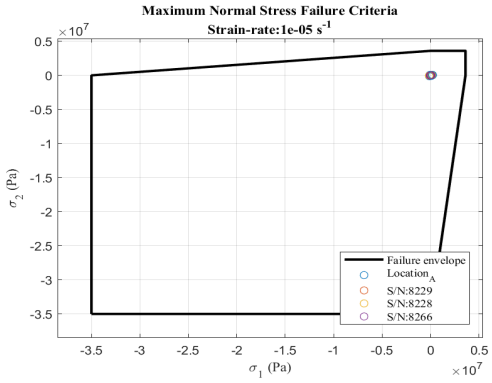

a.

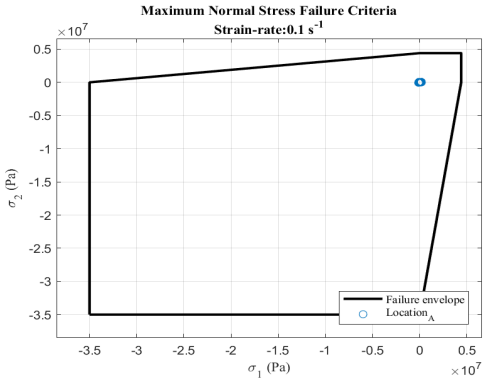

b.

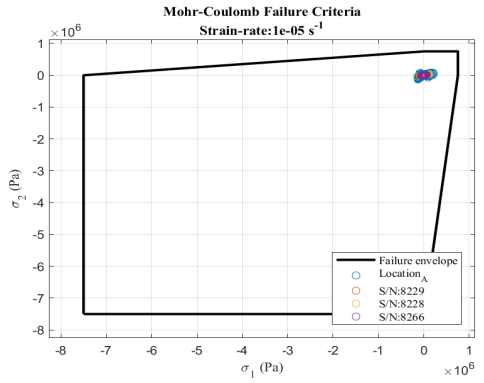

c.

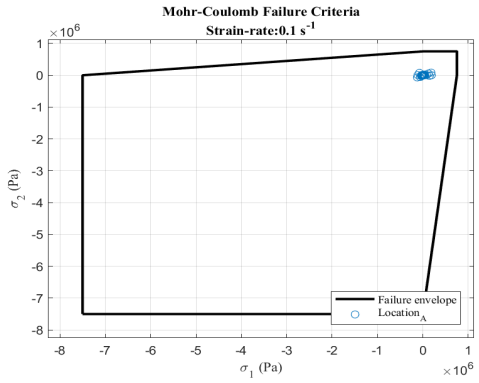

d.

Figure A.30 Failure criterion envelopes, 5 x 5 lumber, test date: 13 Aug 19

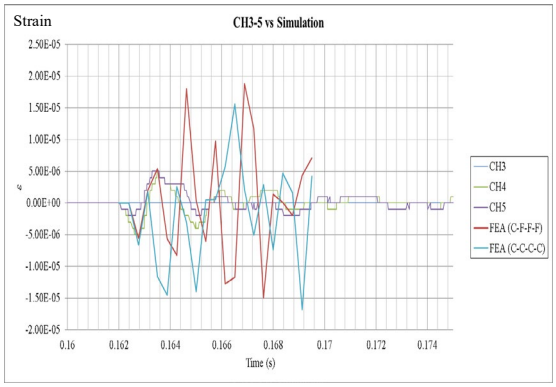

a.

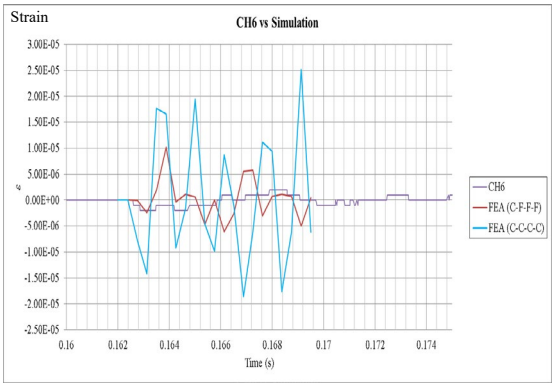

b.

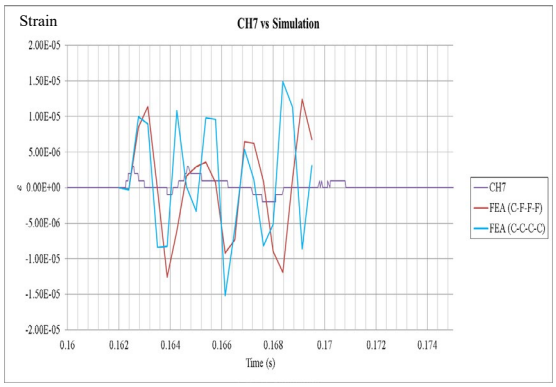

c.

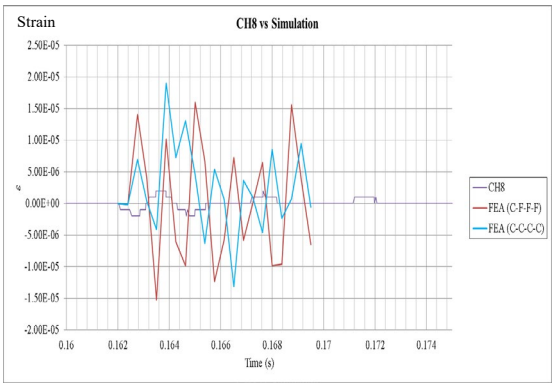

d.

Figure A.31 Strain response and FEA comparison, 5 x 5 lumber, test date: 13 Aug 19

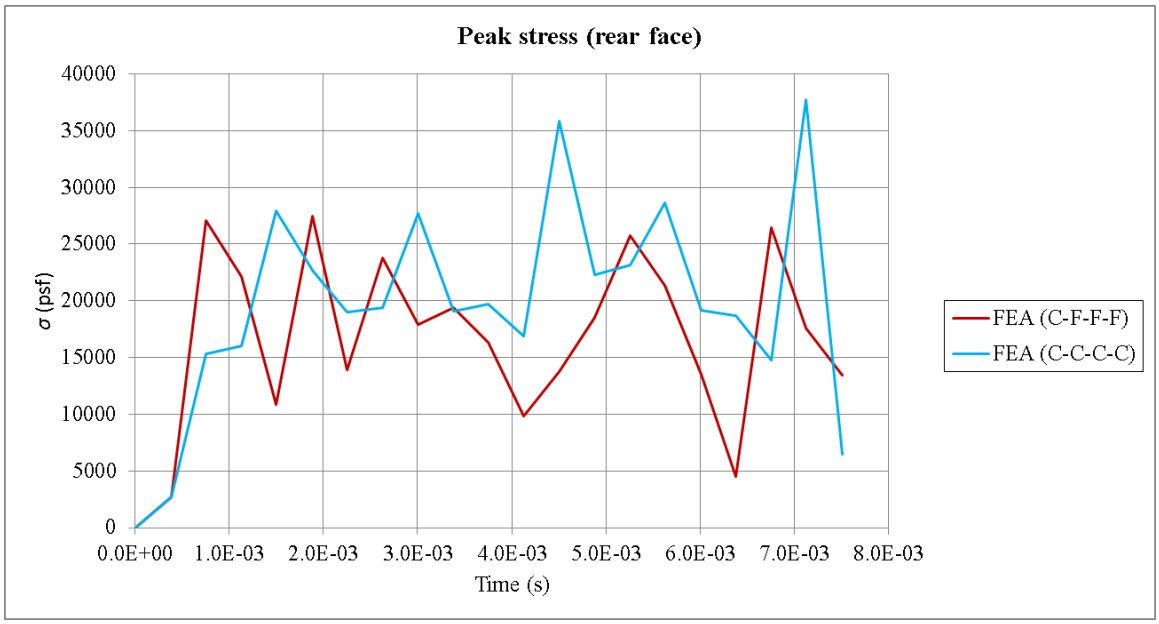

Figure A.32 FEA peak rear face stress, 5 x 5 lumber, test date: 13 Aug 19

F, Roof bolts, 13 August 2019

Figure A.33 Roof bolts

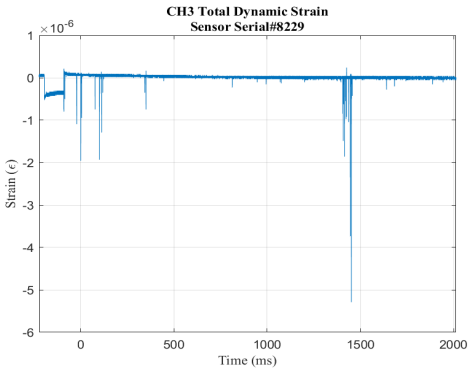

a.

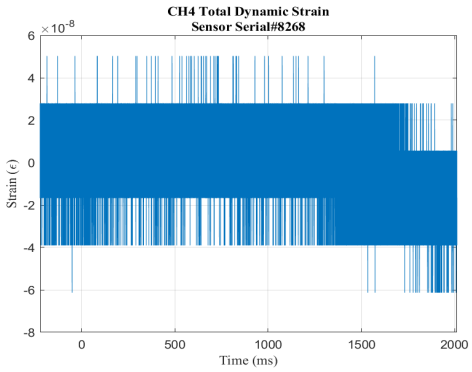

b.

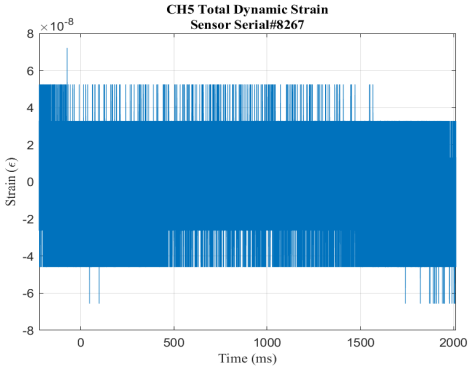

c.

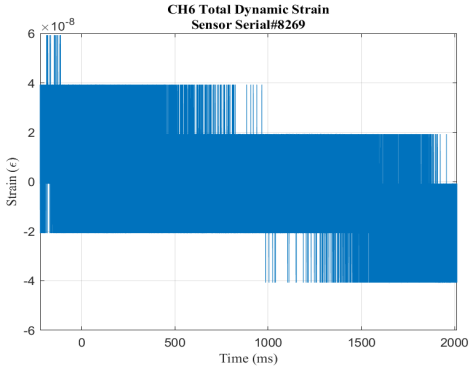

d.

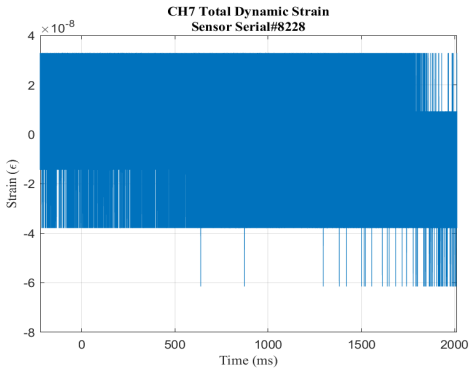

e.

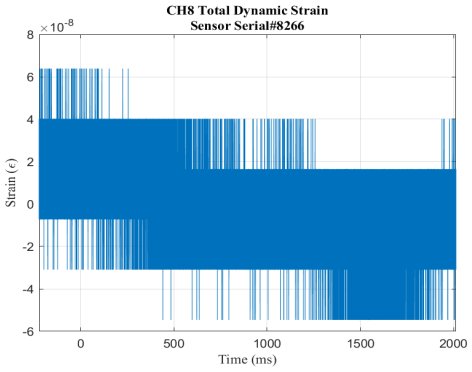

f.

Figure A.34 Strain response, roof bolts, 13 Aug 19

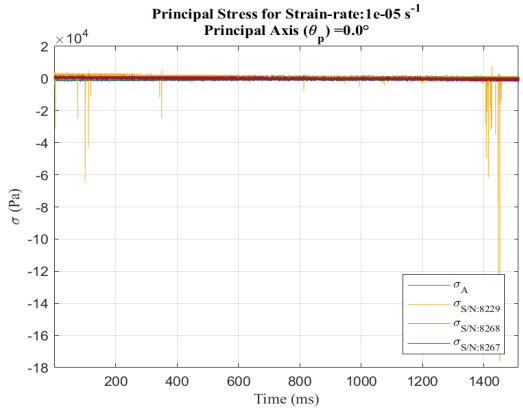

a.

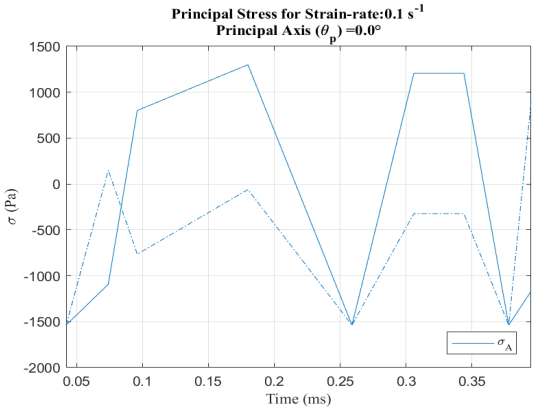

b.

Figure A.35 Principal stress at strain rate, roof bolts, test date: 13 Aug 19

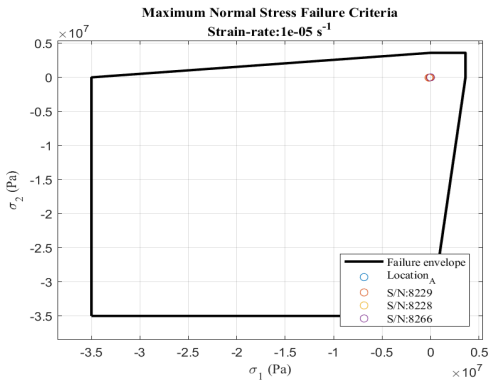

a.

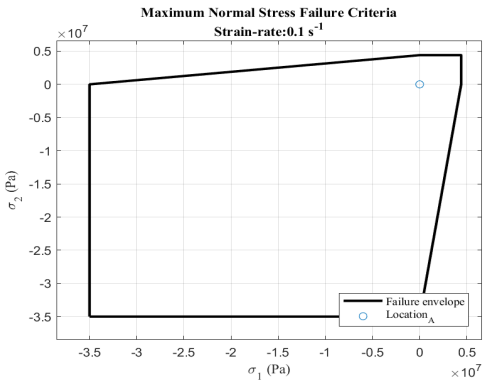

b.

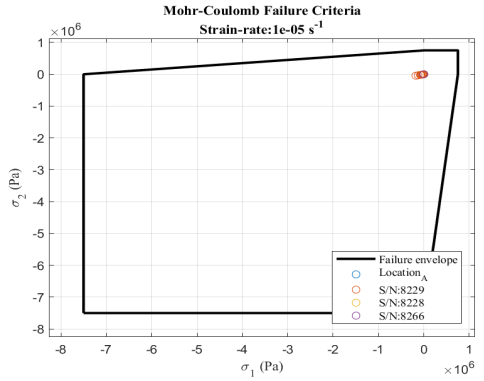

c.

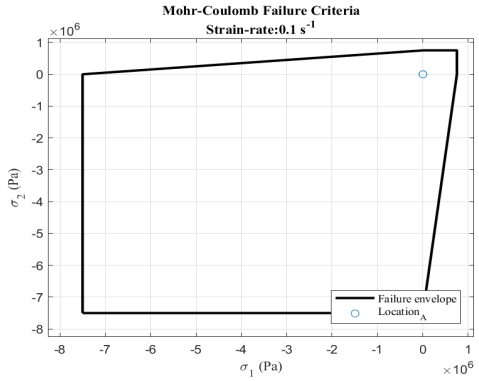

d.

Figure A.36 Failure criterion envelopes, roof bolts, test date: 13 Aug 19

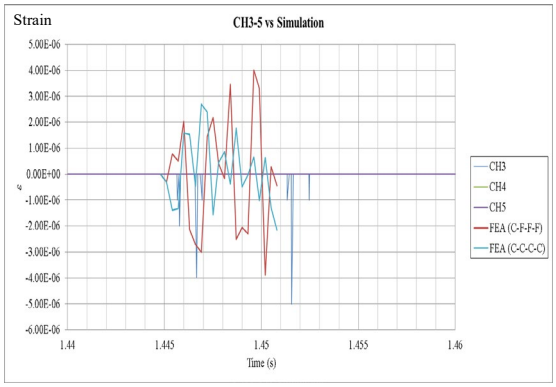

a.

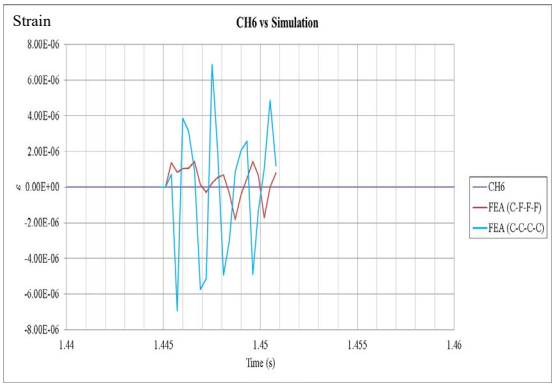

b.

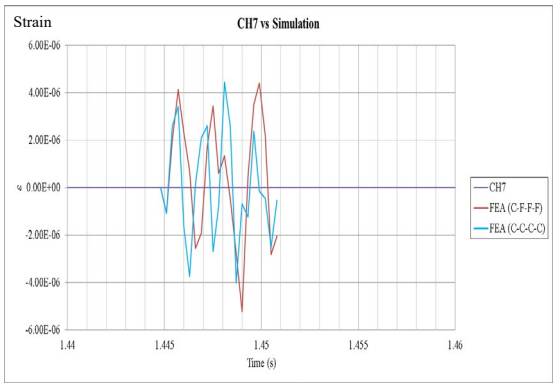

c.

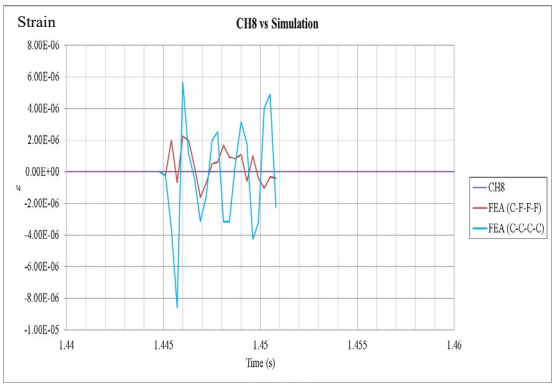

d.

Figure A.37 Strain response and FEA comparison, roof bolts, test date: 13 Aug 19

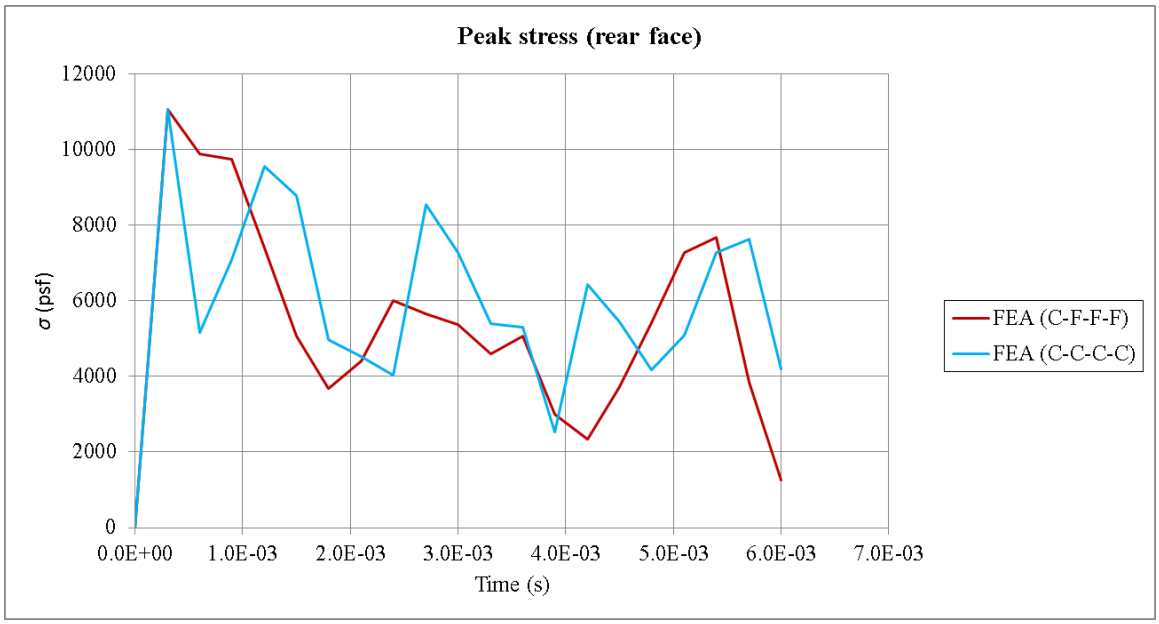

Figure A.38 FEA peak rear face stress, roof bolts, test date: 13 Aug 19

G, Concrete (10 lb), 13 August 2019

Figure A.39 Concrete (10 lb)

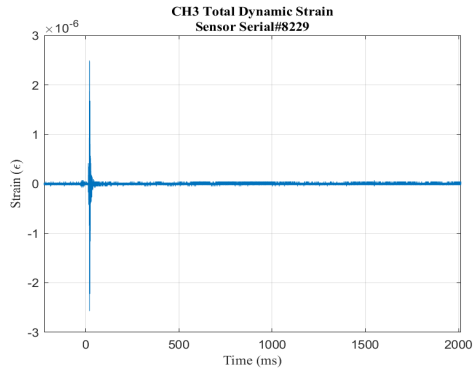

a.

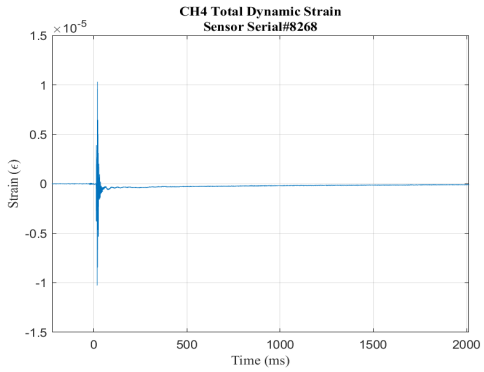

b.

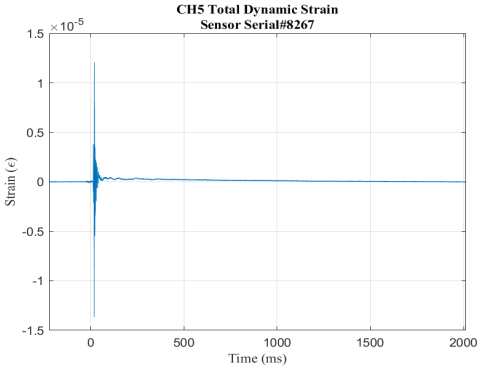

c.

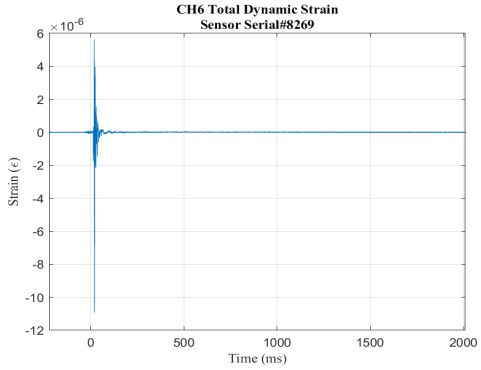

d.

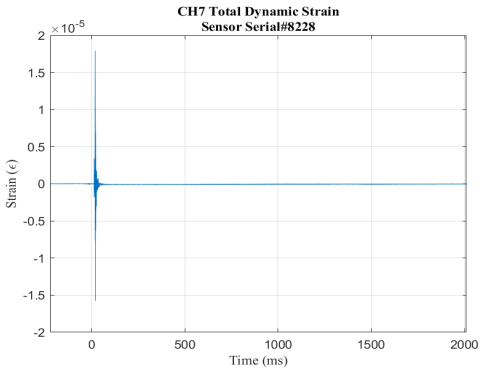

e.

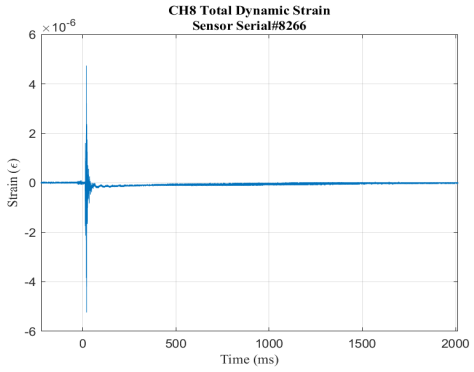

f.

Figure A.40 Strain response, concrete (10 lb) test date: 13 Aug 19

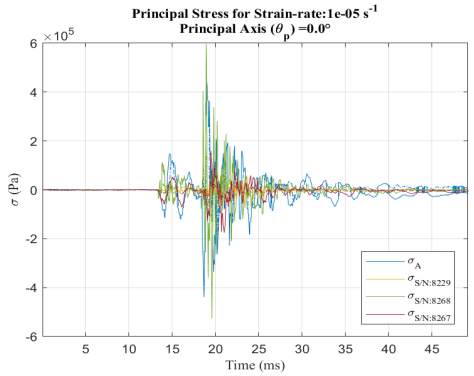

a.

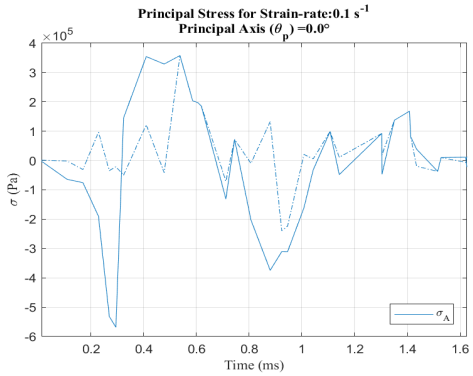

b.

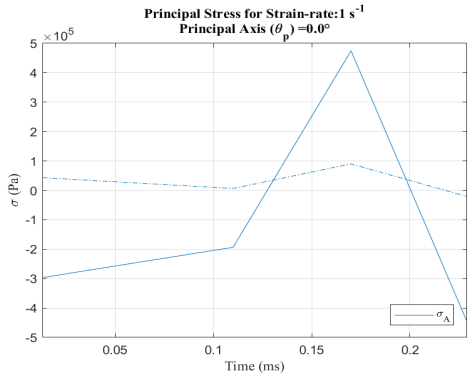

c.

Figure A.41 Principal stress at strain rate, concrete (10 lb), test date: 13 Aug 19

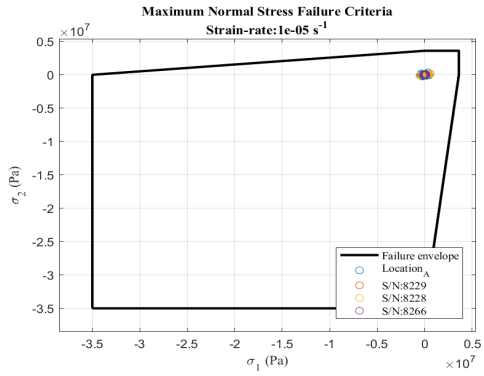

a.

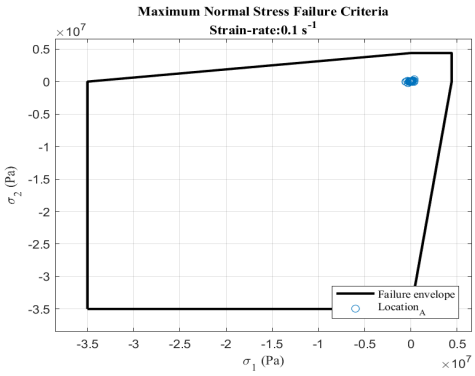

b.

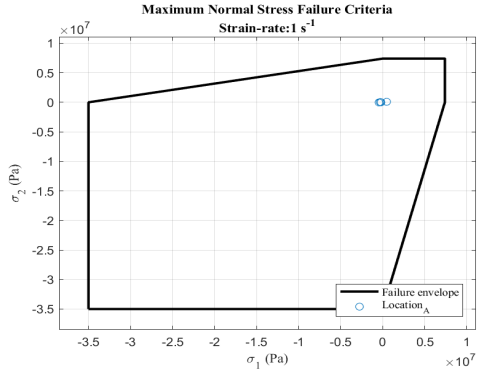

c.

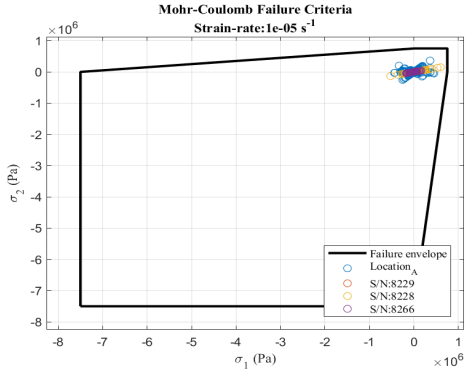

d.

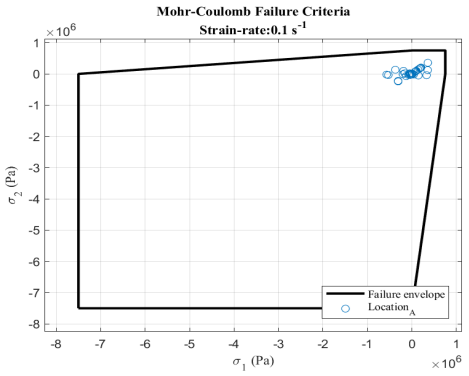

e

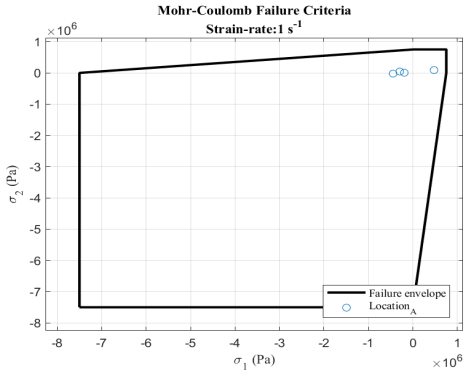

f

Figure A.42 Failure criterion envelopes, concrete (10 lb), test date: 13 Aug 19

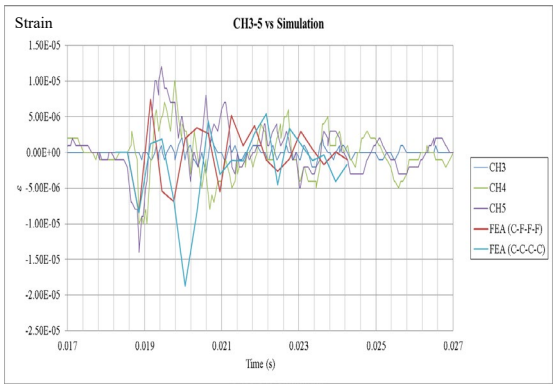

a.

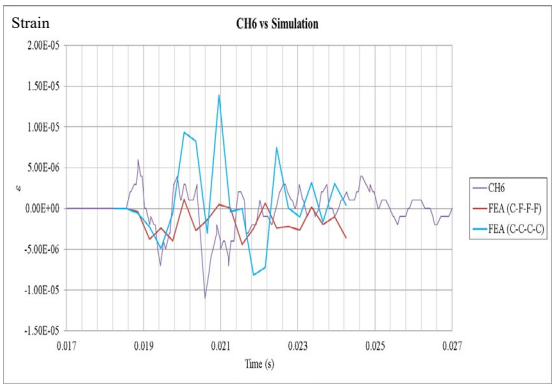

b.

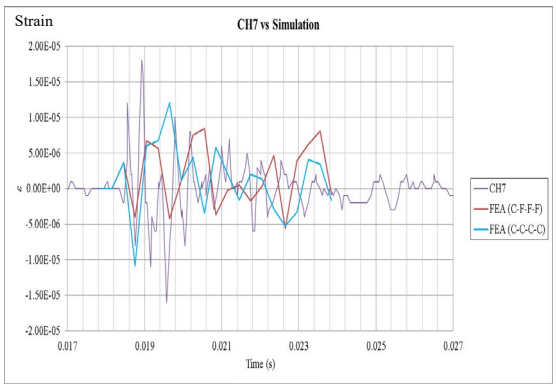

c.

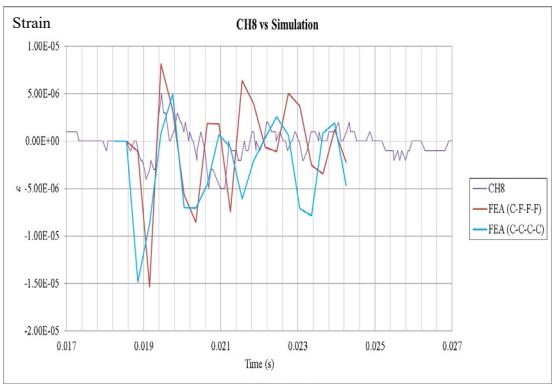

d.

Figure A.43 Strain response and FEA comparison, concrete (10 lb), test date: 13 Aug 19

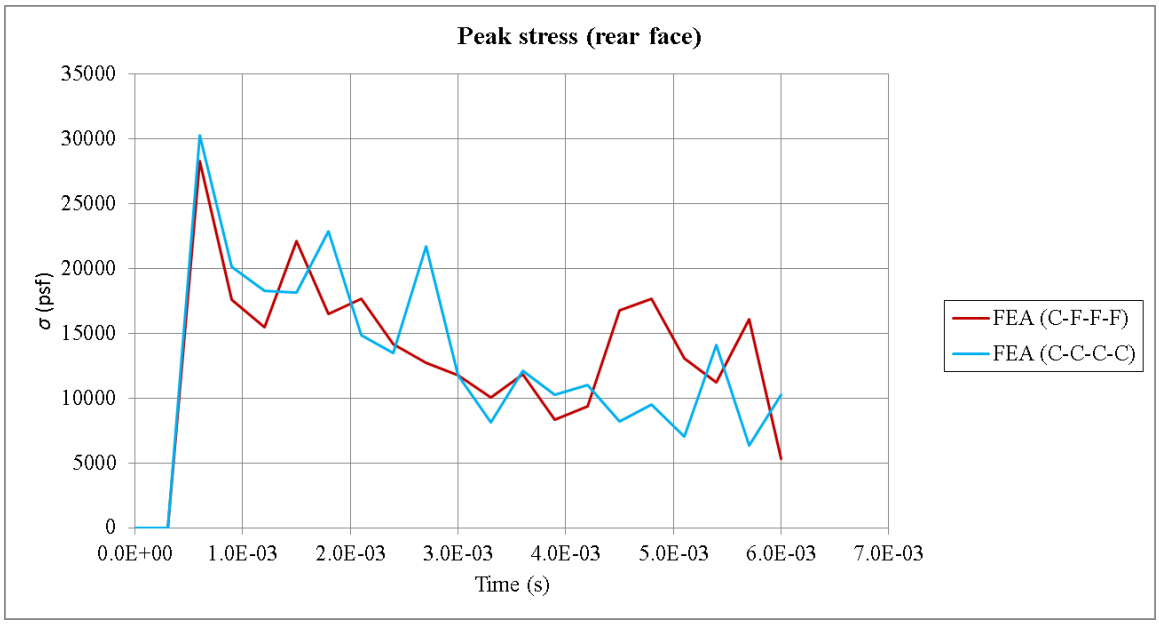

Figure A.44 FEA peak rear face stress, concrete (10 lb), test date: 13 Aug 19

H, Concrete (20 lb), 27 August 2019

Figure A.45 Concrete (20 lb)

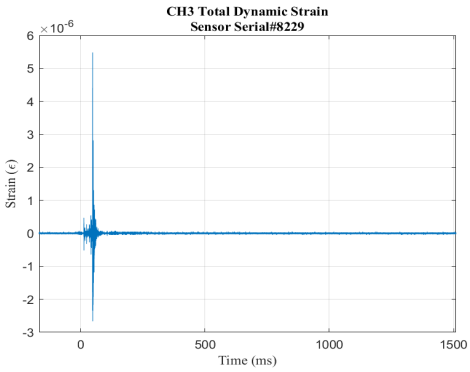

a.

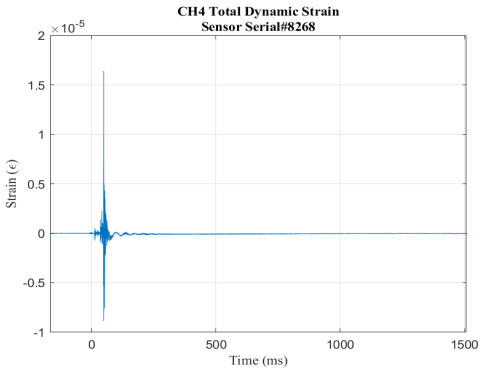

b.

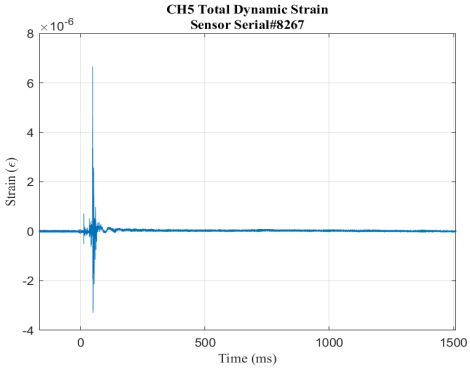

c.

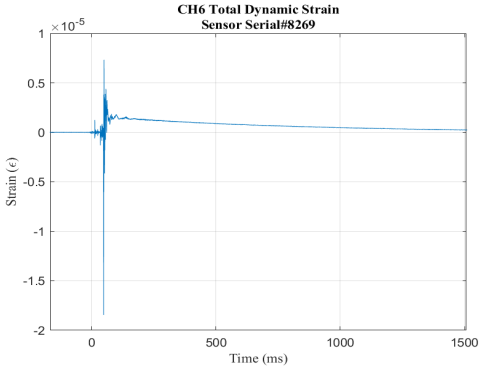

d.

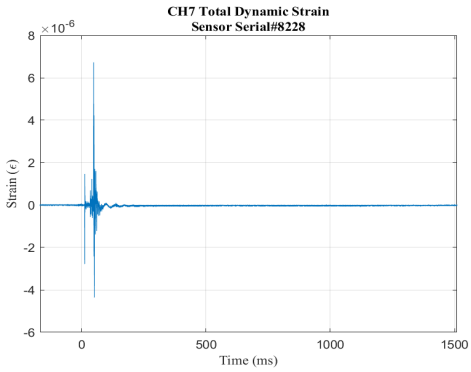

e.

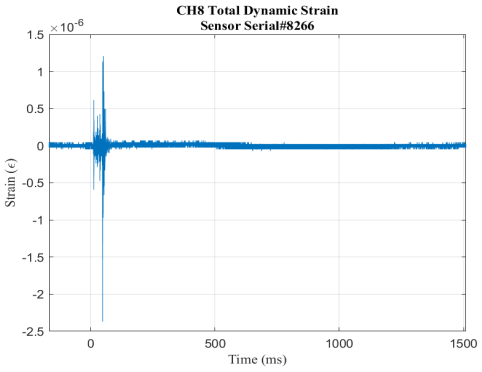

f.

Figure A.46 Strain response, concrete (20 lb), test date: 27 Aug 19

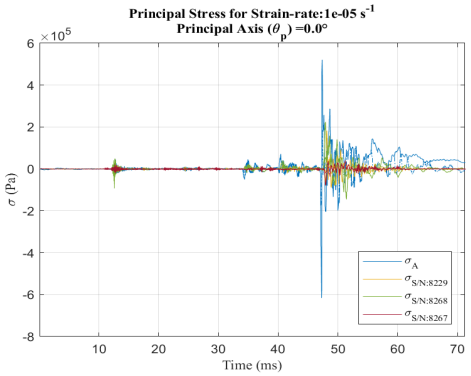

a.

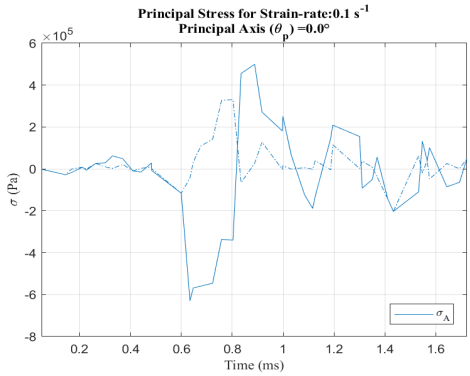

b.

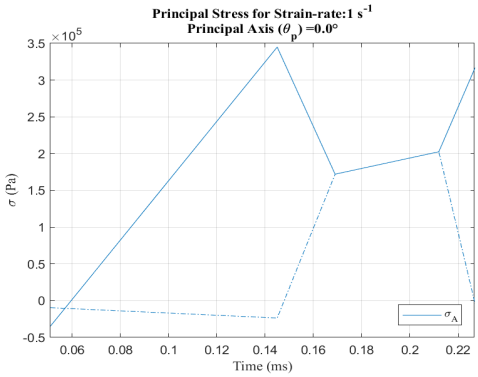

c.

Figure A.47 Principal stress at strain rate, concrete (20 lb), test date: 27 Aug 19

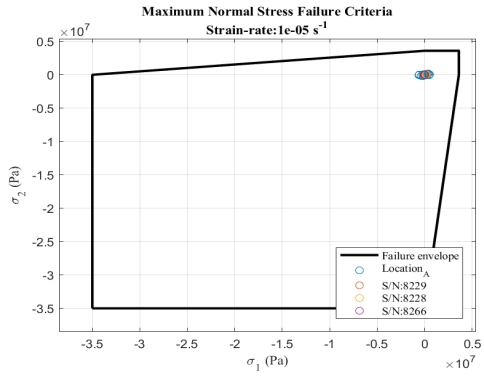

a.

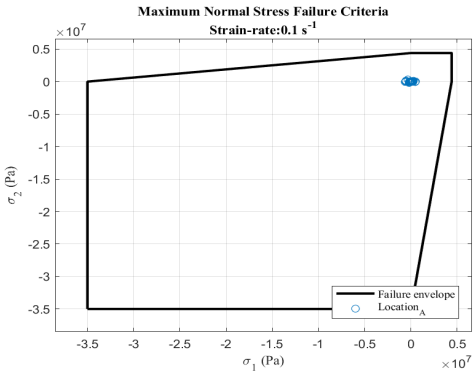

b.

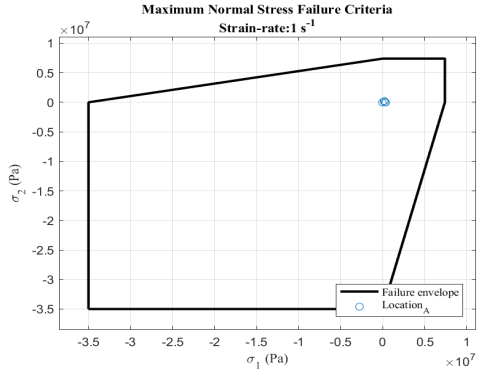

c.

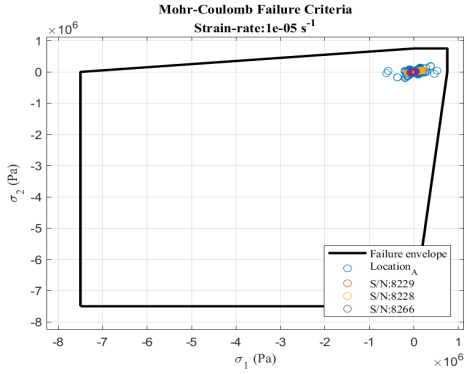

d.

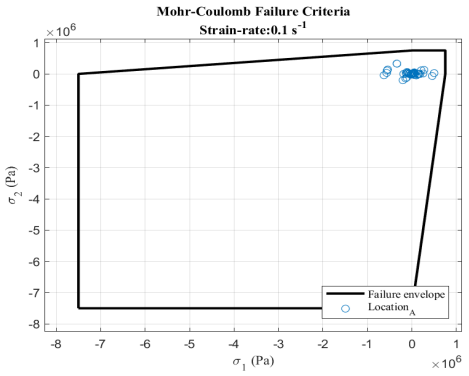

e.

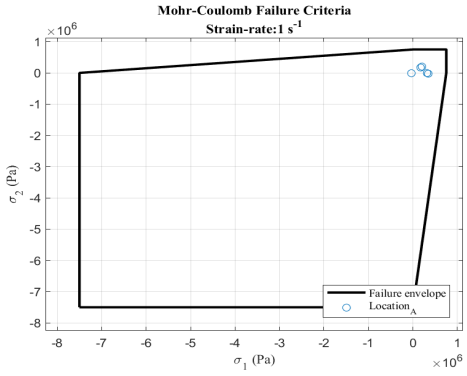

f.

Figure A.48 Failure criterion envelopes, concrete (20 lb), test date: 27 Aug 19

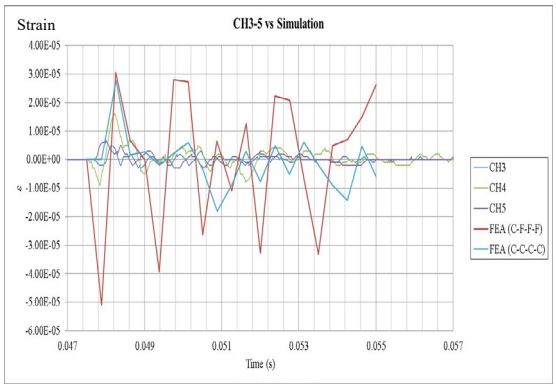

a.

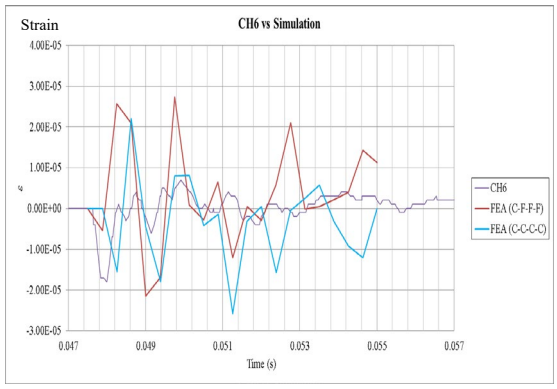

b.

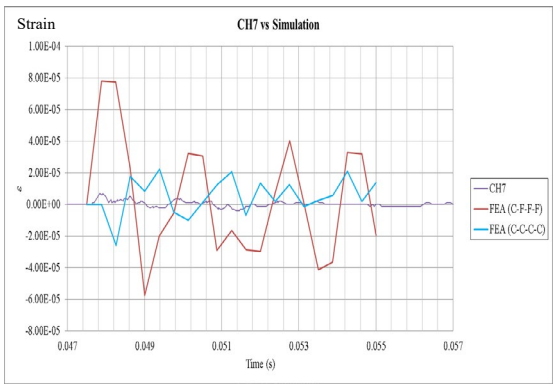

c.

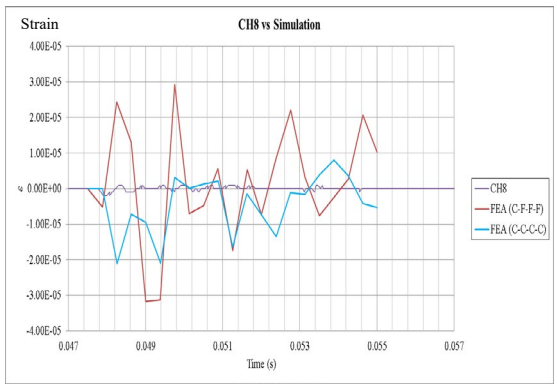

d.

Figure A.49 Strain response and FEA comparison, concrete (20 lb), test date: 27 Aug 19

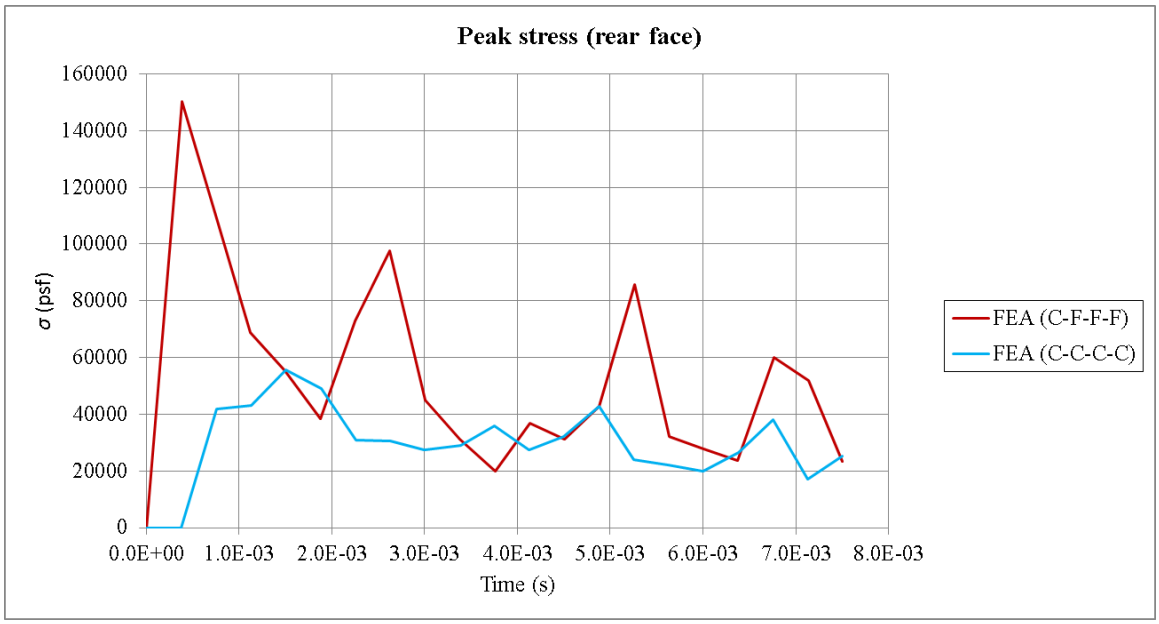

Figure A.50 FEA peak rear face stress, concrete (20 lb), test date: 27 Aug 19

I, Concrete (30 lb), 27 August 2019

Figure A.51 Concrete (30 lb)

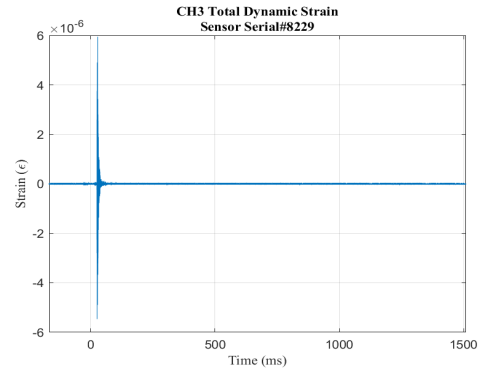

a.

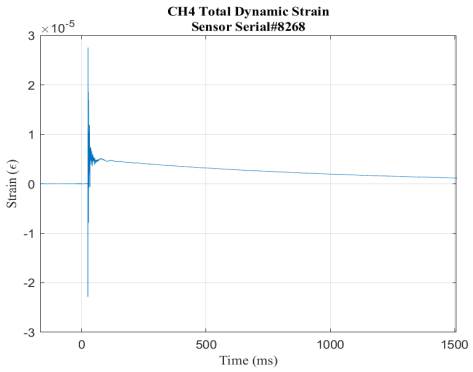

b.

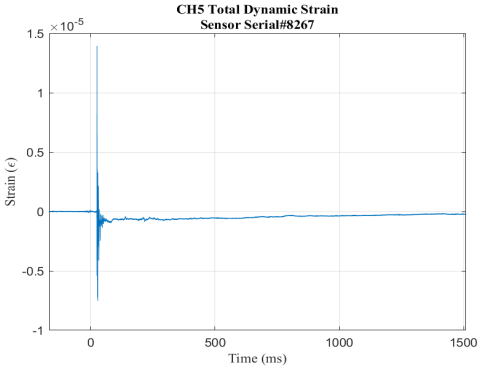

c.

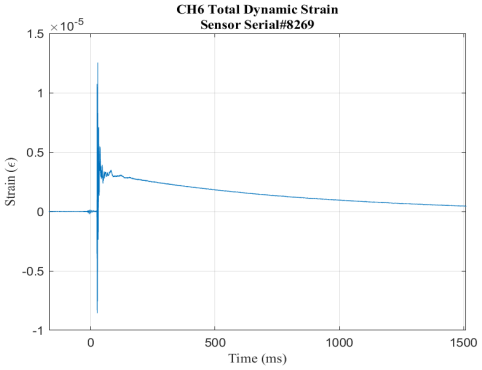

d.

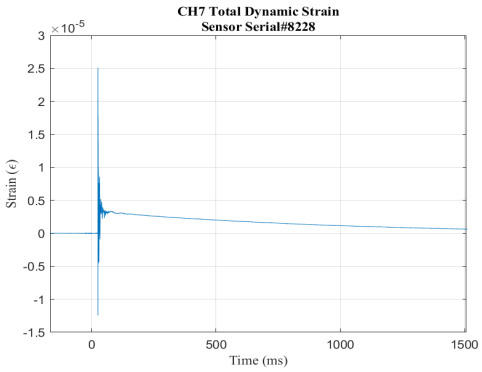

e.

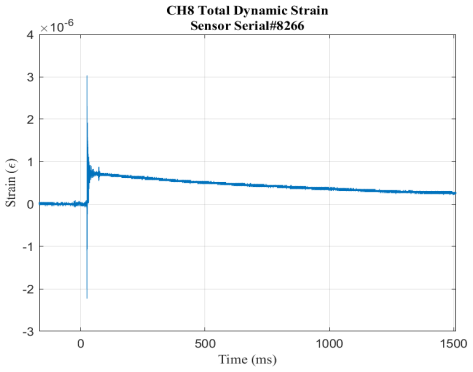

f.

Figure A.52 Strain response, concrete (30 lb), test date: 27 Aug 19

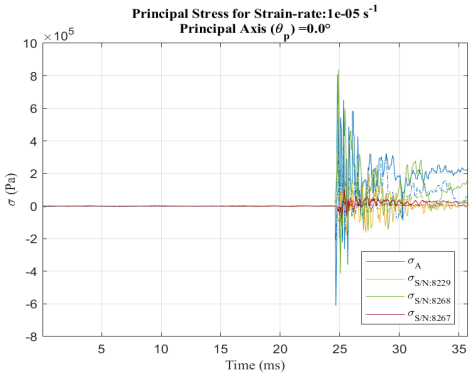

a.

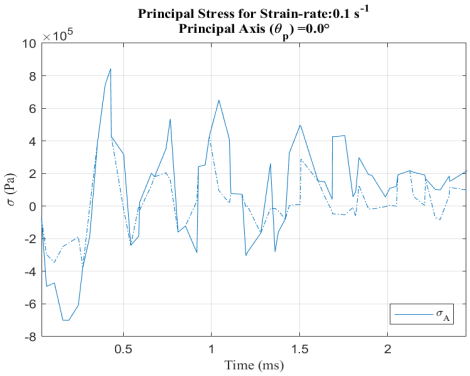

b.

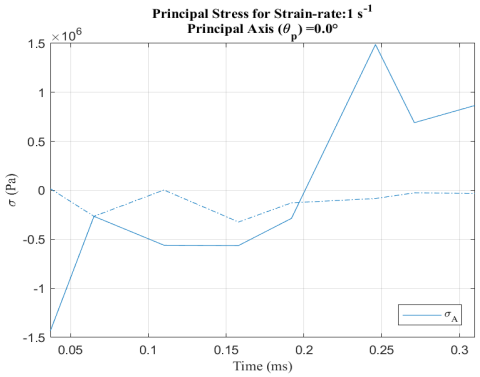

c.

Figure A.53 Principal stress at strain rate, concrete (30 lb), test date: 27 Aug 19

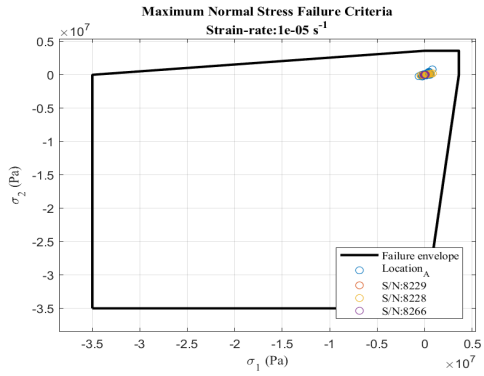

a.

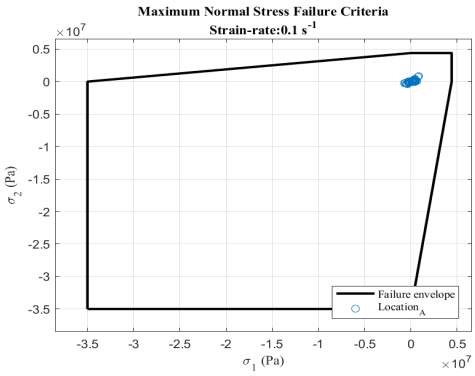

b.

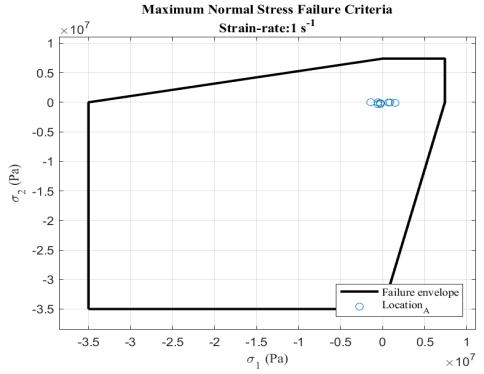

c.

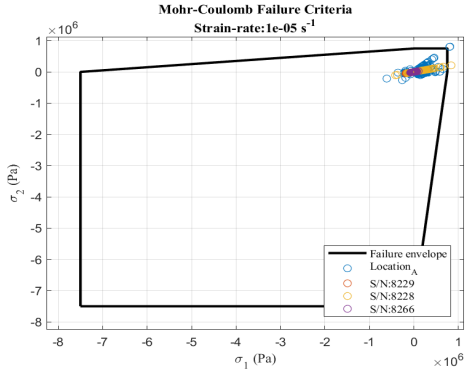

d.

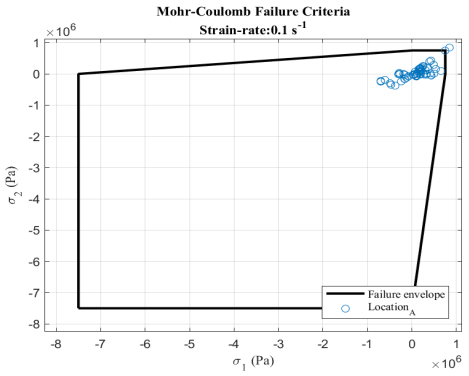

e

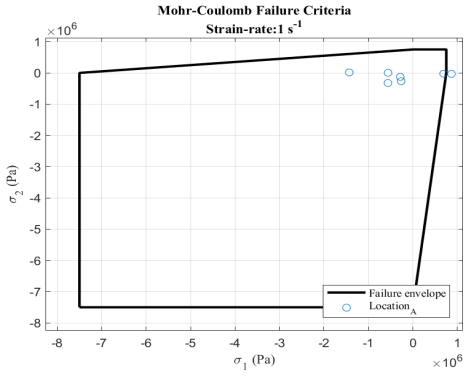

f

Figure A.54 Failure criterion envelopes, concrete (30 lb), test date; 27 Aug 19

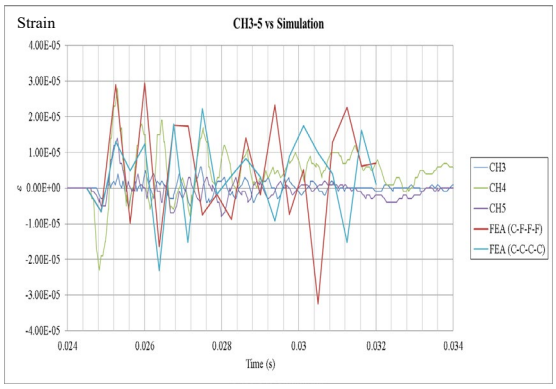

a.

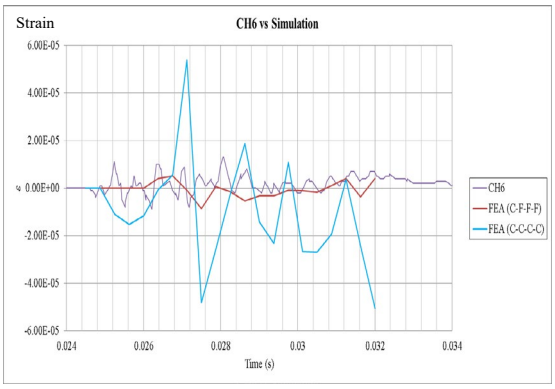

b.

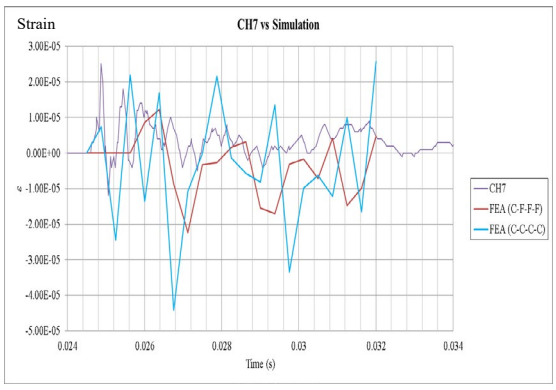

c.

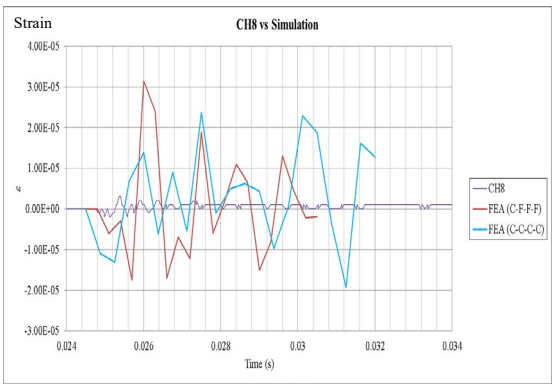

d.

Figure A.55 Strain response and FEA comparison, concrete (30 lb), test date: 27 Aug

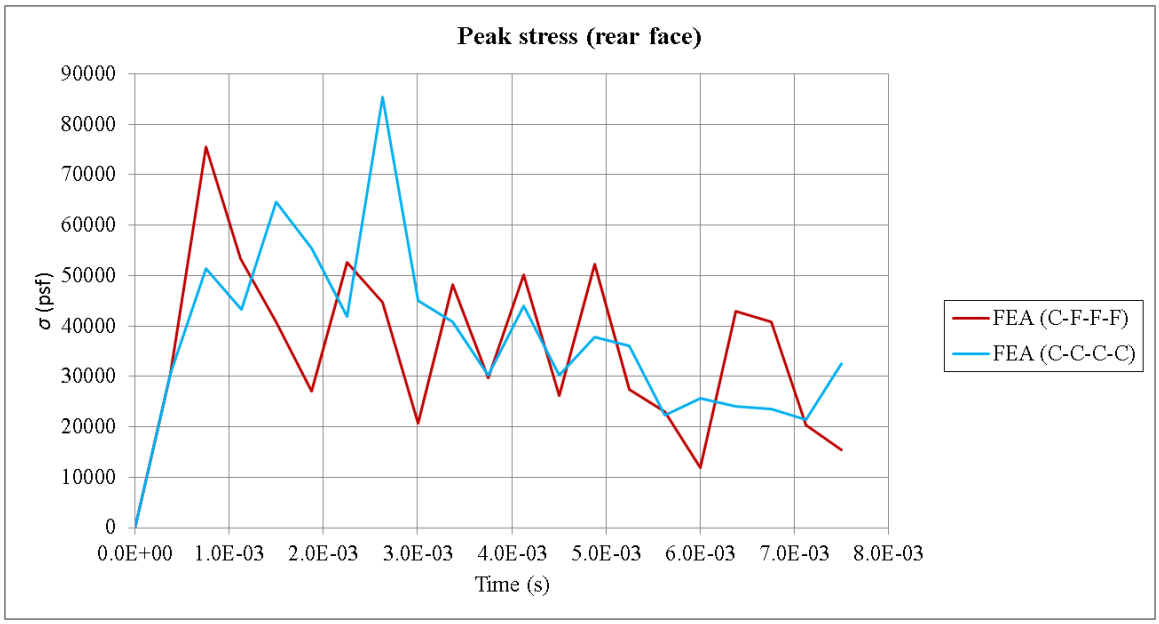

Figure A.56 FEA peak rear face stress, concrete (30 lb), test date: 27 Aug 19

J, Steel penetrator (10 lb), 27 August 2019

Figure A.57 Steel penetrator (10 lb)

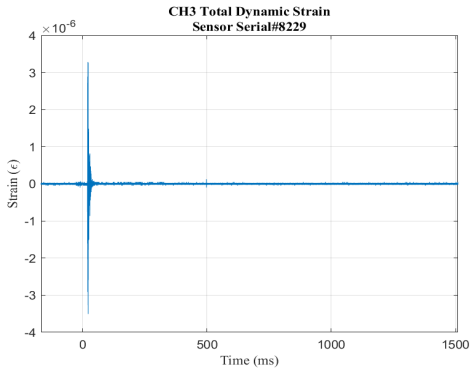

a.

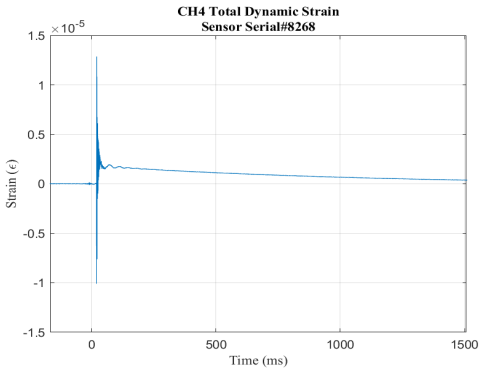

b.

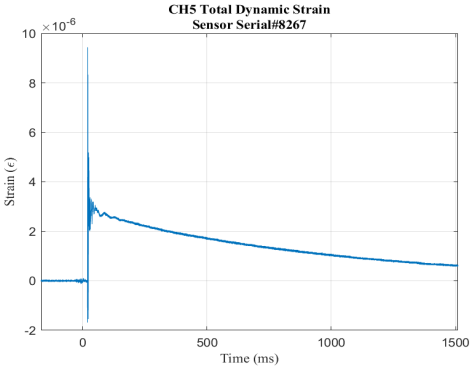

c.

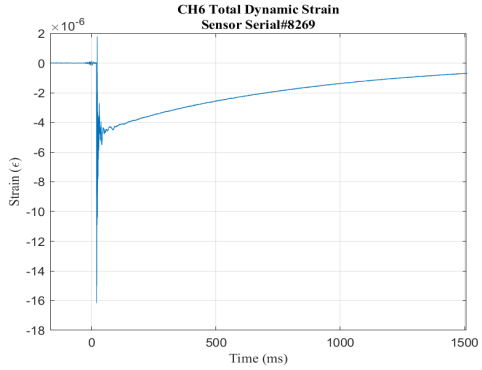

d.

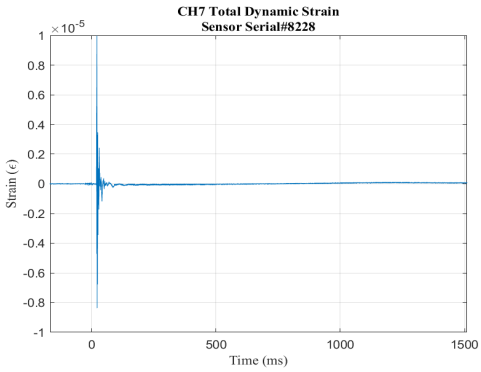

e.

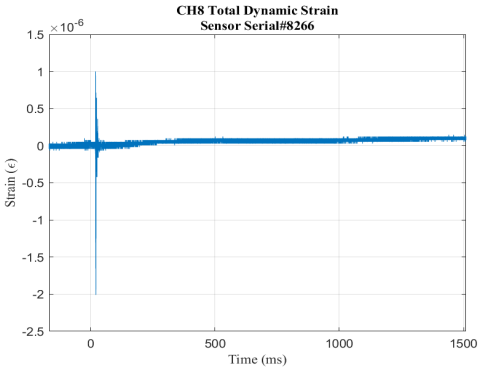

f.

Figure A.58 Strain response, steel penetrator (10 lb), test date: 27 Aug 19

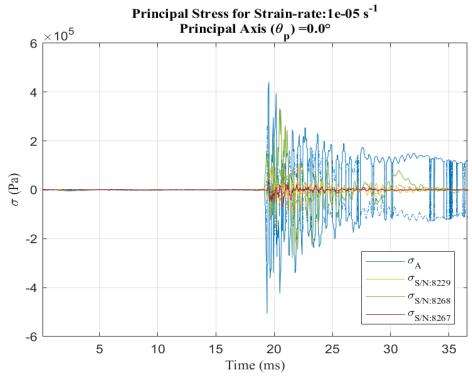

a.

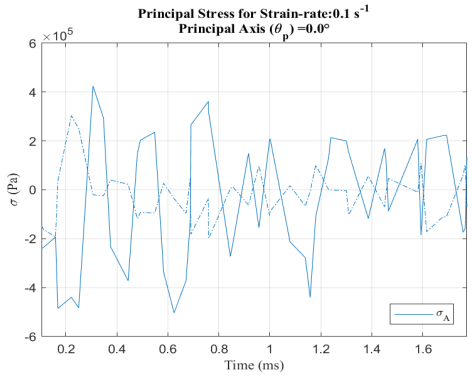

b.

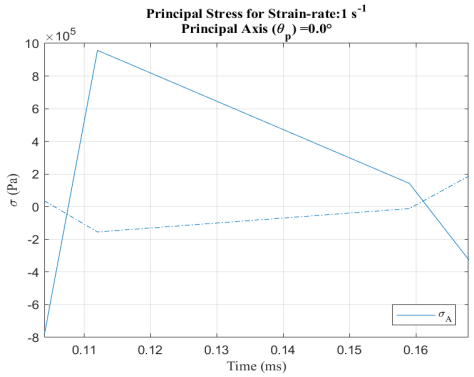

c.

Figure A.59 Principal stress at strain rate, steel penetrator (10 lb), test date: 27 Aug 19

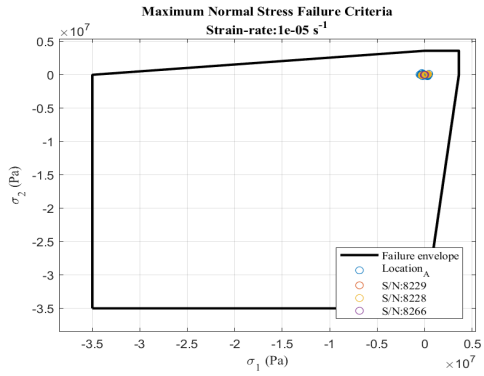

a.

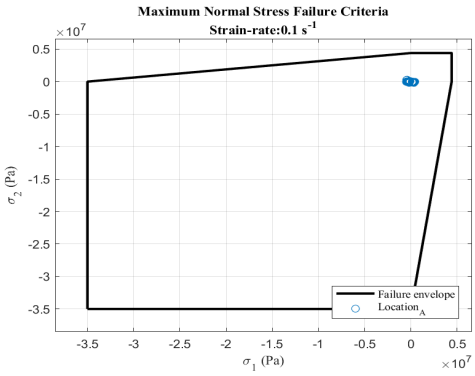

b.

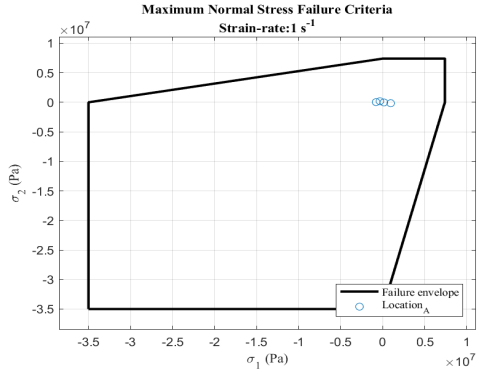

c.

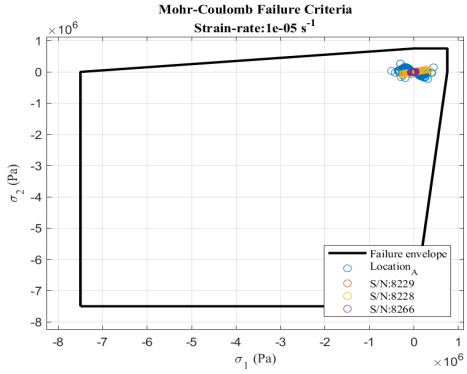

d.

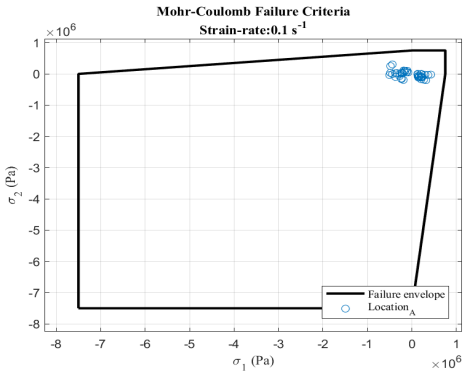

e.

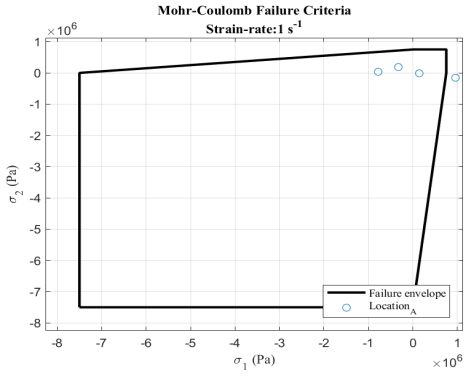

f.

Figure A.60 Failure criterion envelopes, steel penetrator (10 lb), test date: 27 Aug 19

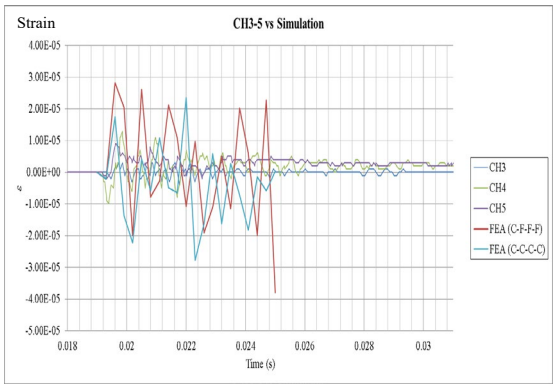

a.

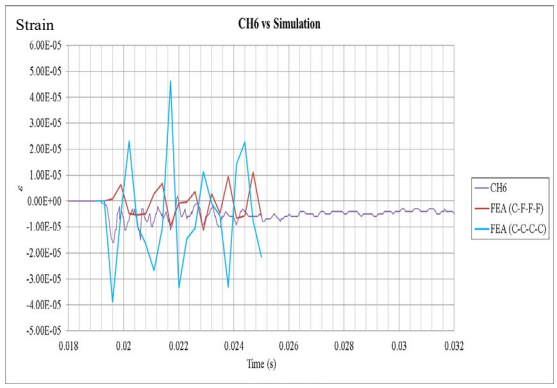

b.

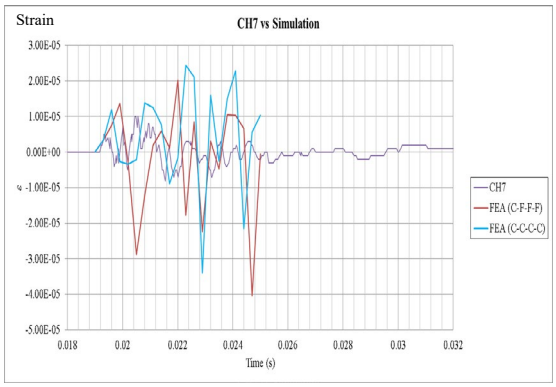

c.

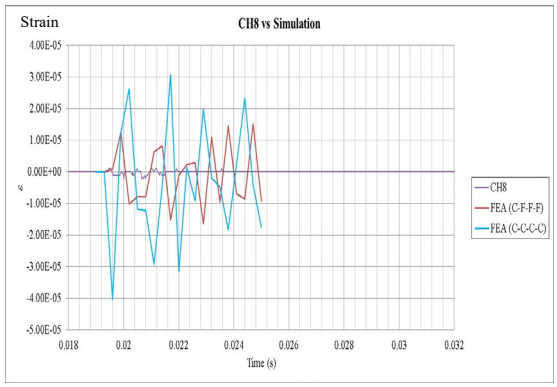

d.

Figure A.61 Strain response and FEA comparison, steel penetrator (10 lb), test date: 27 Aug 19

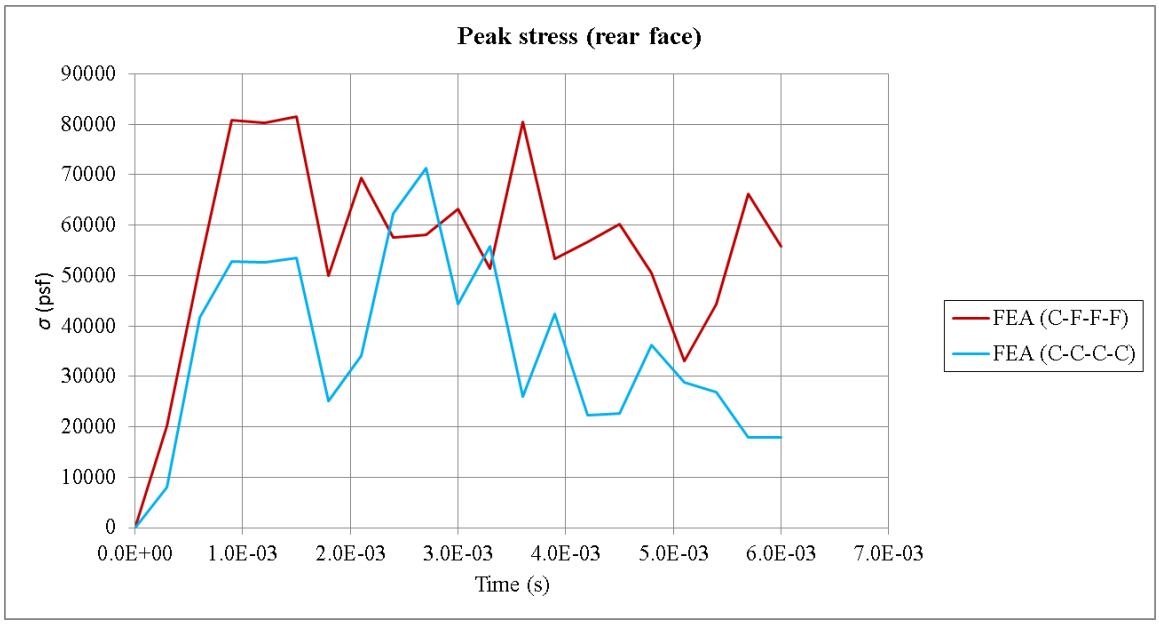

Figure A.62 FEA peak rear face stress, steel penetrator (10 lb), test date: 27 Aug 19

K, Steel rail (25 lb), 6 September 2019

Figure A.63 Steel rail (25 lb)

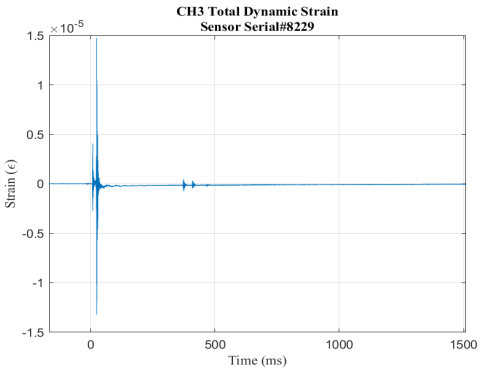

a.

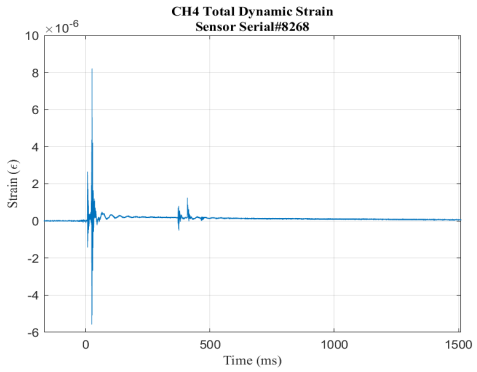

b.

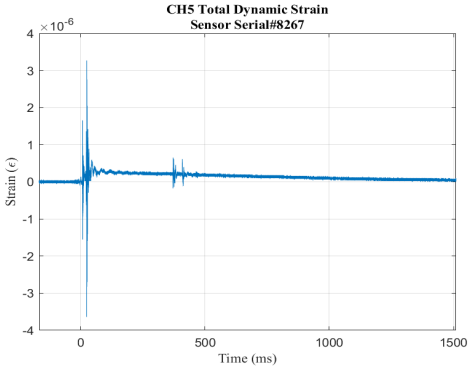

c.

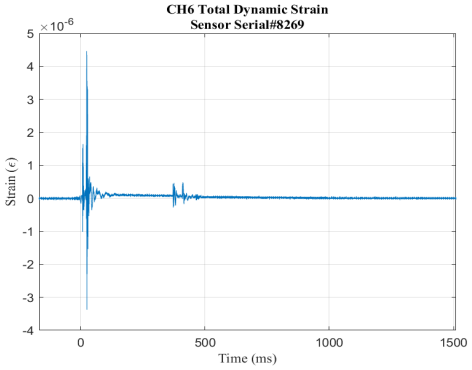

d.

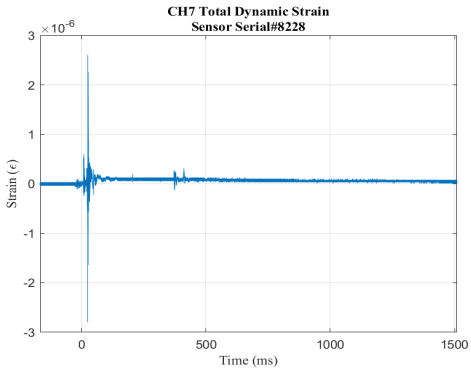

e.

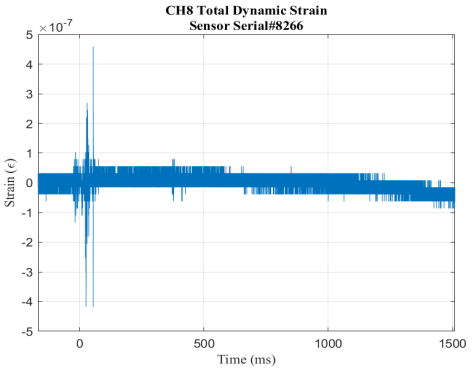

f.

Figure A.64 Strain response, steel rail (25 lb), test date: 6 Sep 19

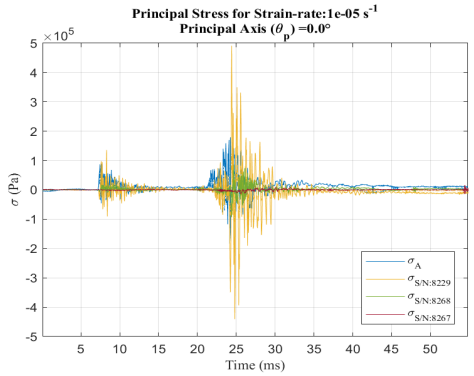

a.

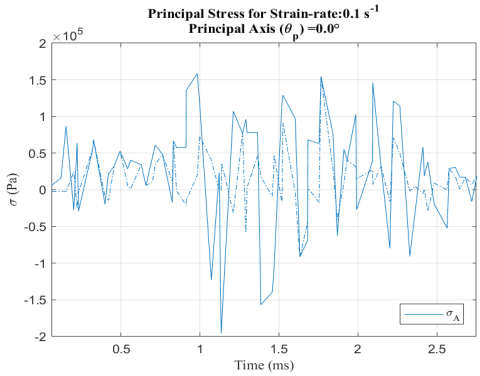

b.

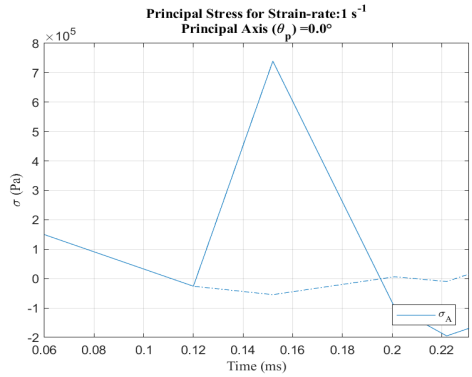

c.

Figure A.65 Principal stress at strain-rate, steel rail (25 lb), test date: 6 Sep 19

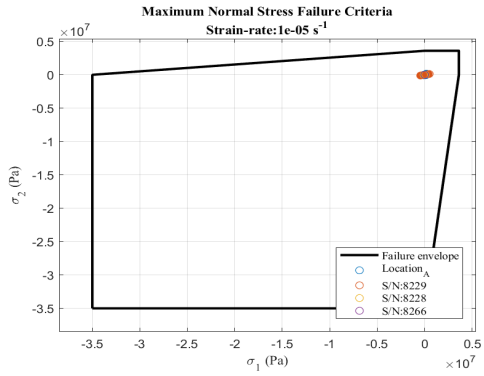

a.

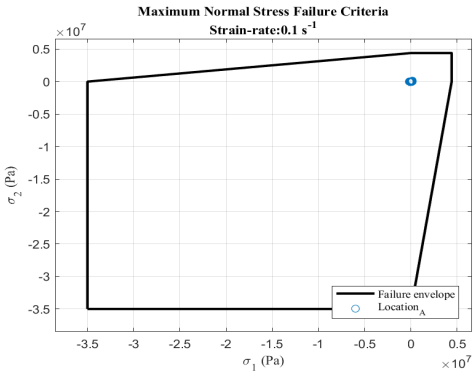

b.

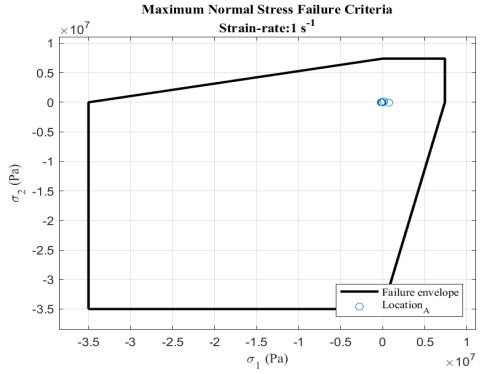

c.

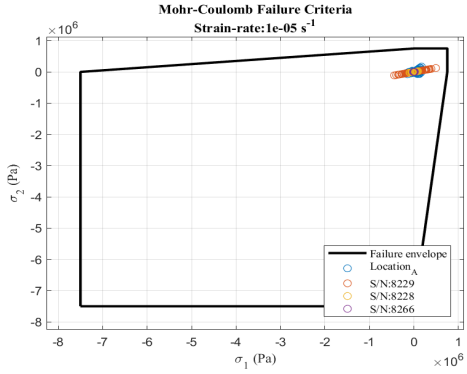

d.

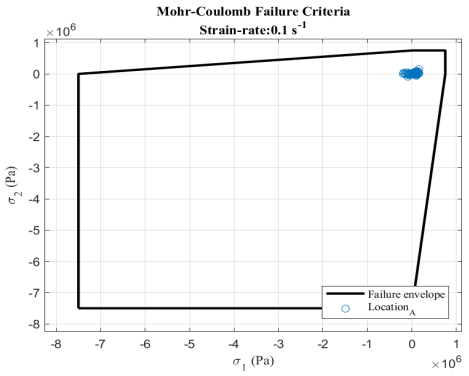

e.

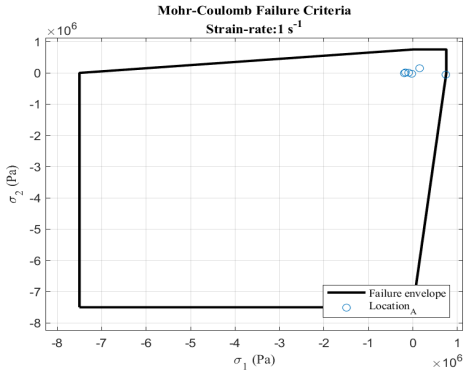

f.

Figure A.66 Failure criterion envelopes, steel rail (25 lb), test date: 6 Sep 19

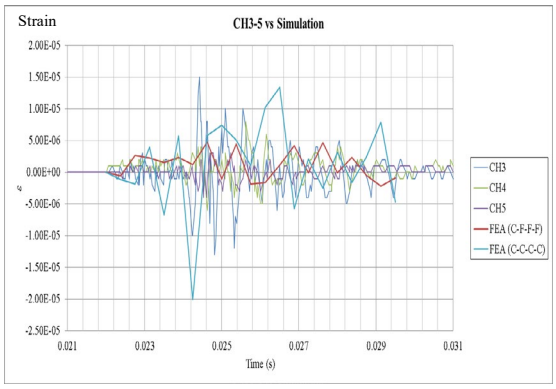

a.

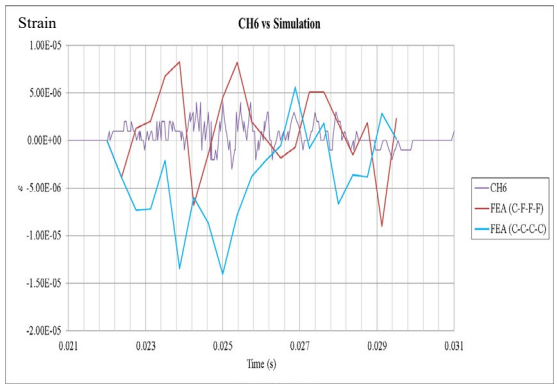

b.

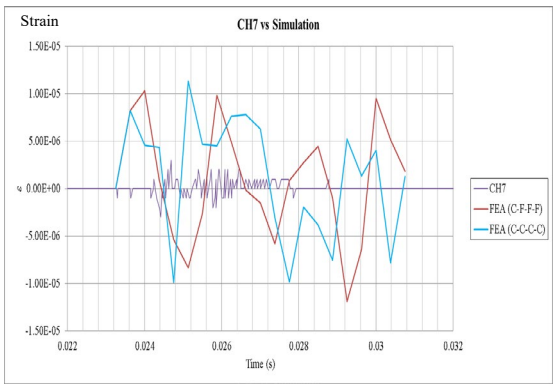

c.

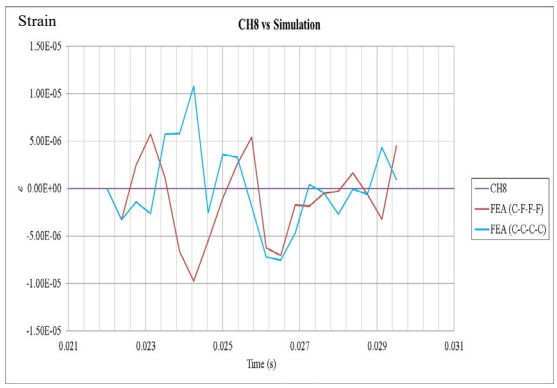

d.

Figure A.67 Strain response and FEA comparison, steel rail (25 lb), test date: 6 Sep 19

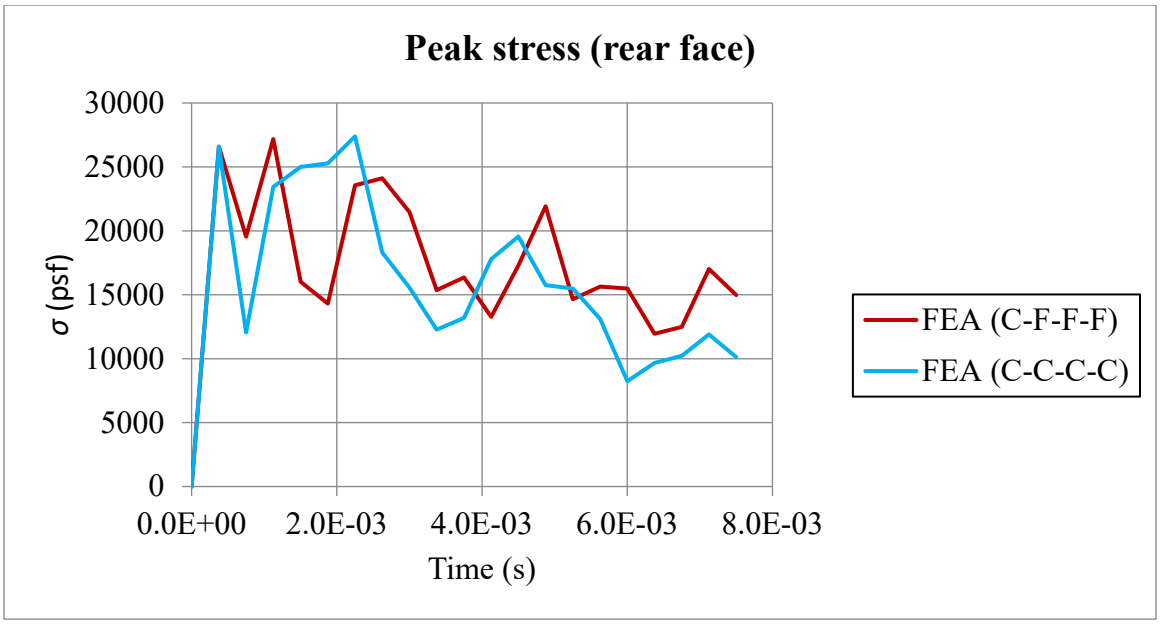

Figure A.68 FEA peak rear face stress, steel rail (25 lb), test date: 6 Sep 19

L, Steel penetrator (20 lb), 6 September 2019

Figure A.69 Steel penetrator (20 lb), test date: 6 Sep 19

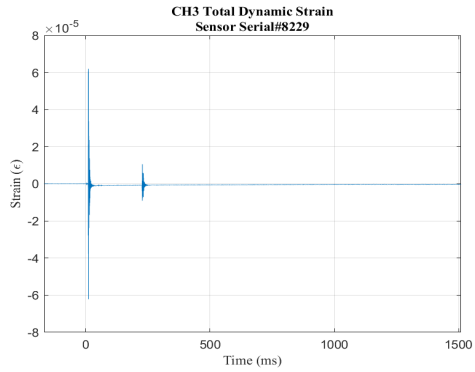

a.

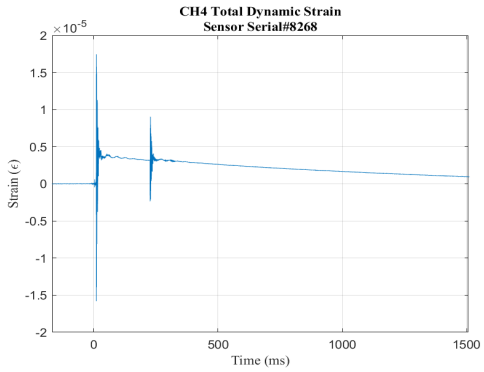

b.

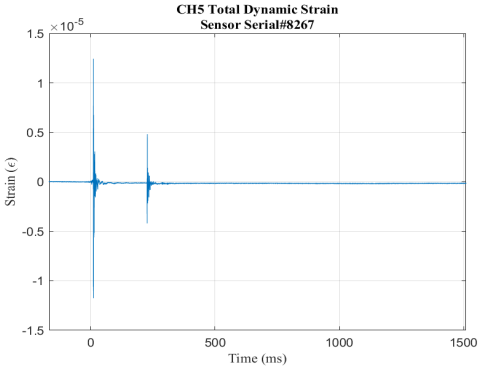

c.

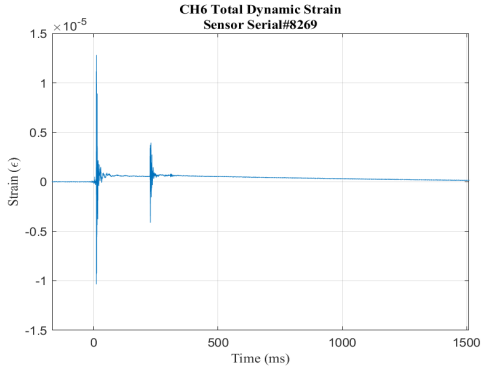

d.

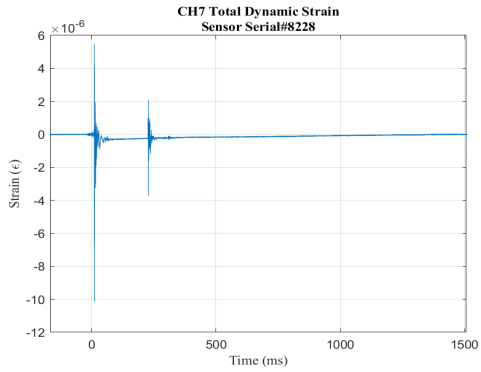

e.

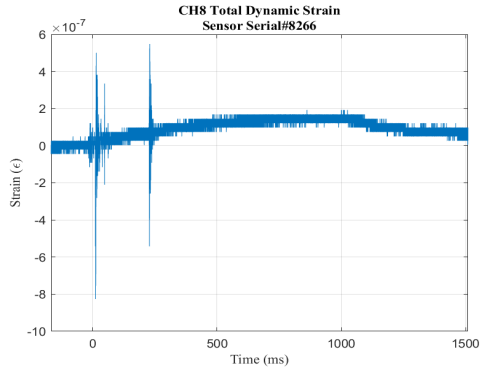

f.

Figure A.70 Strain response, steel penetrator (20 lb), test date: 6 Sep 19

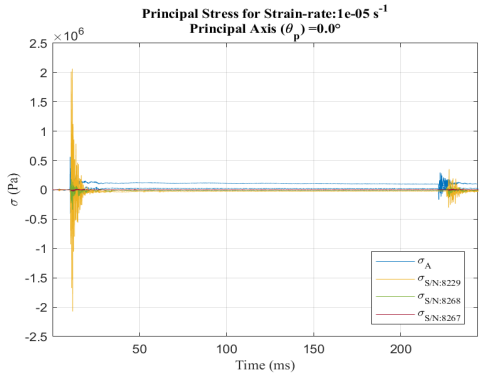

a.

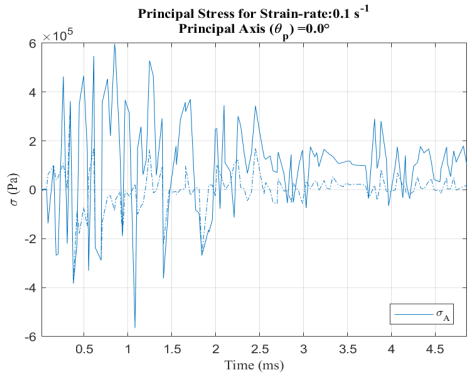

b.

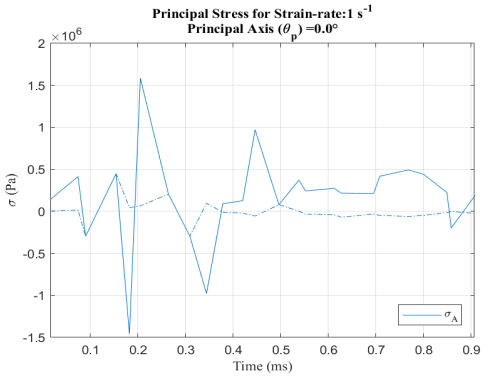

c.

Figure A.71 Principal stress at strain rate, steel penetrator (20 lb), test date: 6 Sep 19

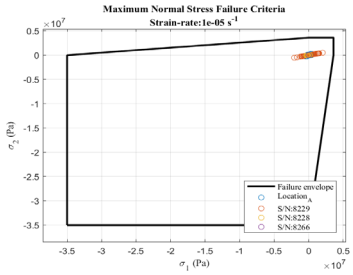

a

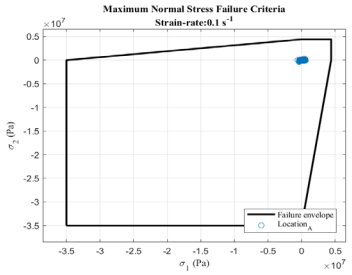

b

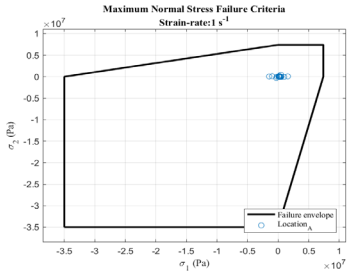

c

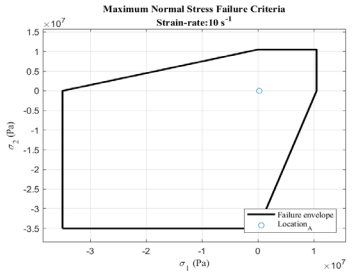

d

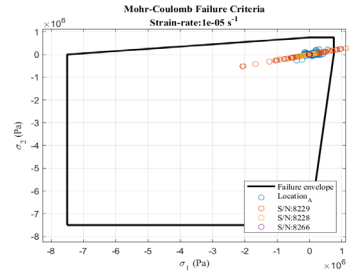

e

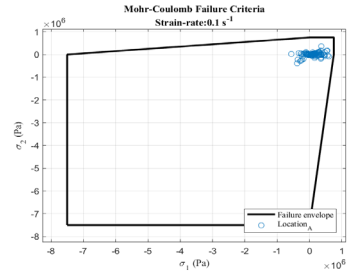

f

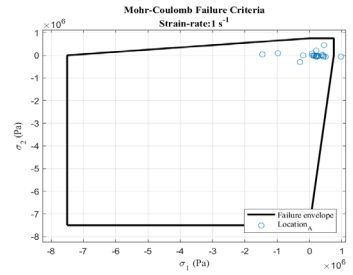

g.

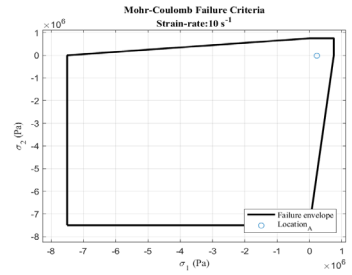

h.

Figure STYLEREF \s "Heading 1" A. SEQ Figure * ARABIC \s 1 72 Failure criterion envelopes, steel penetrator (20 lb), test date: 6 Sep 19

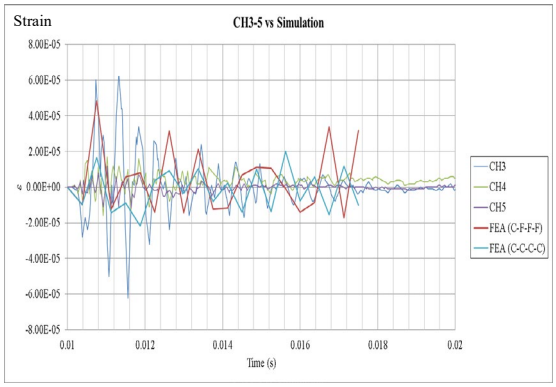

a.

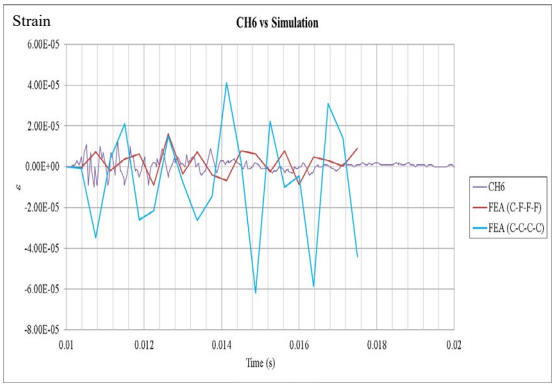

b.

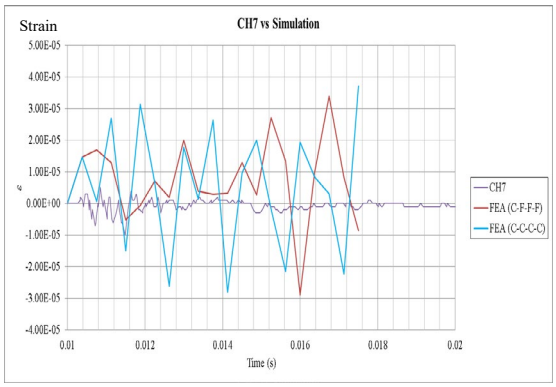

c.

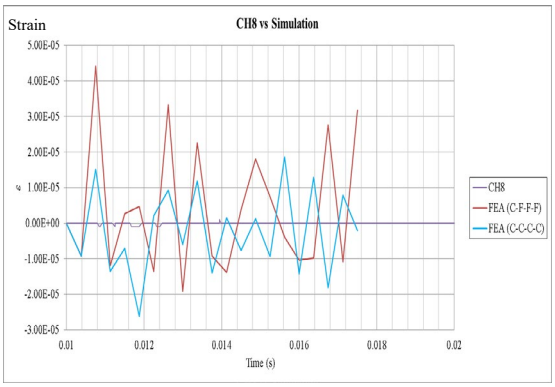

d.

Figure A.73 Strain response and FEA comparison, steel penetrator (20 lb), test date: 6 Sep 19

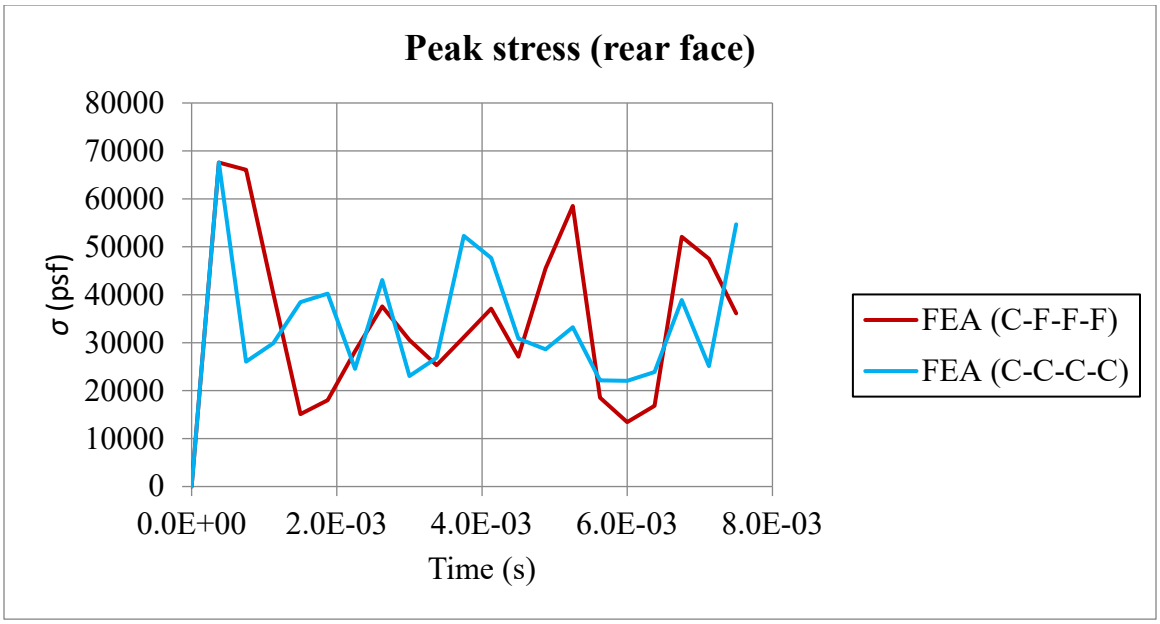

Figure A.74 FEA peak rear face stress, steel penetrator (20 lb), test date: 6 Sep 19

M, Steel penetrator (30 lb), 6 September 2019

Figure A.75 Steel penetrator (30 lb), test date: 6 Sep 19

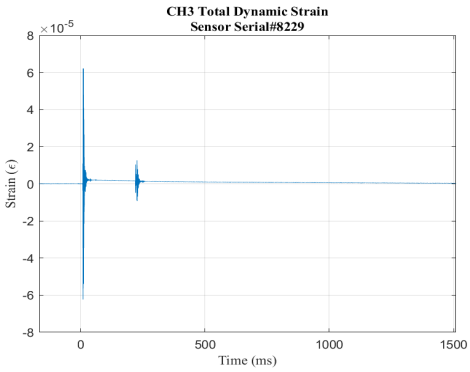

a.

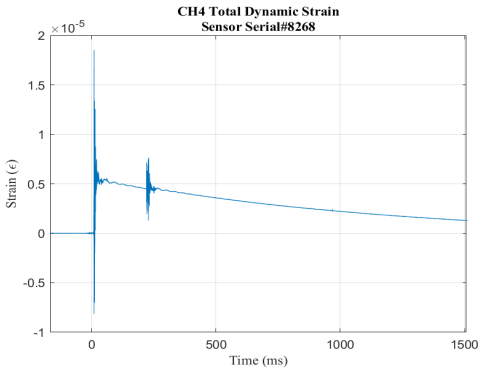

b.

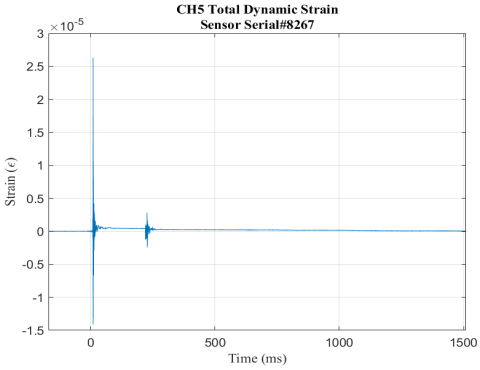

c.

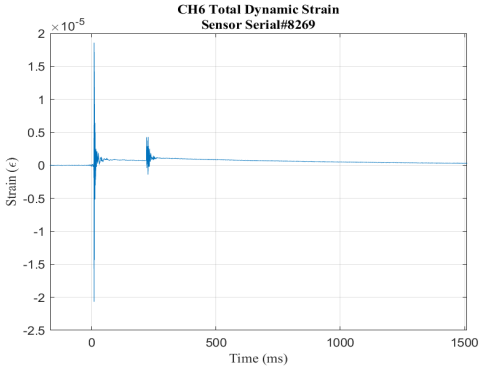

d.

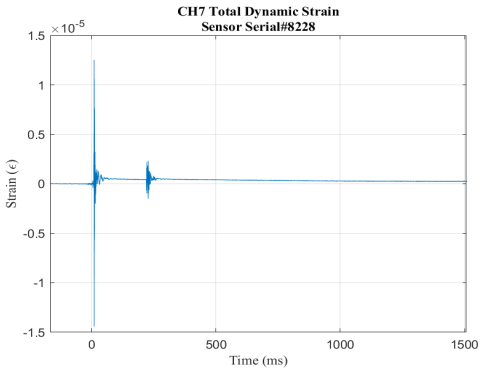

e.

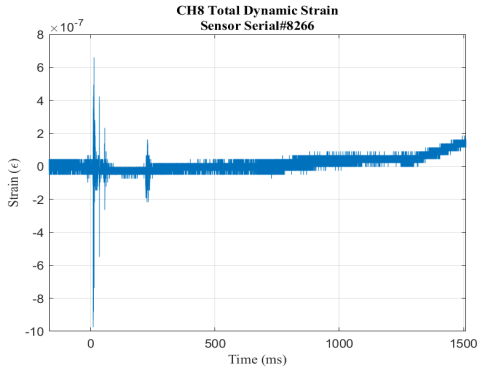

f.

Figure A.76 Strain response, steel penetrator (30 lb), test date: 6 Sep 19

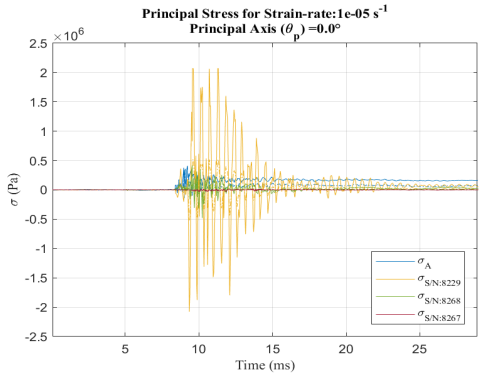

a.

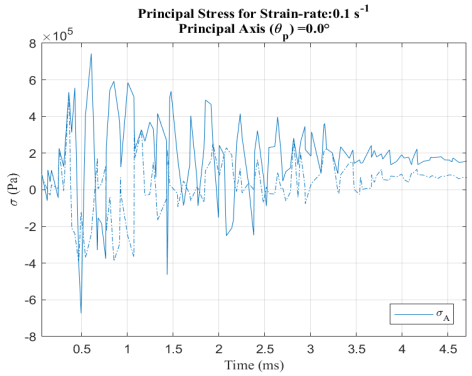

b.

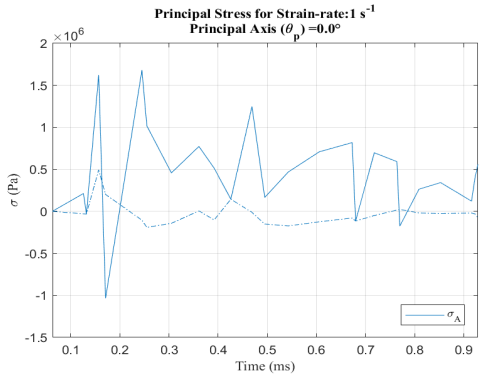

c.

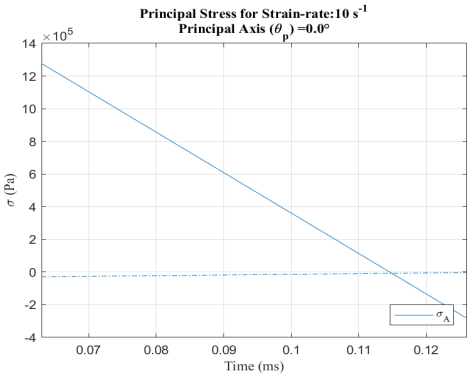

d.

Figure A.77 Principal stress at strain rate, steel penetrator (30 lb), test date: 6 Sep 19

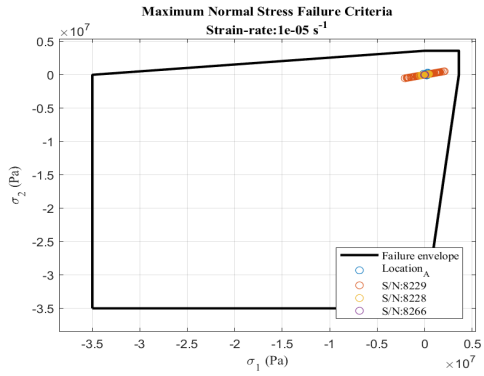

a.

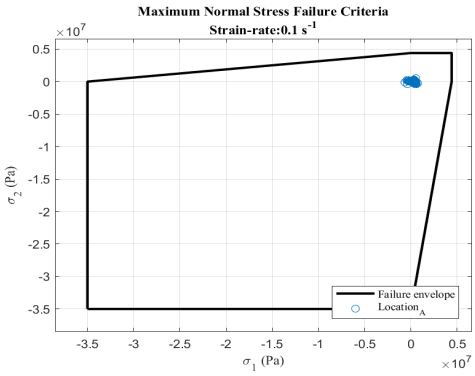

b.

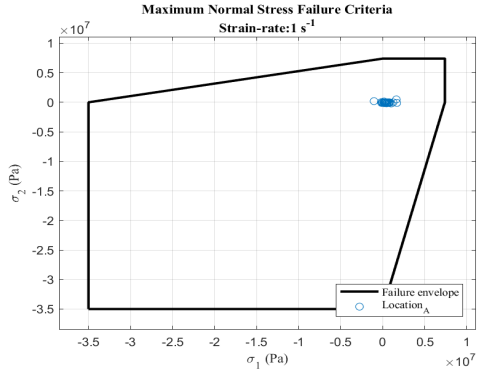

c.

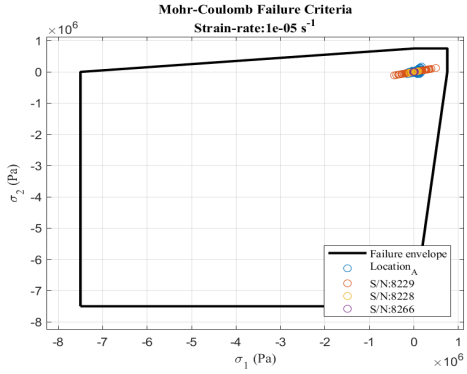

d.

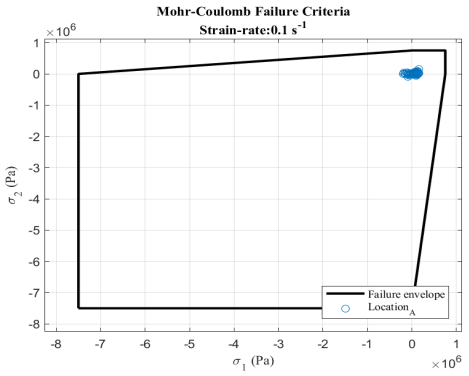

e.

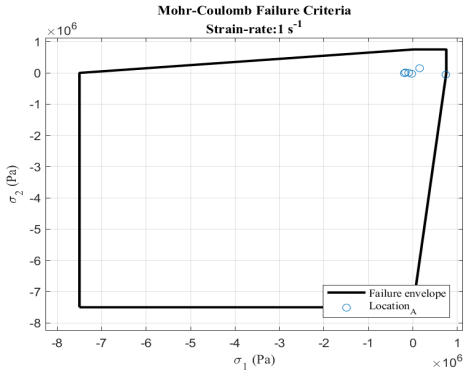

f.

Figure A.78 Failure criterion envelopes, steel penetrator (30 lb), test date: 6 Sep 19

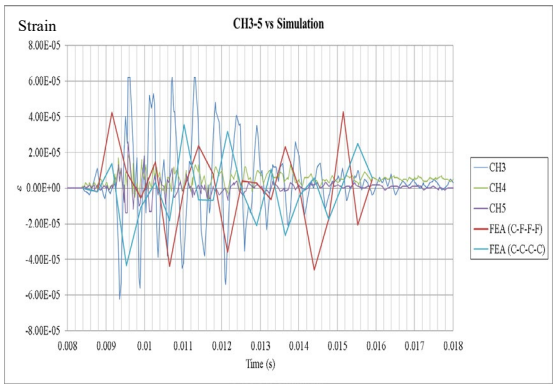

a.

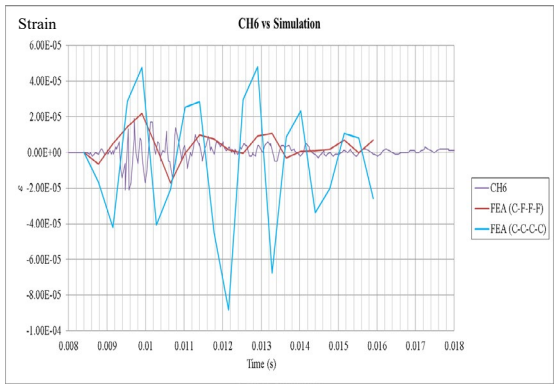

b.

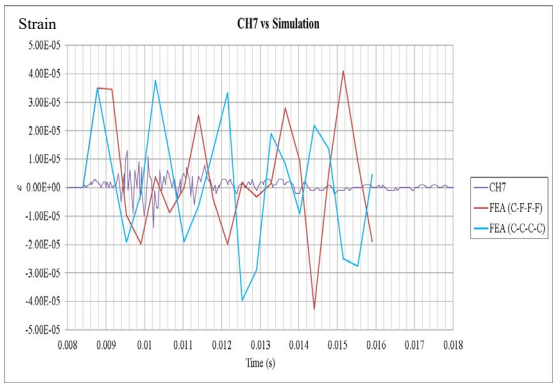

c.

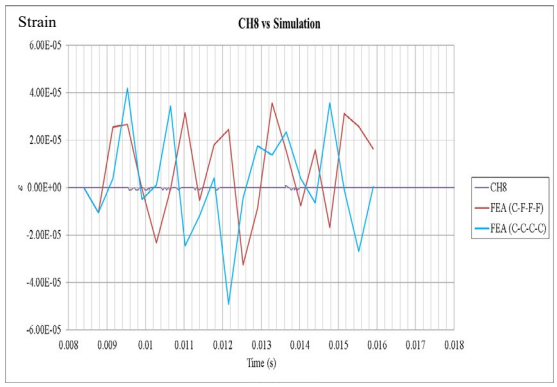

d.

Figure A.79 Strain response and FEA comparison, steel penetrator (30 lb), test date: 6 Sep 19

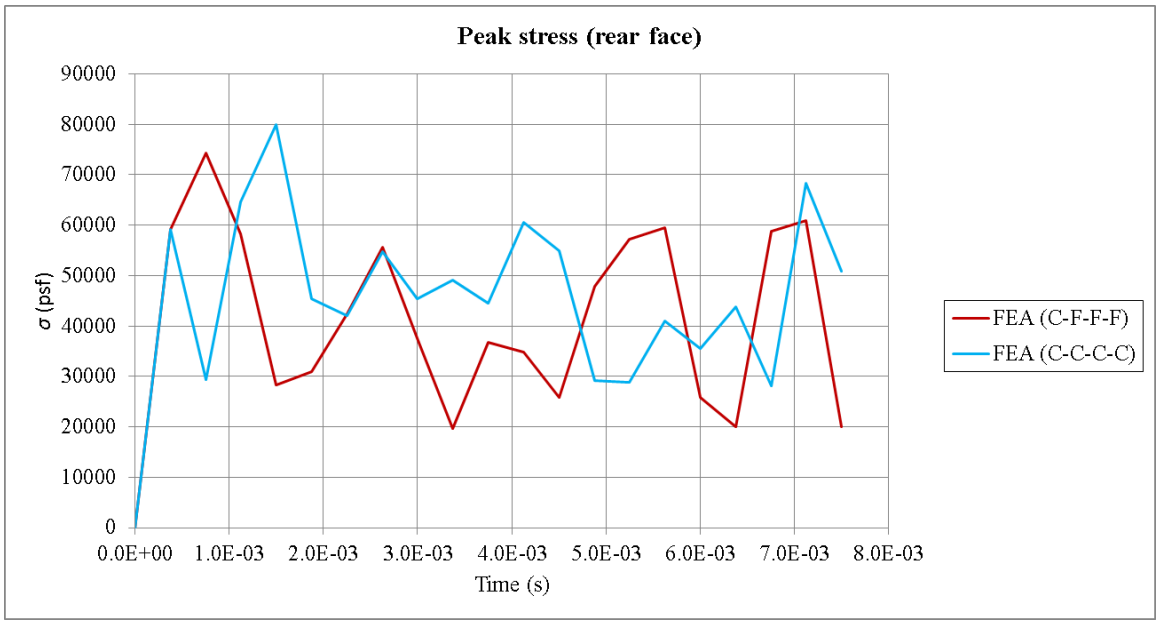

Figure A.80 FEA peak rear face stress, steel penetrator (30 lb), test date: 6 Sep 19

N, Steel rail (35 lb), 19 September 2019

Figure A.81 Steel rail (35 lb)

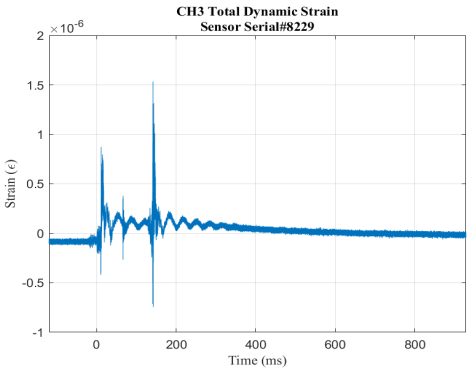

a.

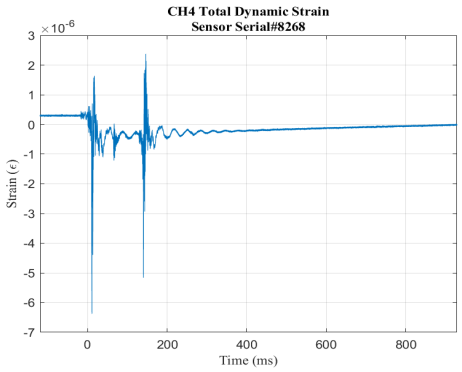

b.

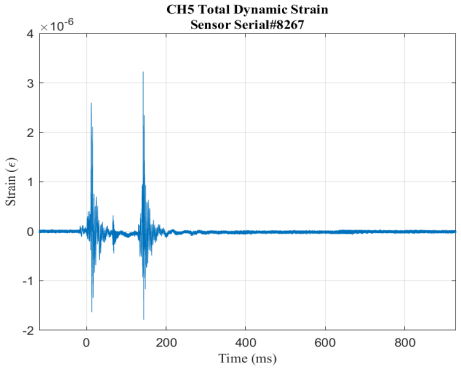

c.

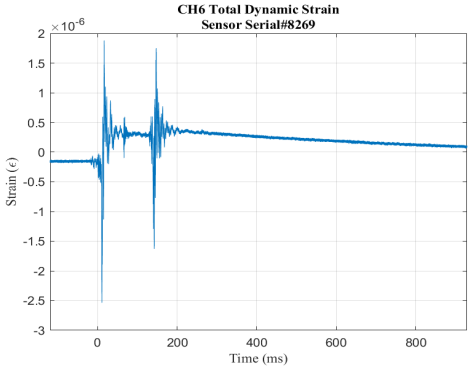

d.

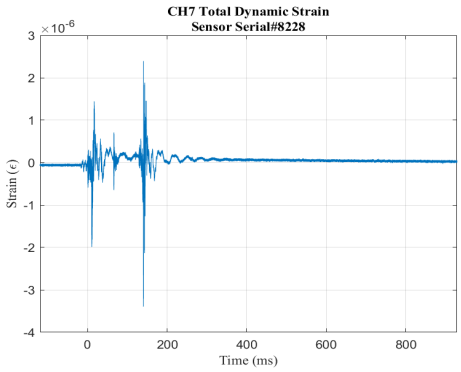

e.

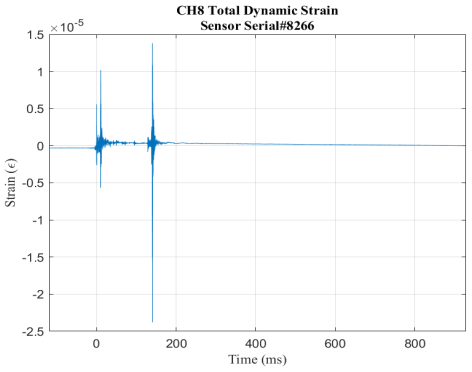

f.

Figure A.82 Strain response, steel rail (35 lb), test date: 19 Sep 19

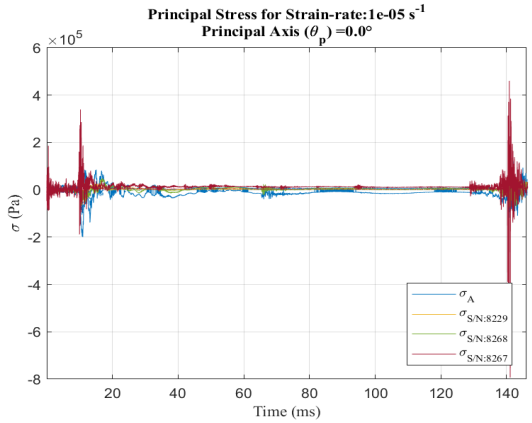

a.

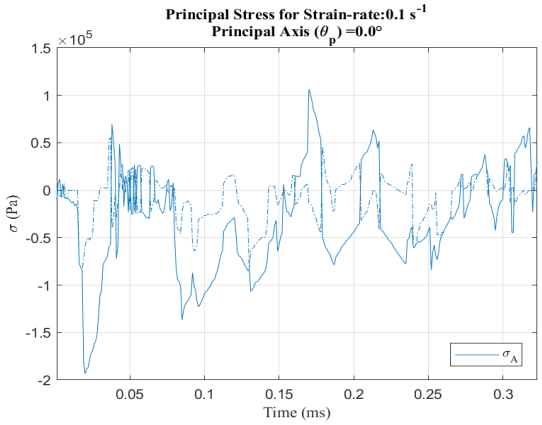

b.

Figure A.83 Principal stress at strain rate, steel rail (35 lb), test date: 19 Sep 19

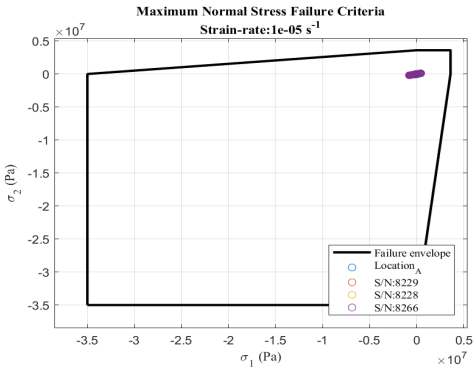

a.

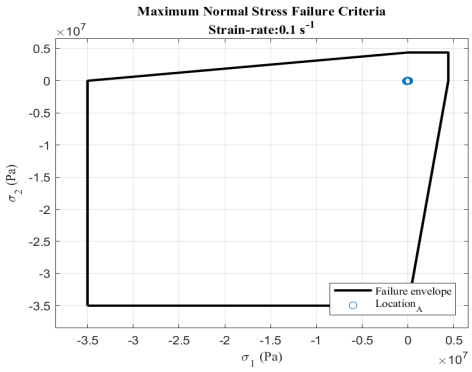

b.

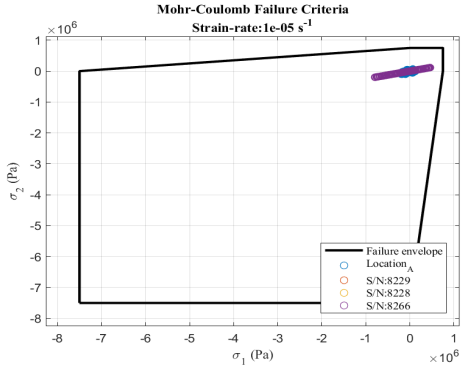

c.

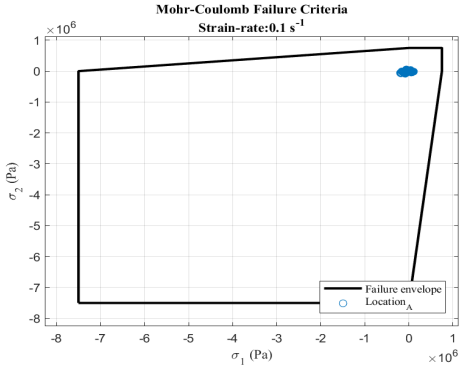

d.

Figure A.84 Failure criterion envelopes, steel rail (35 lb), test date: 19 Sep 19

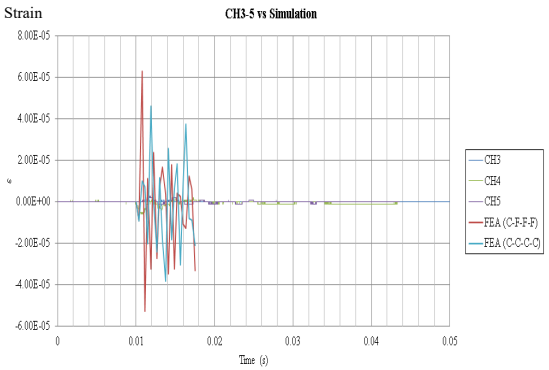

a.

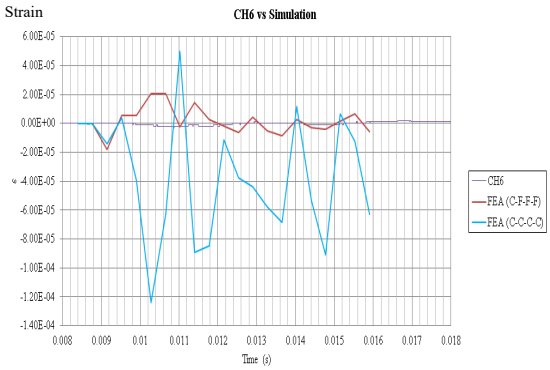

b.

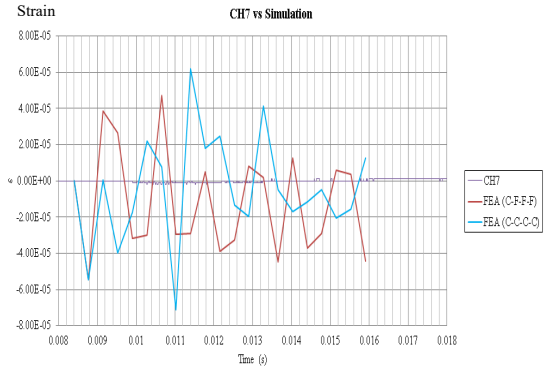

c.

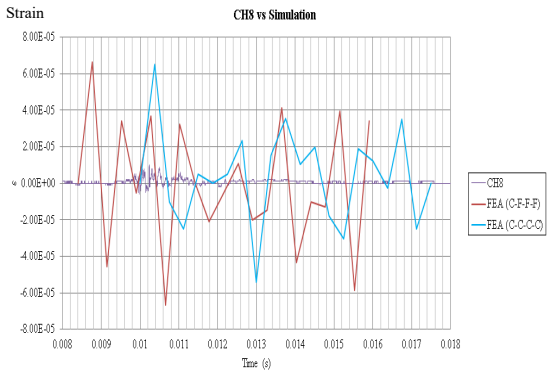

d.

Figure A.85 Strain response and FEA comparison, steel rail (35 lb), test date: 19 Sep 19

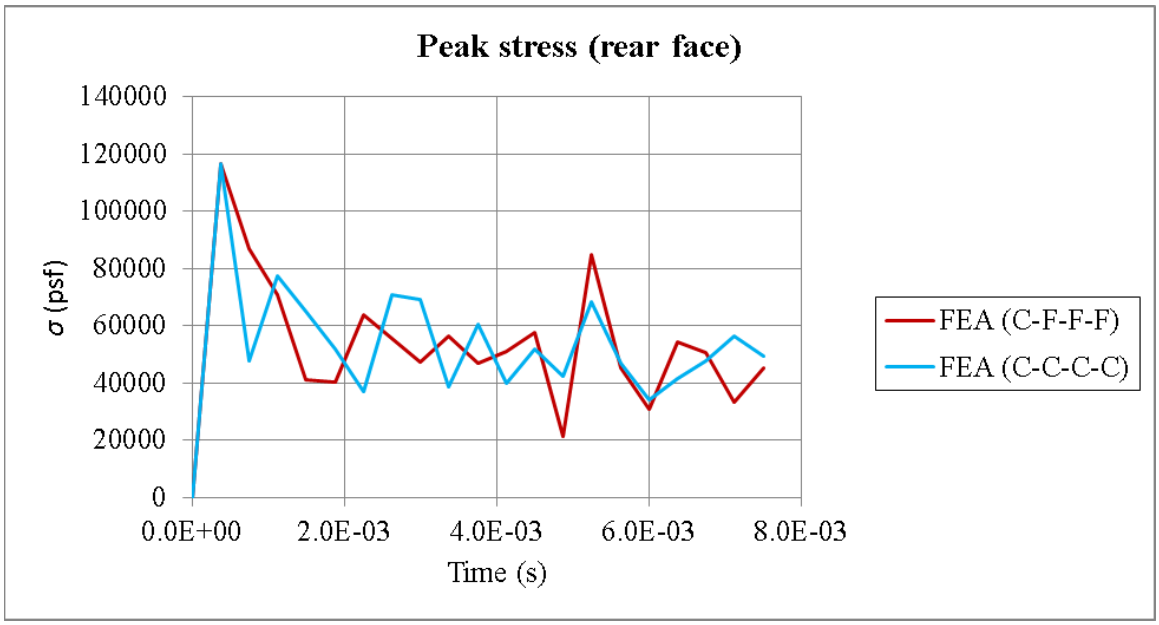

Figure A.86 FEA peak rear face stress, steel rail (35 lb), test date: 19 Sep 19

O, Steel penetrator (20 lb), 19 September 2019

Figure A.87 Steel penetrator (20 lb), test date: 19 Sep 19

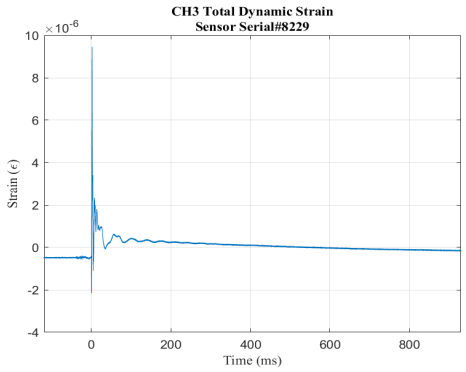

a.

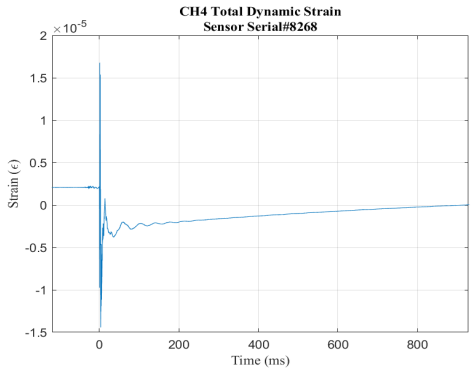

b.

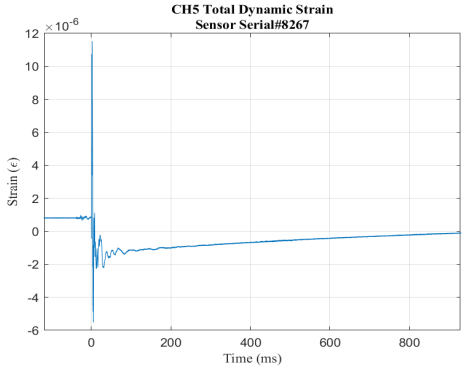

c.

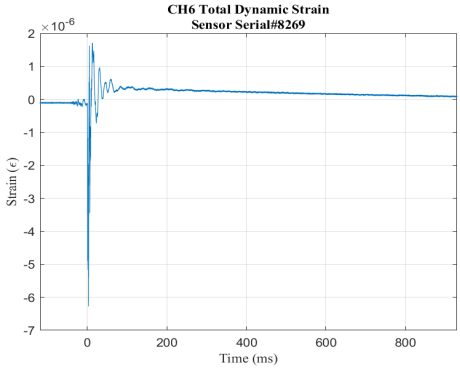

d.

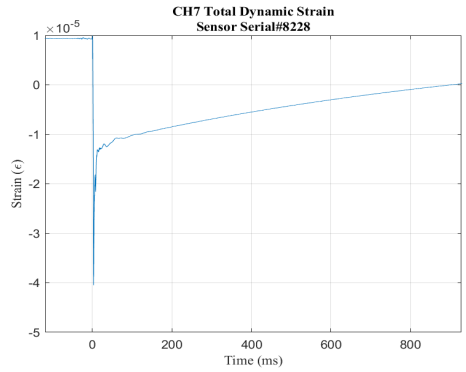

e.

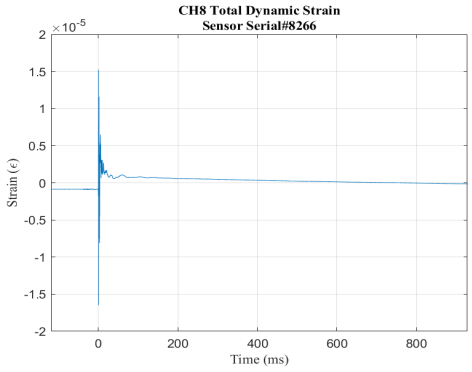

f.

Figure A.88 Strain response, steel penetrator (20 lb), test date: 19 Sep 19

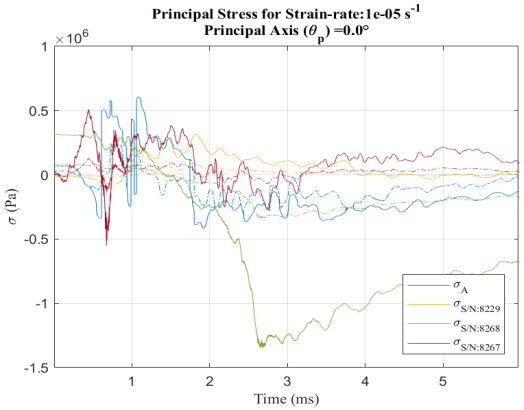

a.

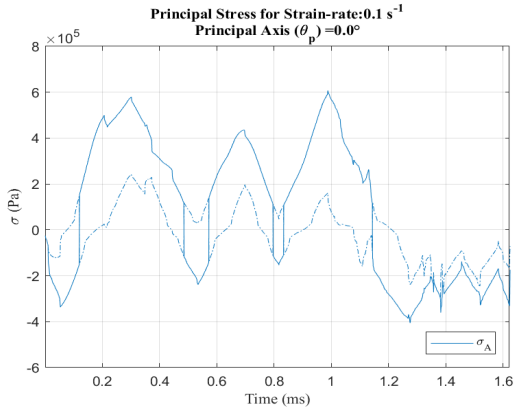

b.

Figure A.89 Principal stress at strain rate, steel penetrator (20 lb), test date: 19 Sep 19

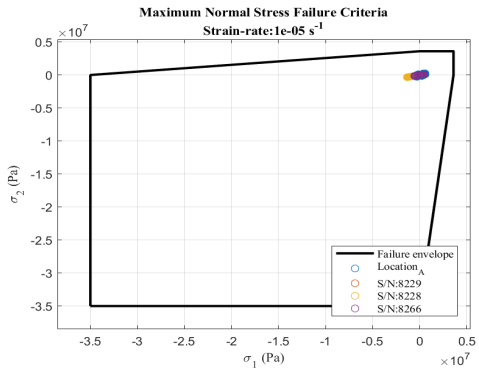

a.

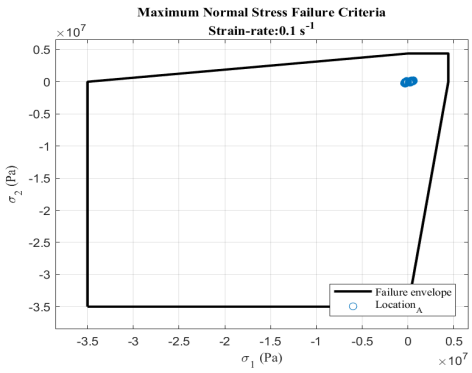

b.

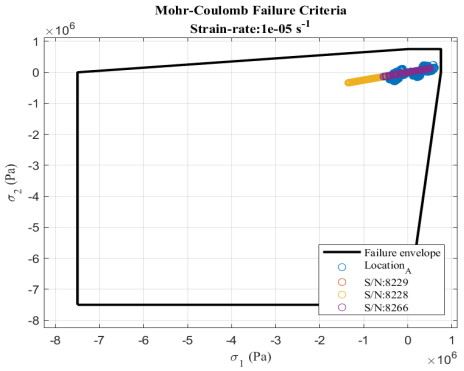

c.

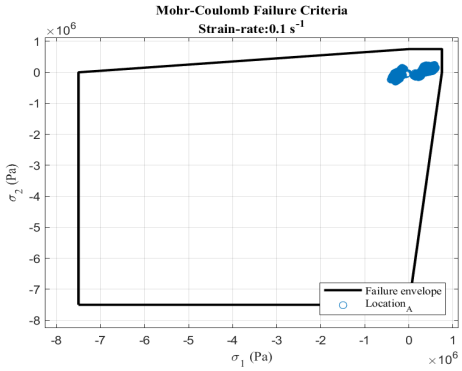

d.

Figure A.90 Failure criterion envelopes, steel penetrator (20 lb), test date: 19 Sep 19

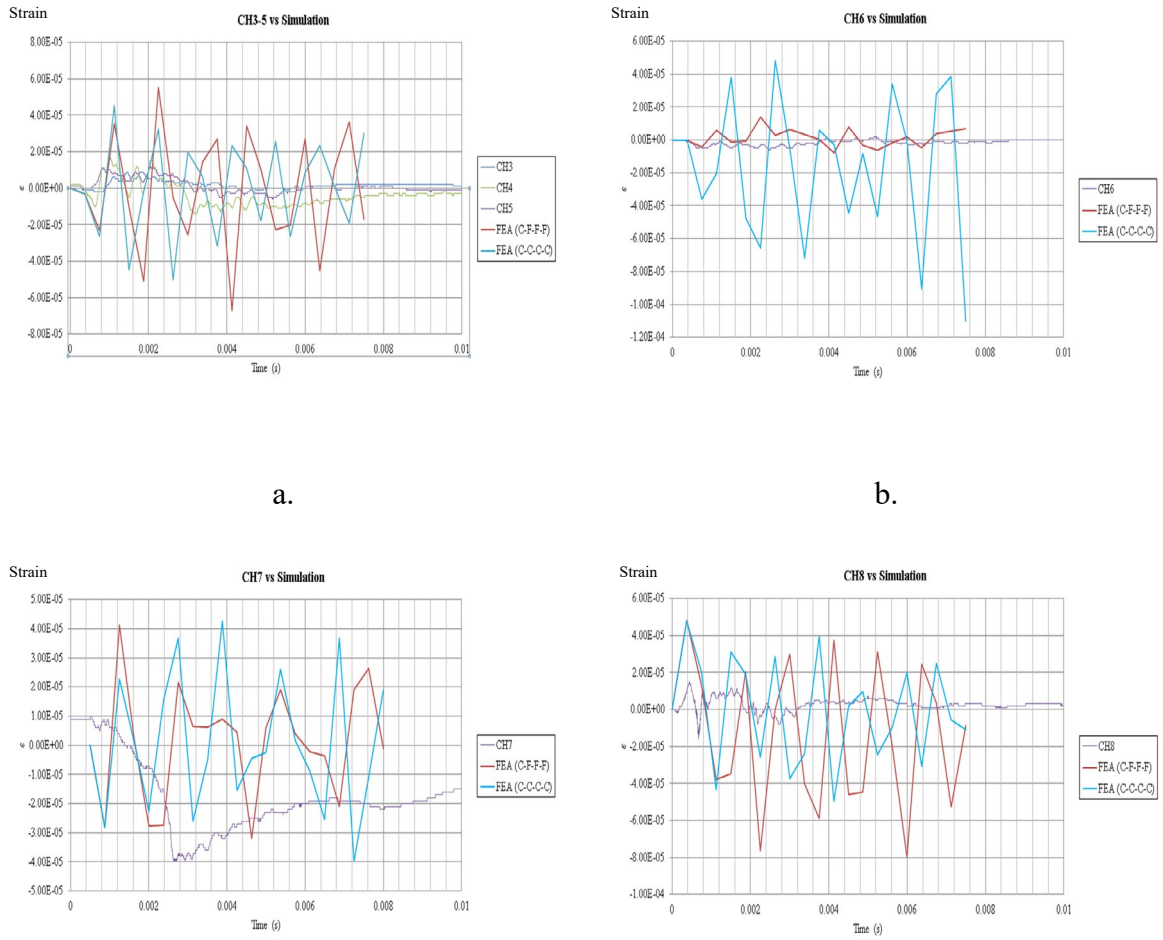

Figure A.91 Strain response and FEA comparison, steel penetrator (20 lb), test date: 19 Sep 19

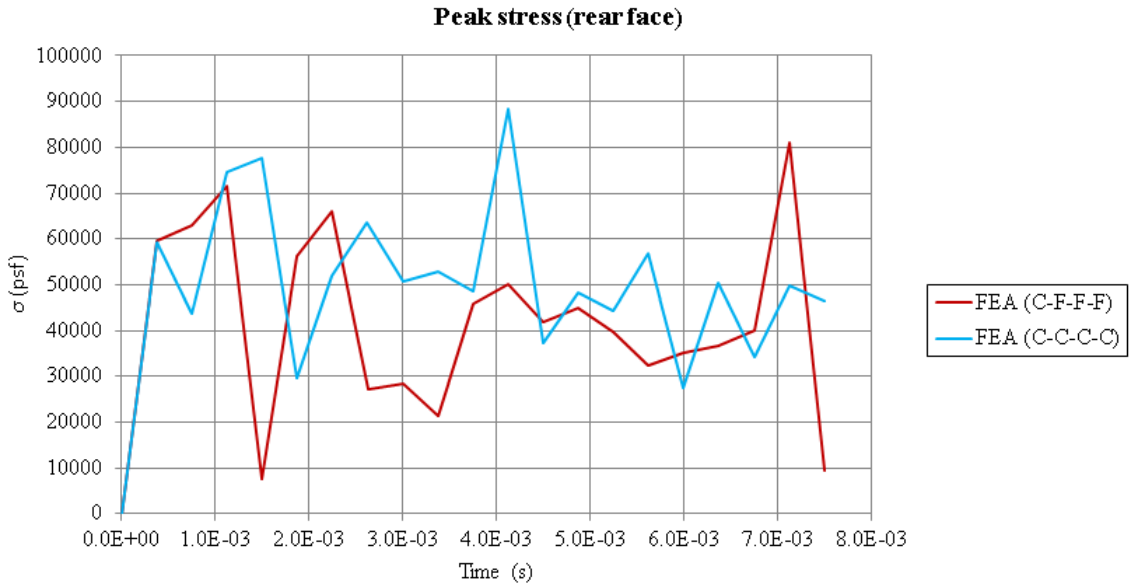

Figure A.92 FEA peak rear face stress, steel penetrator (20 lb), test date: 19 Sep 19

P, Steel penetrator (30 lb), 19 September 2019

Figure A.93 Steel penetrator (30 lb), test date: 19 Sep 19

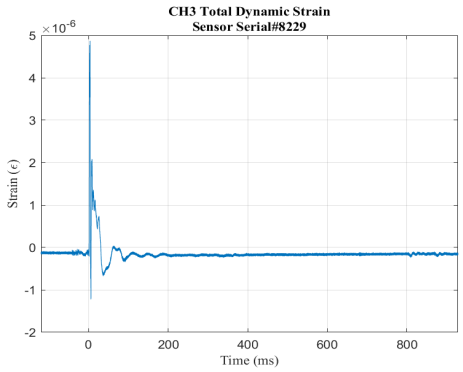

a.

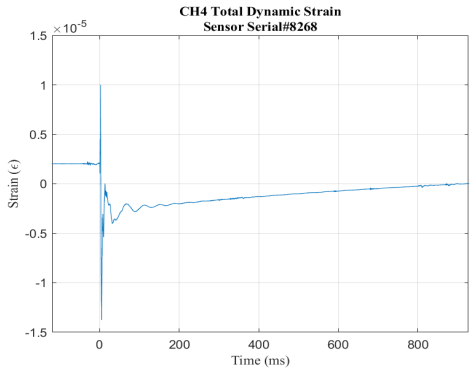

b.

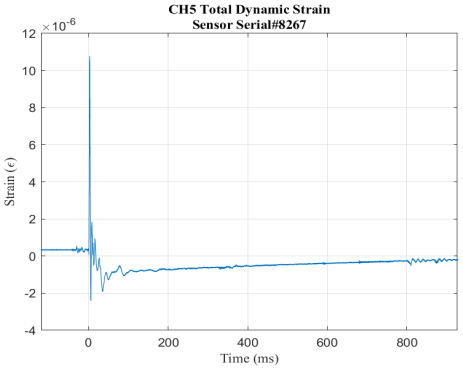

c.

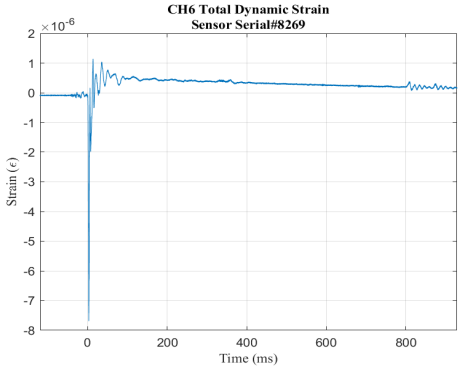

d.

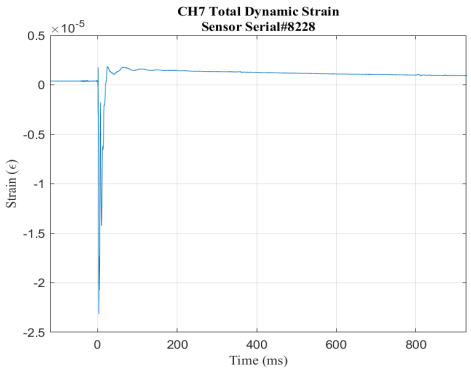

e.

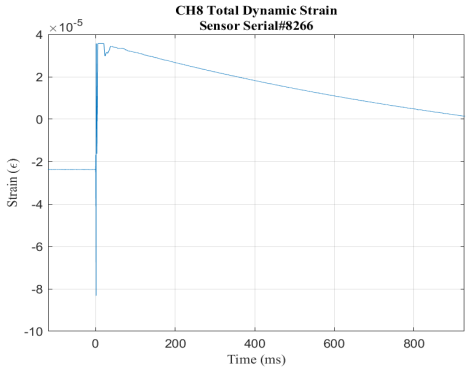

f.

Figure A.94 Strain response, steel penetrator (30 lb), test date: 19 Sep 19

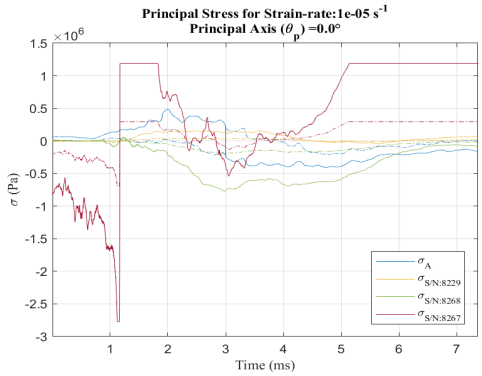

a.

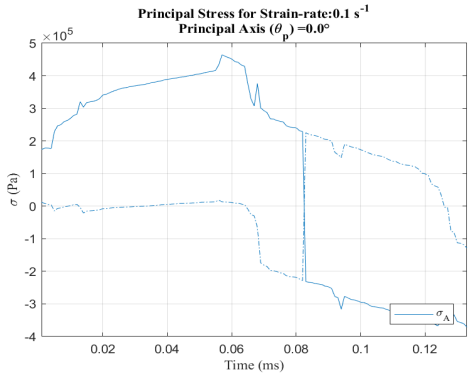

b.

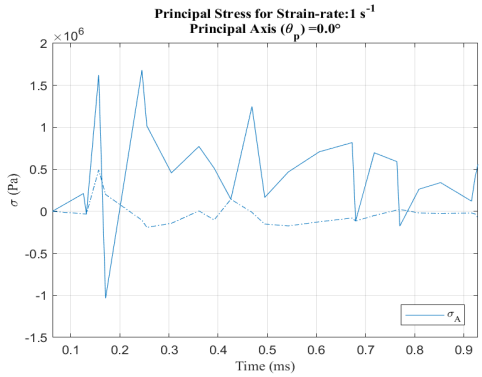

c.

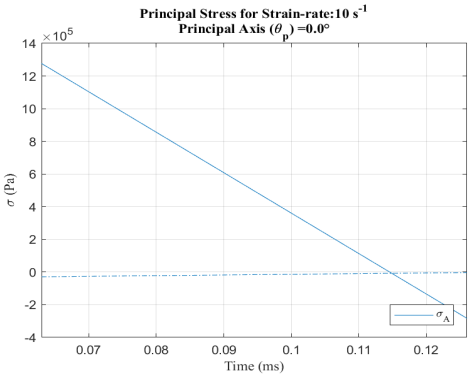

d.

Figure A.95 Principal stress at strain rate, steel penetrator (30 lb), test date: 19 Sep 19

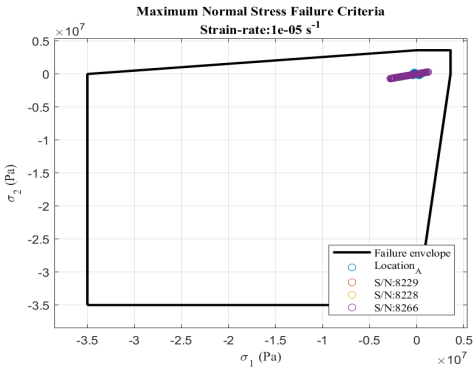

a.

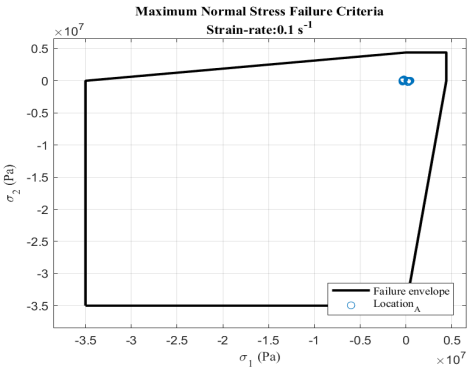

b.

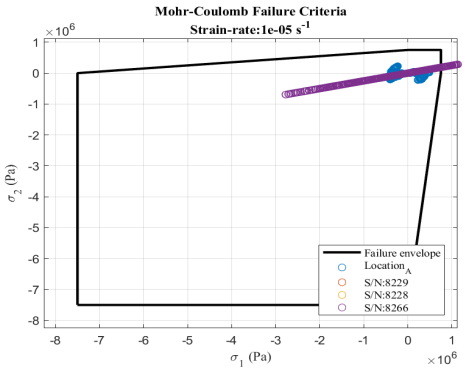

c.

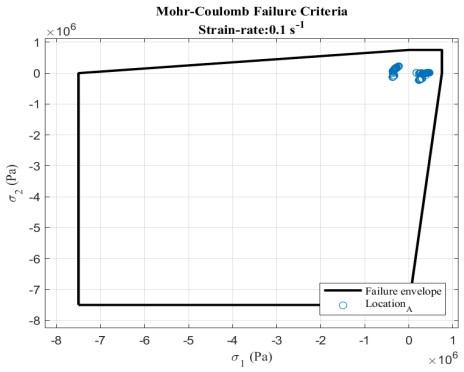

d.

Figure A.96 Failure criterion envelopes, steel penetrator (30 lb), test date: 19 Sep 19

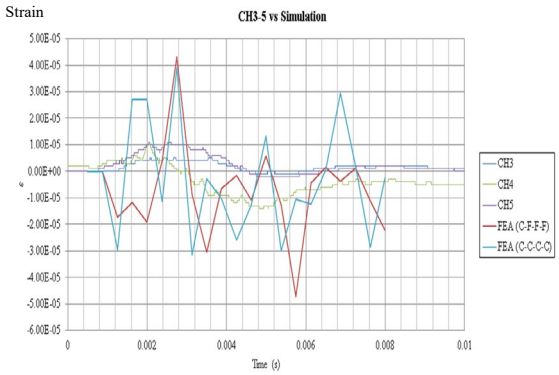

a.

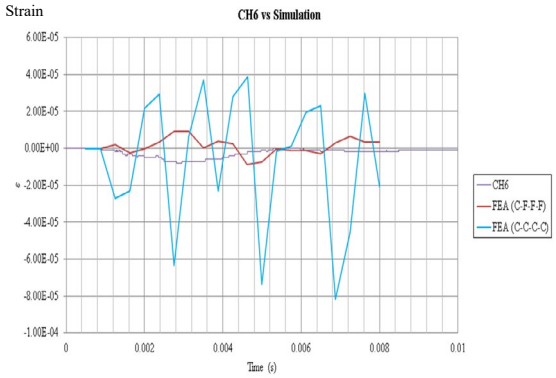

b.

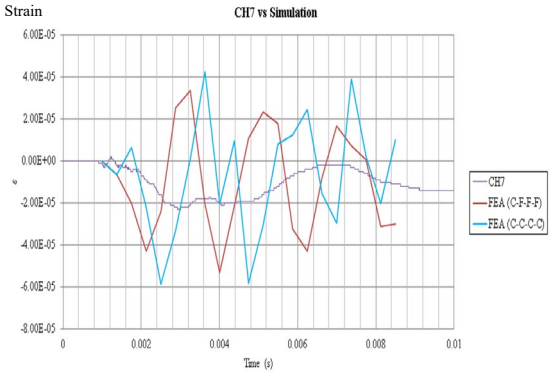

c.

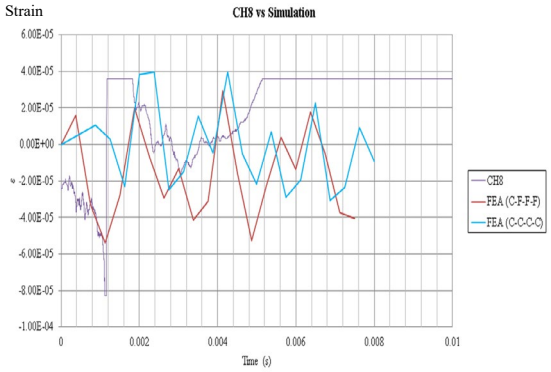

d.

Figure A.97 Strain response and FEA comparison, steel penetrator (30 lb), test date: 6 Sep 19

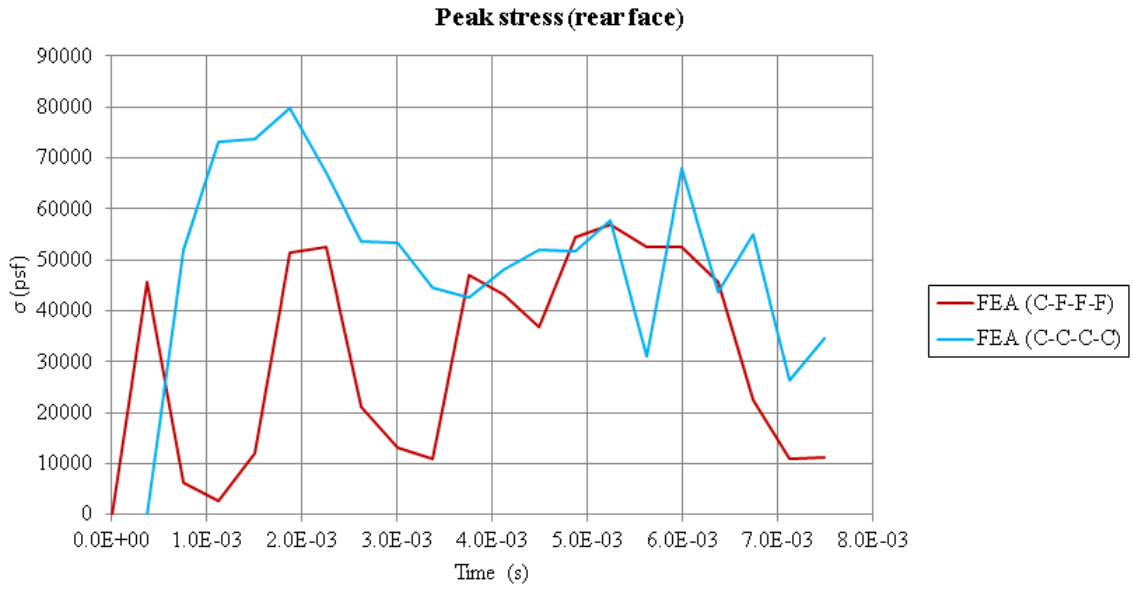

Figure A.98 FEA peak rear face stress, steel penetrator (30 lb), test date: 19 Sep 19

Consolidated Test Data for Comparison

The following figures are a consolidation of penetration and peak values for each test case and the estimated impact energy or modified Weber number.

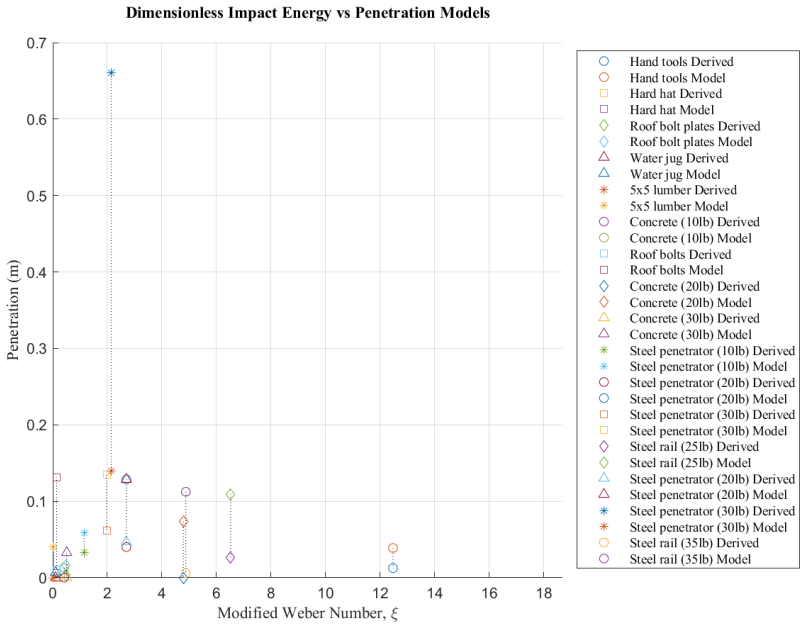

Figure A.99 Dimensionless impact energy for estimated and derived penetration

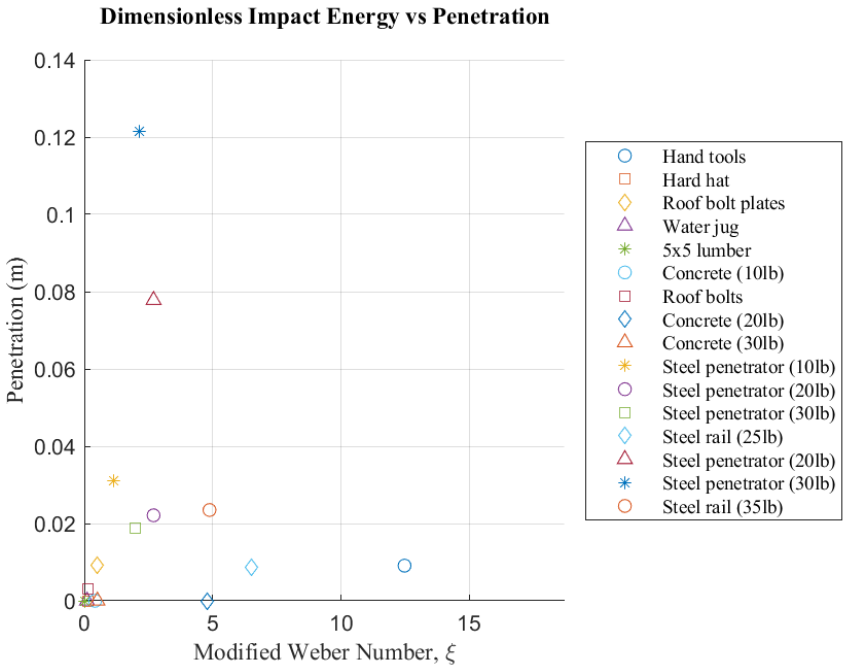

Figure A.100 Dimensionless impact energy and measured penetration

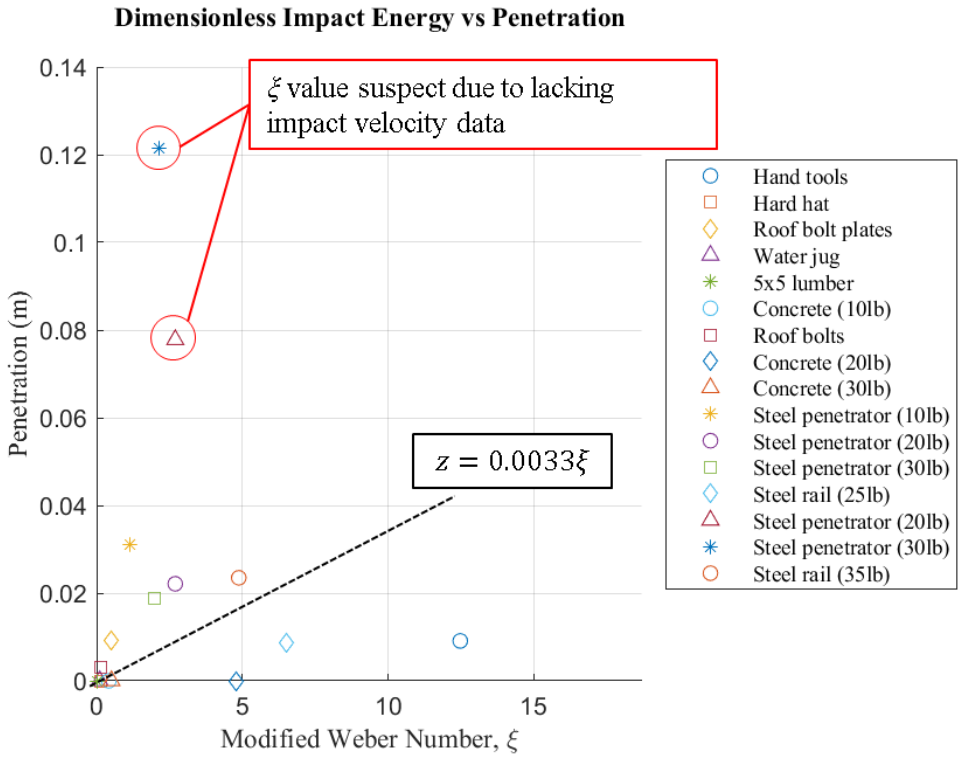

Figure A.101 Dimensionless impact energy and penetration trend

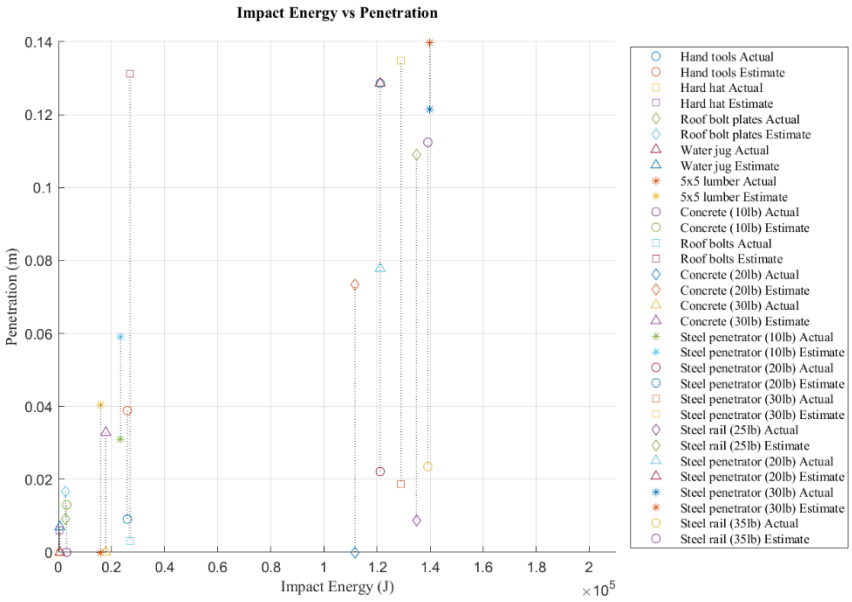

Figure A.102 Impact energy and models for estimated and volume loss derived penetration

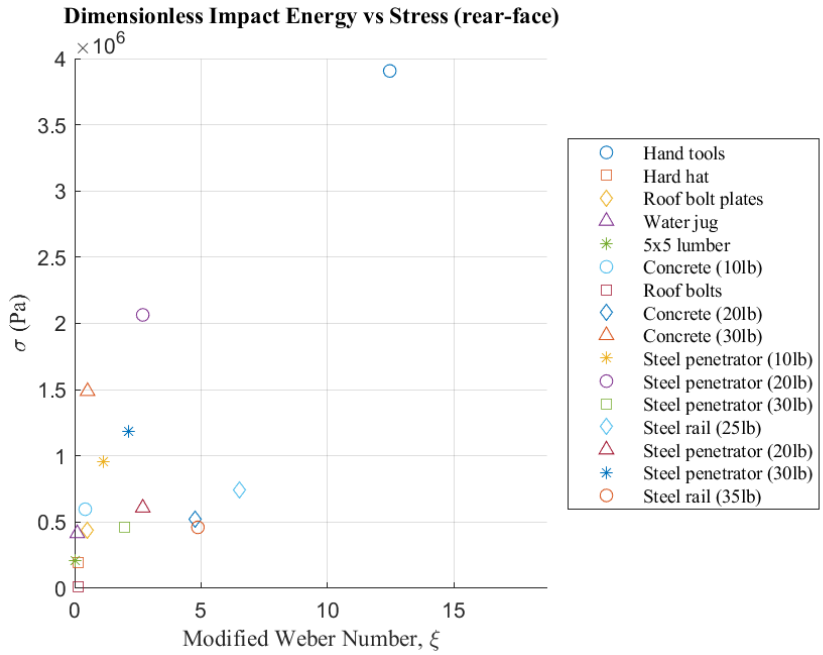

Figure A.103 Dimensionless impact energy and peak rear face stress

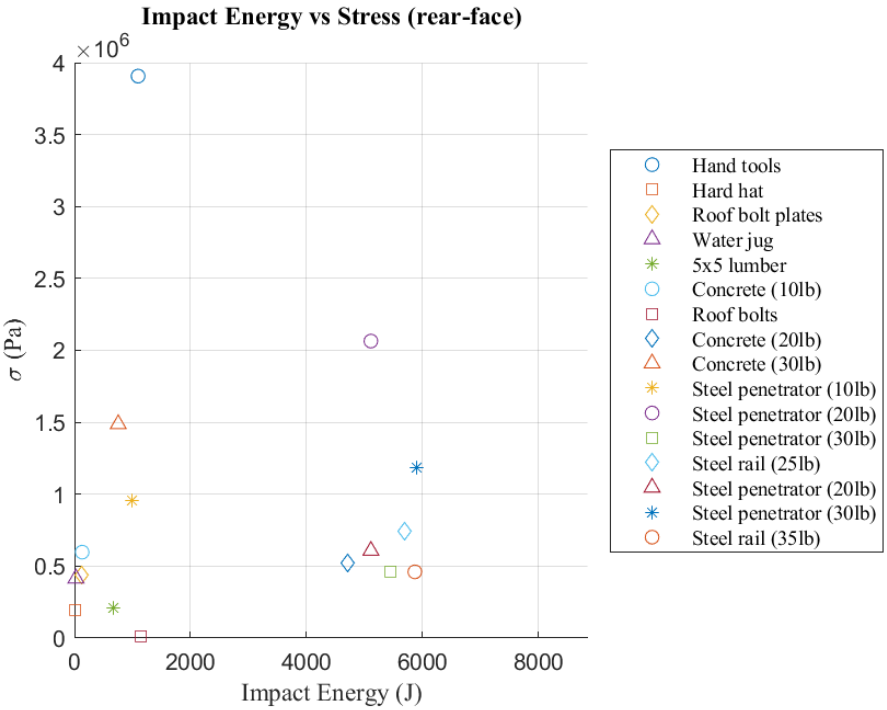

Figure 0.104 Impact energy and peak rear face stress

Appendix B - Reinforced Concrete Seal

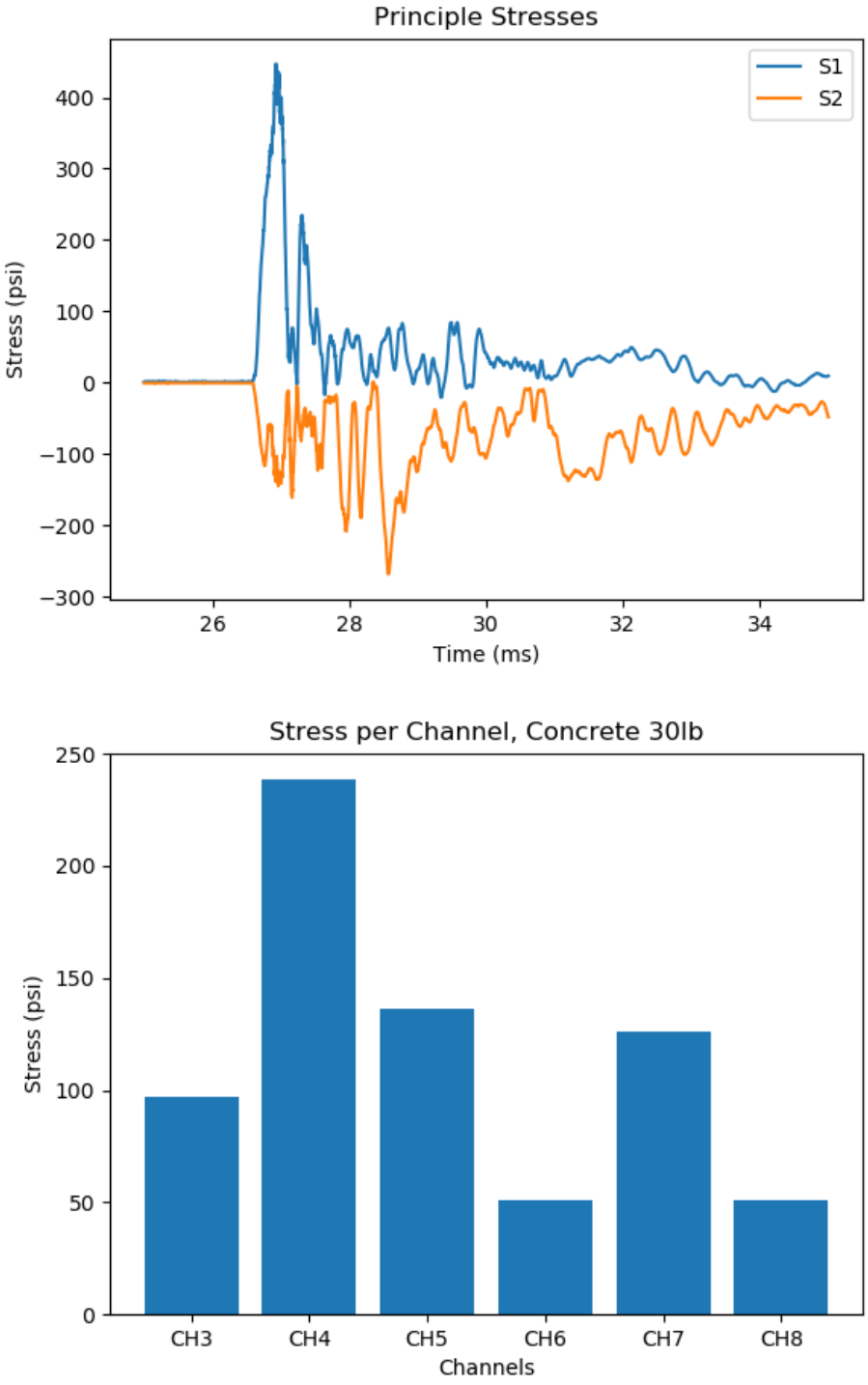

Figure B.1 Concrete Projectile Stresses

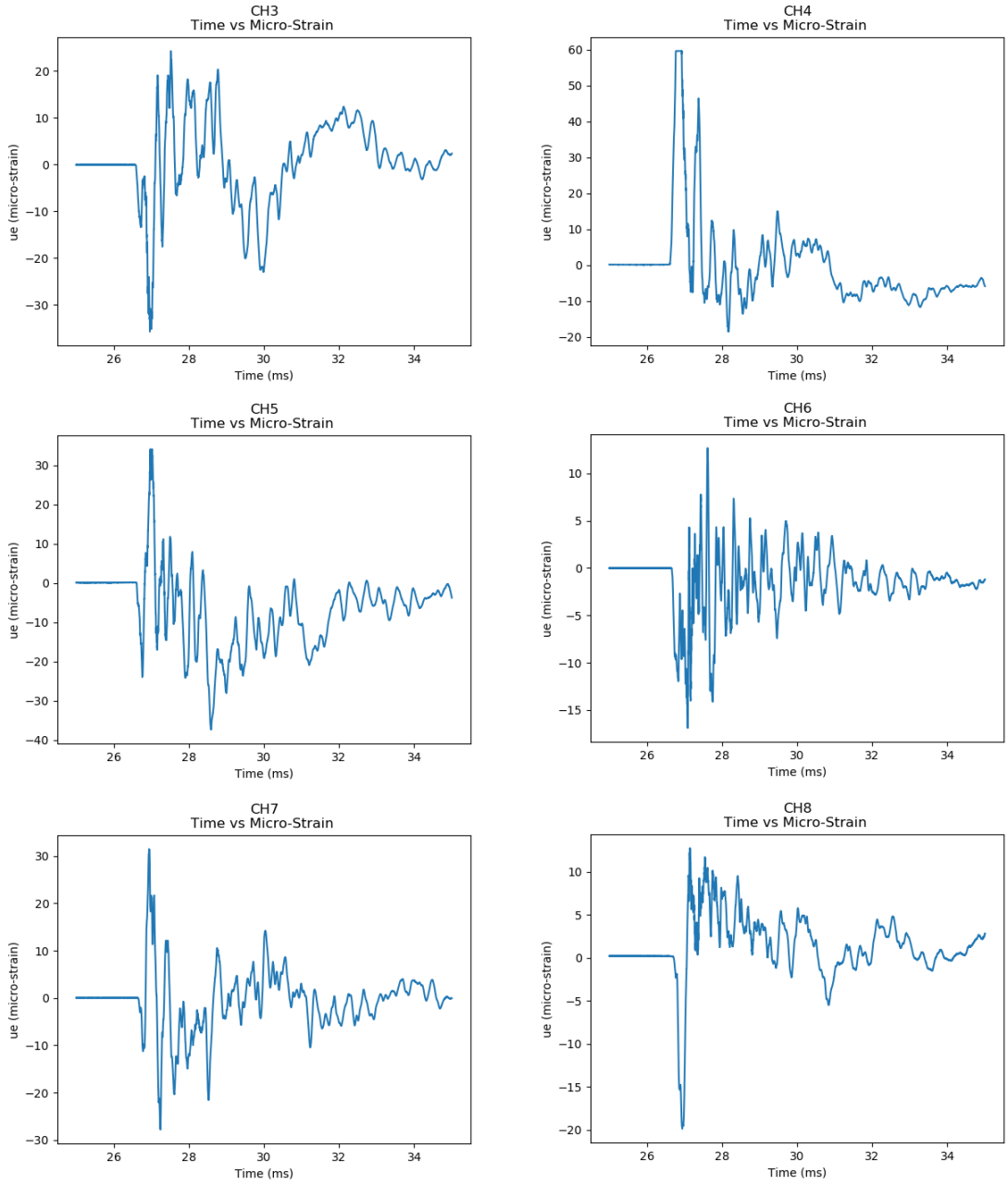

Figure B.2 Concrete Projectile Strains

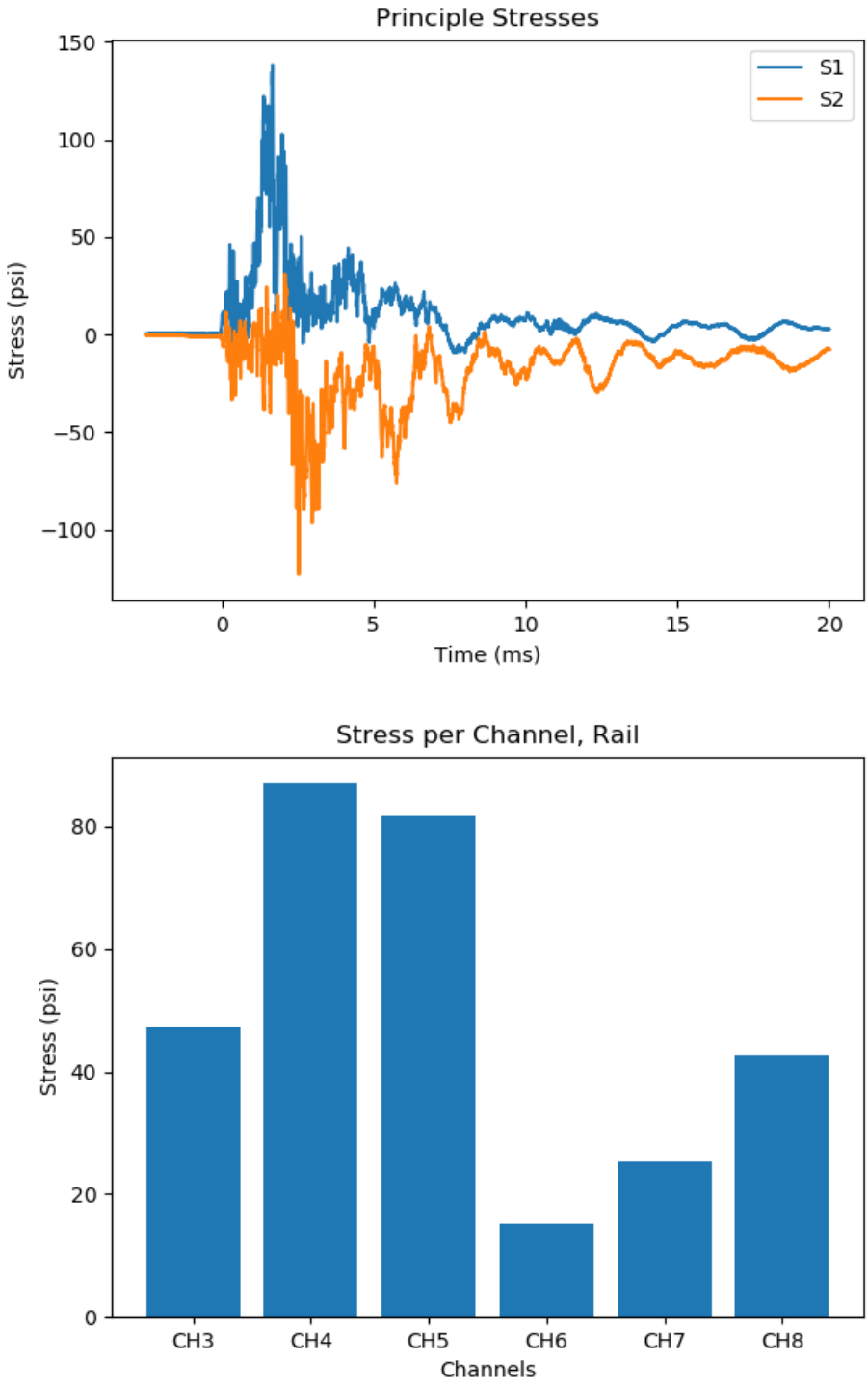

Figure B.3 Rail Projectile Stresses

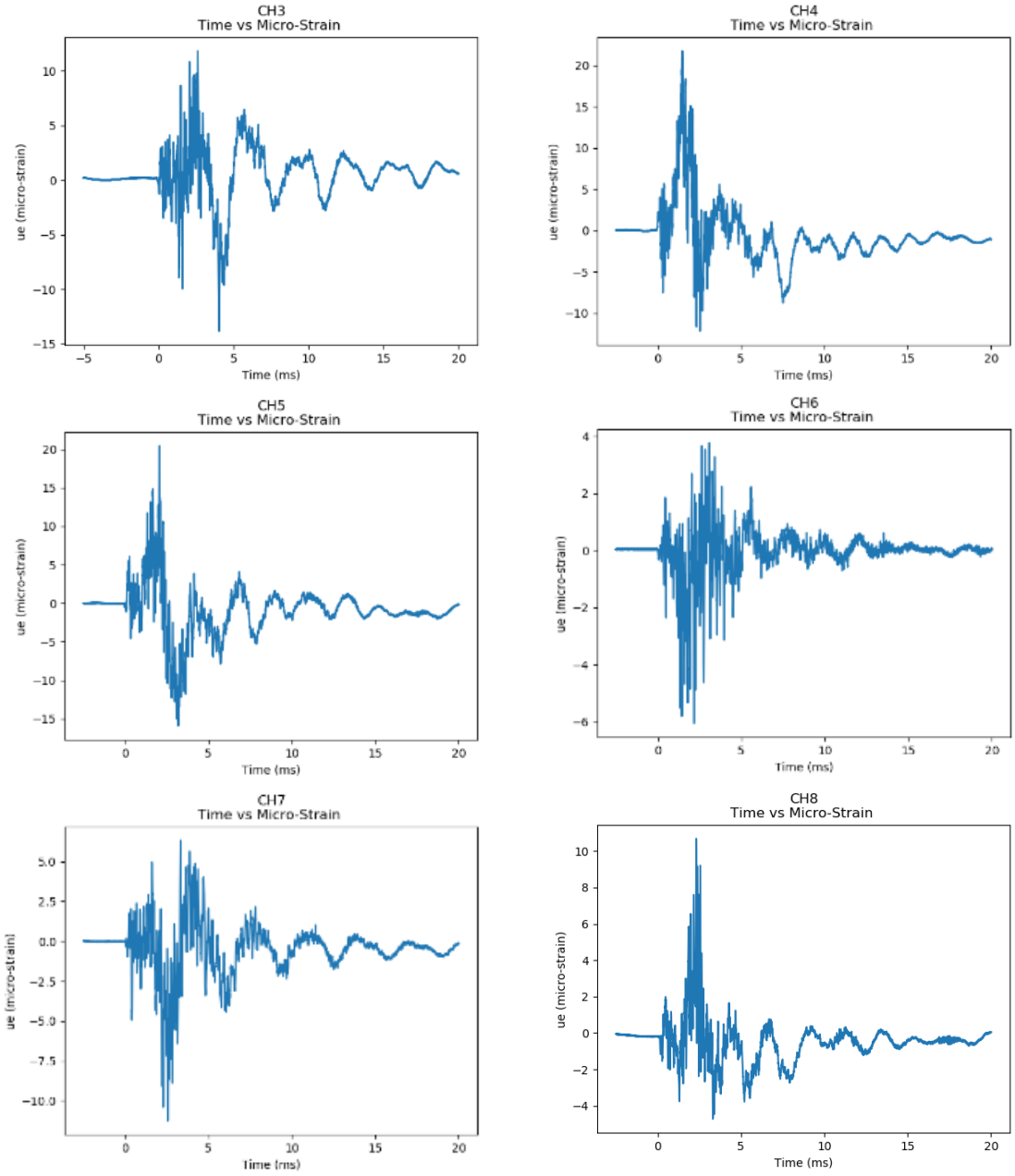

Figure B.4 Rail Projectile Strains

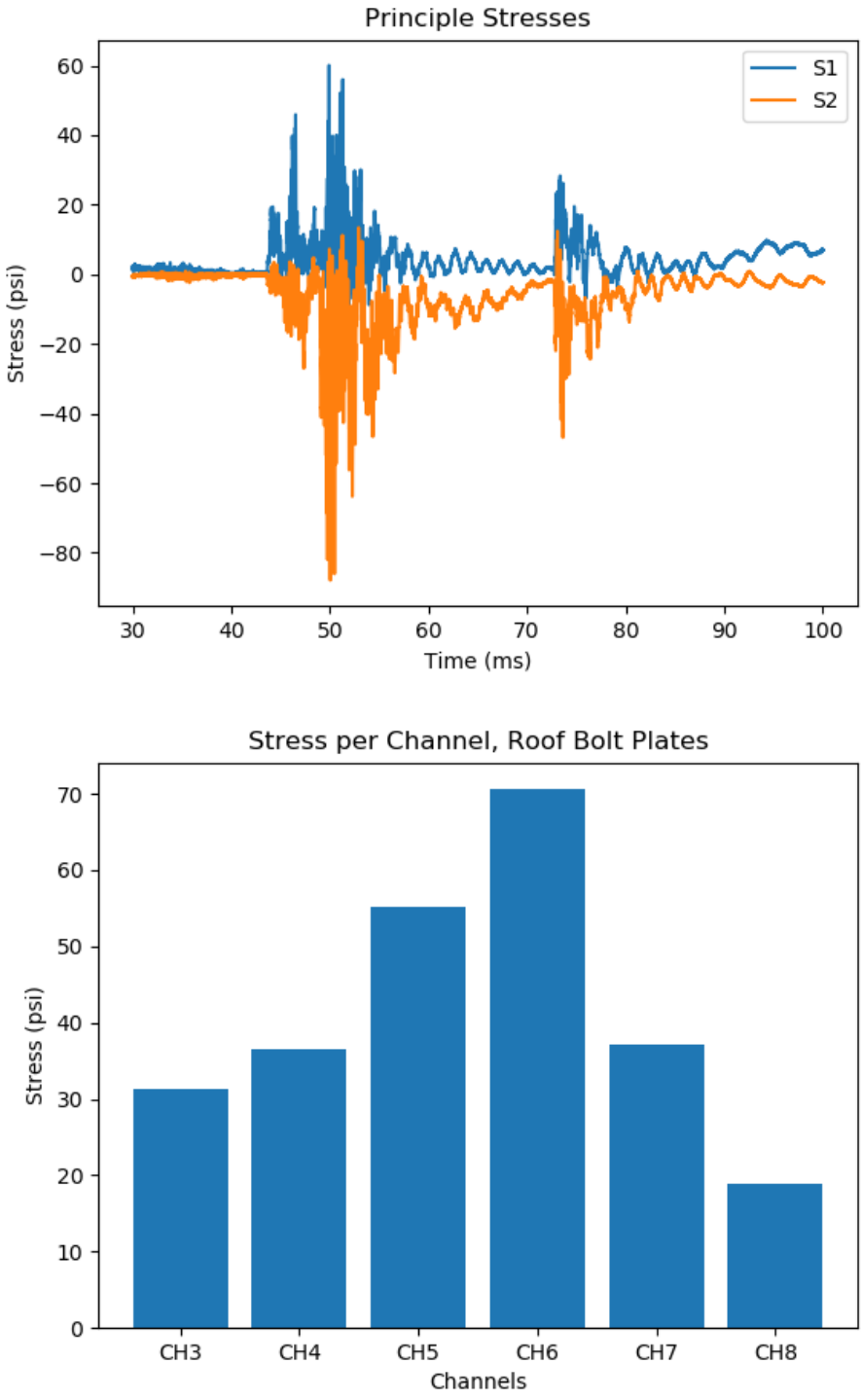

Figure B.5 Roof Bolt Plate Projectile Stresses

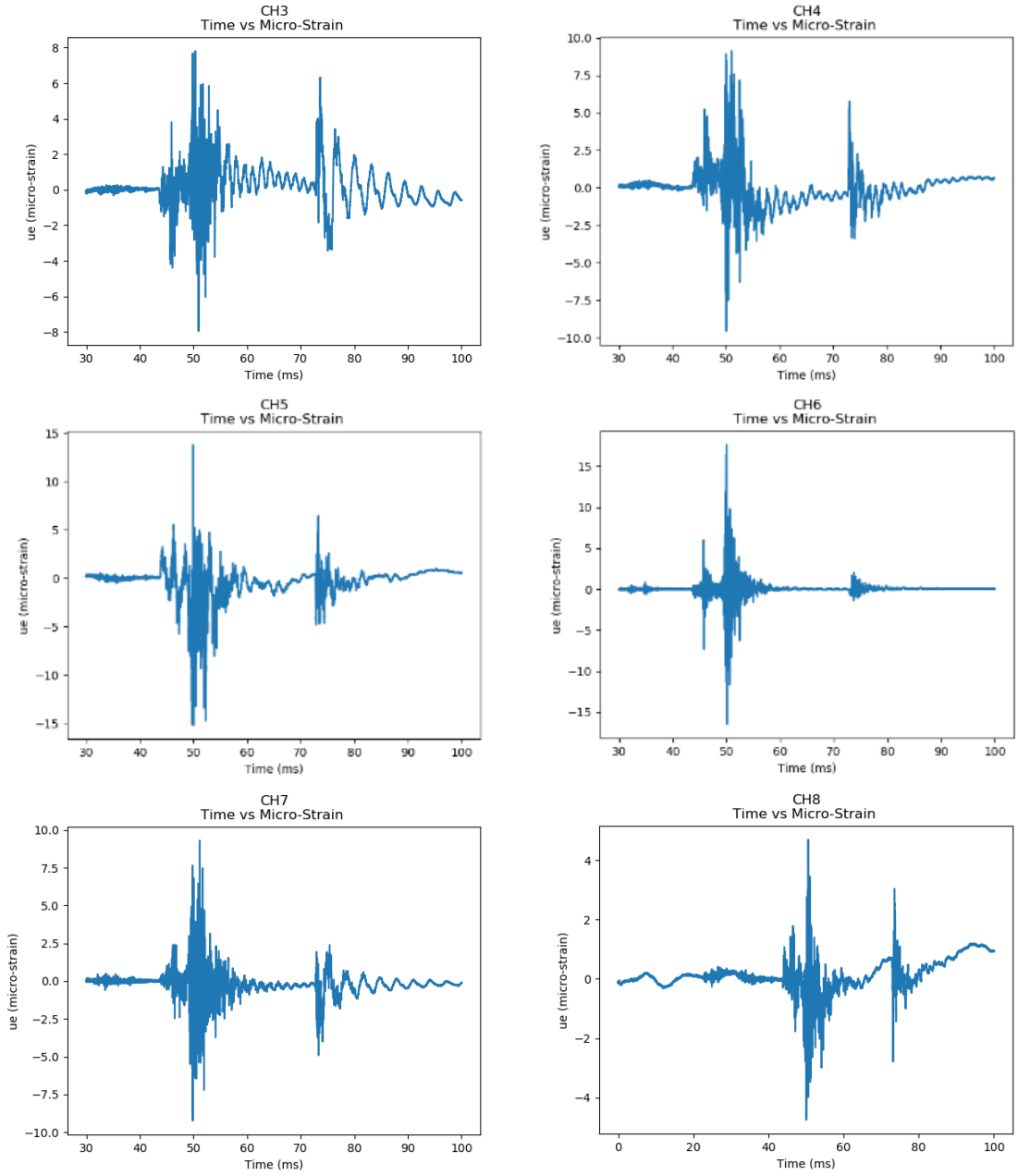

Figure B.6 Roof Bolt Plate Projectile Strains

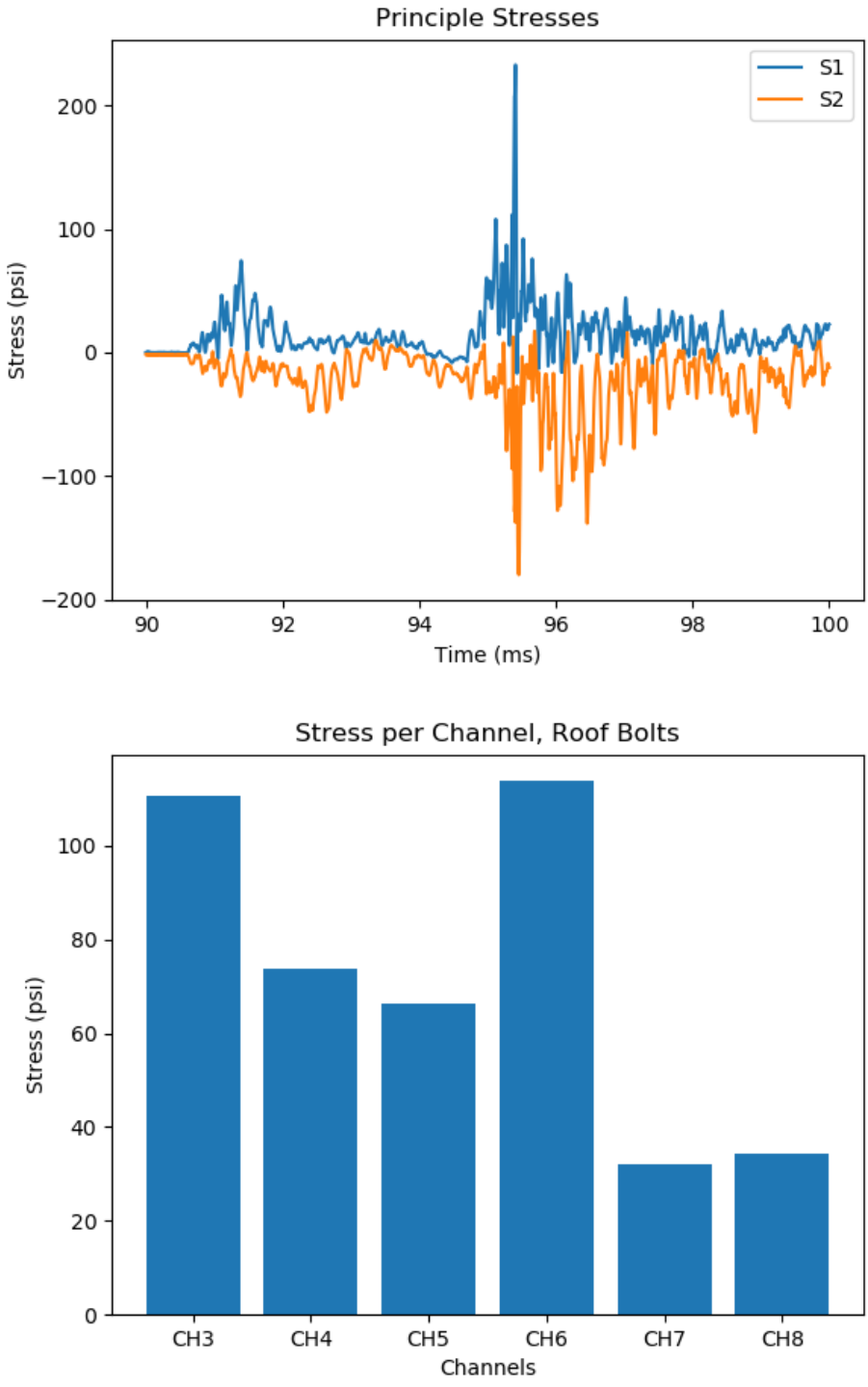

Figure B.7 Roof Bolt Projectile Stresses

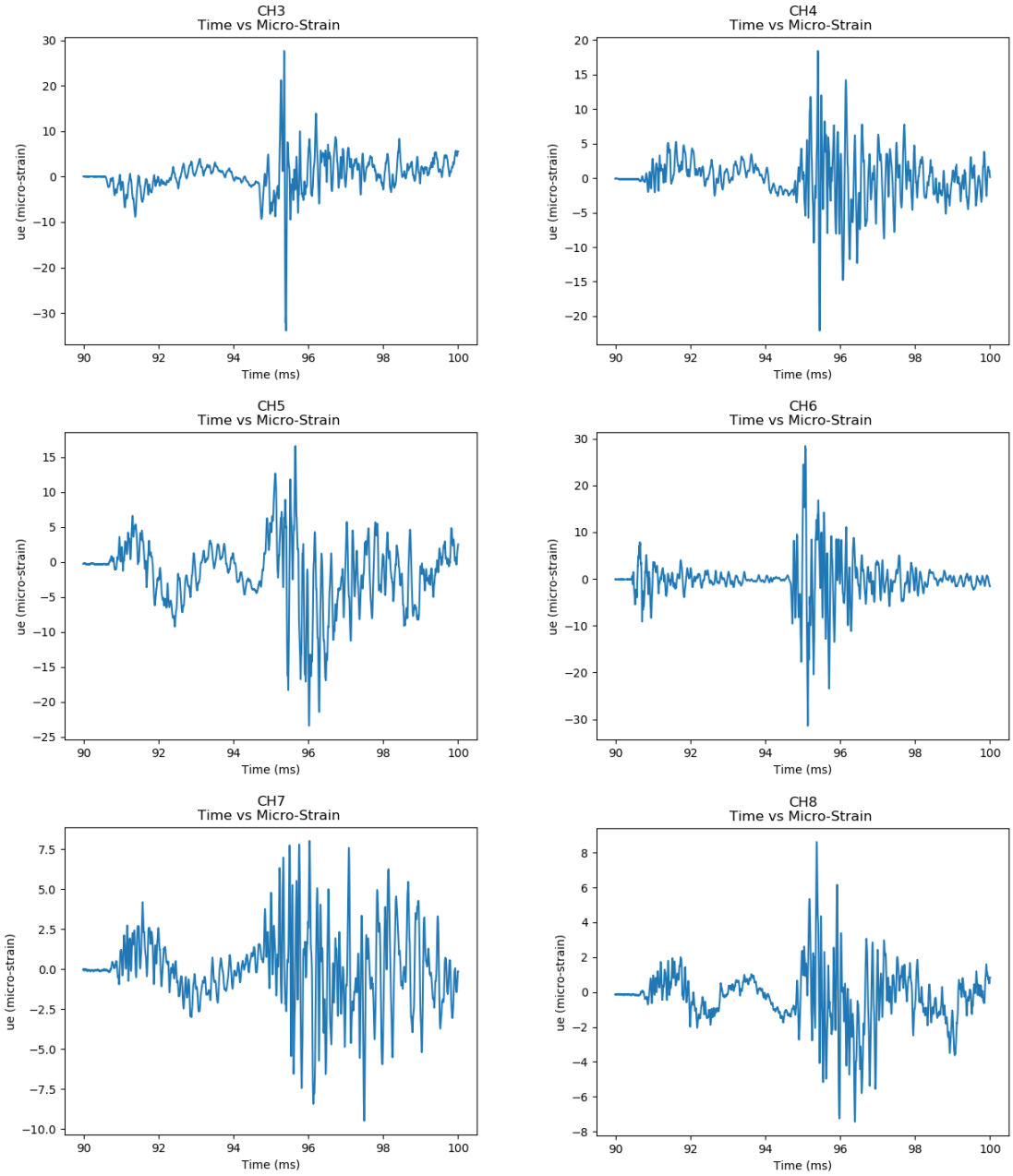

Figure B.8 Roof Bolt Projectile Strains

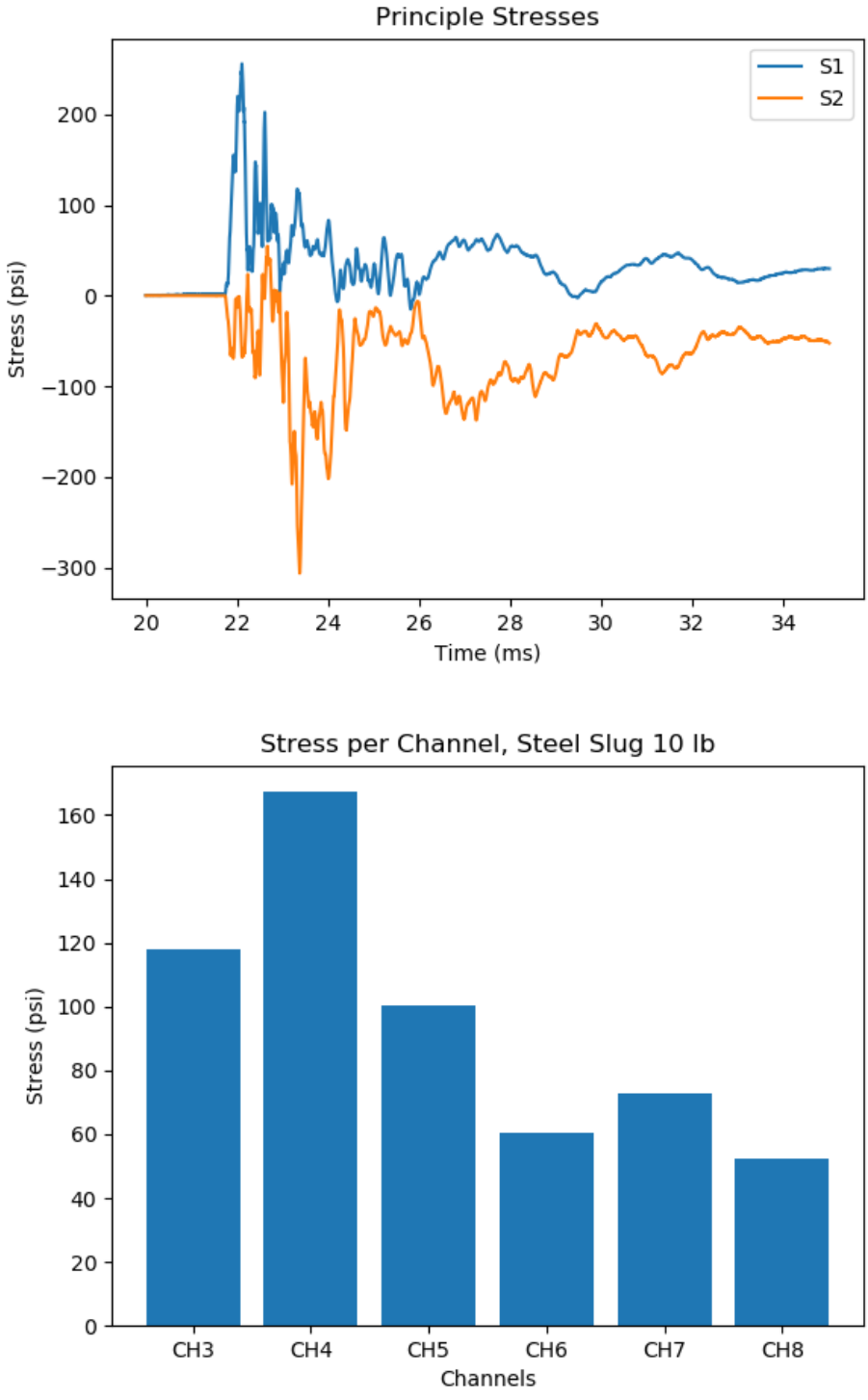

Figure B.9 Steel Slug 10 lb. Projectile Stresses

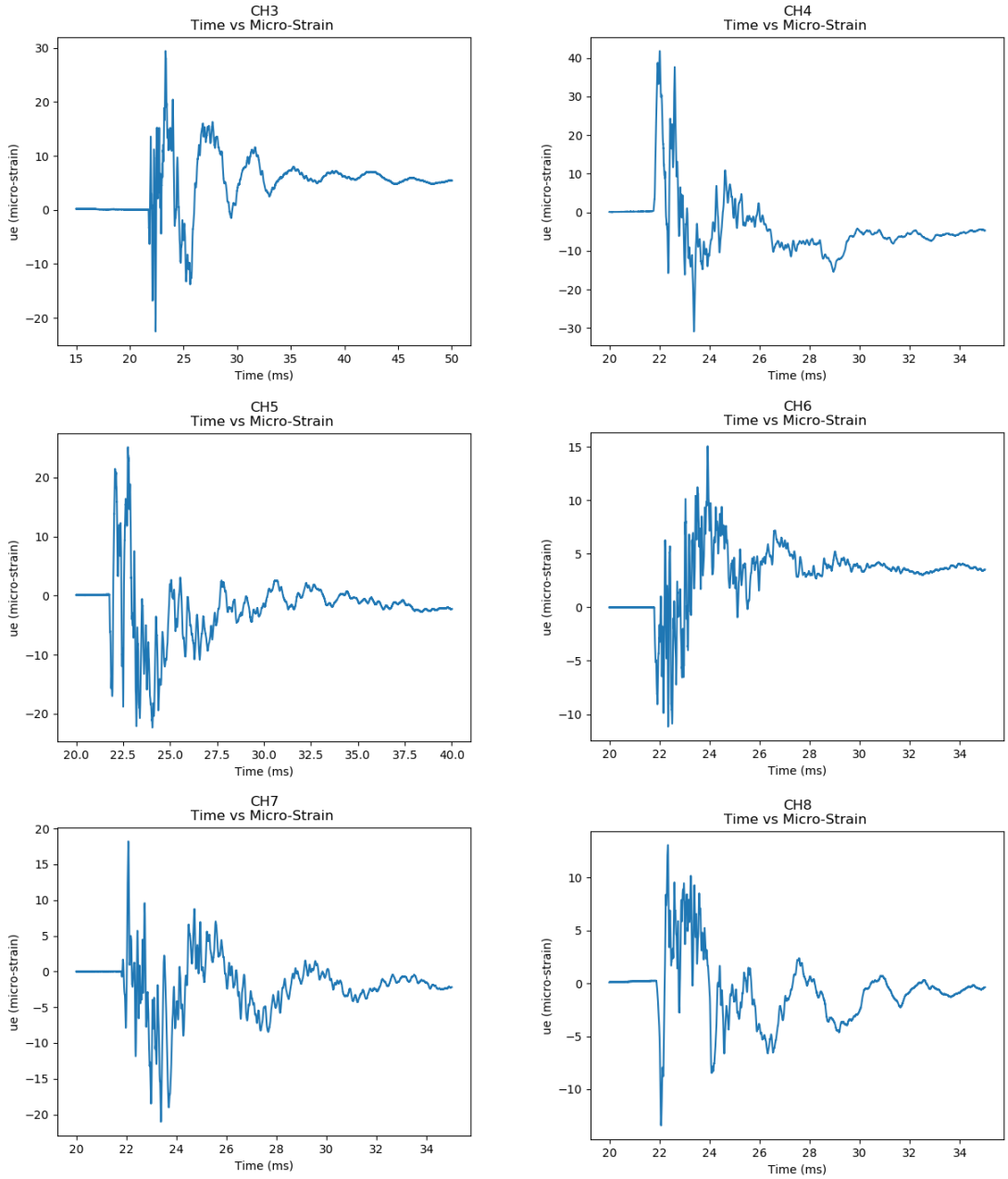

Figure B.10 Steel Slug 10 lb. Projectile Strains

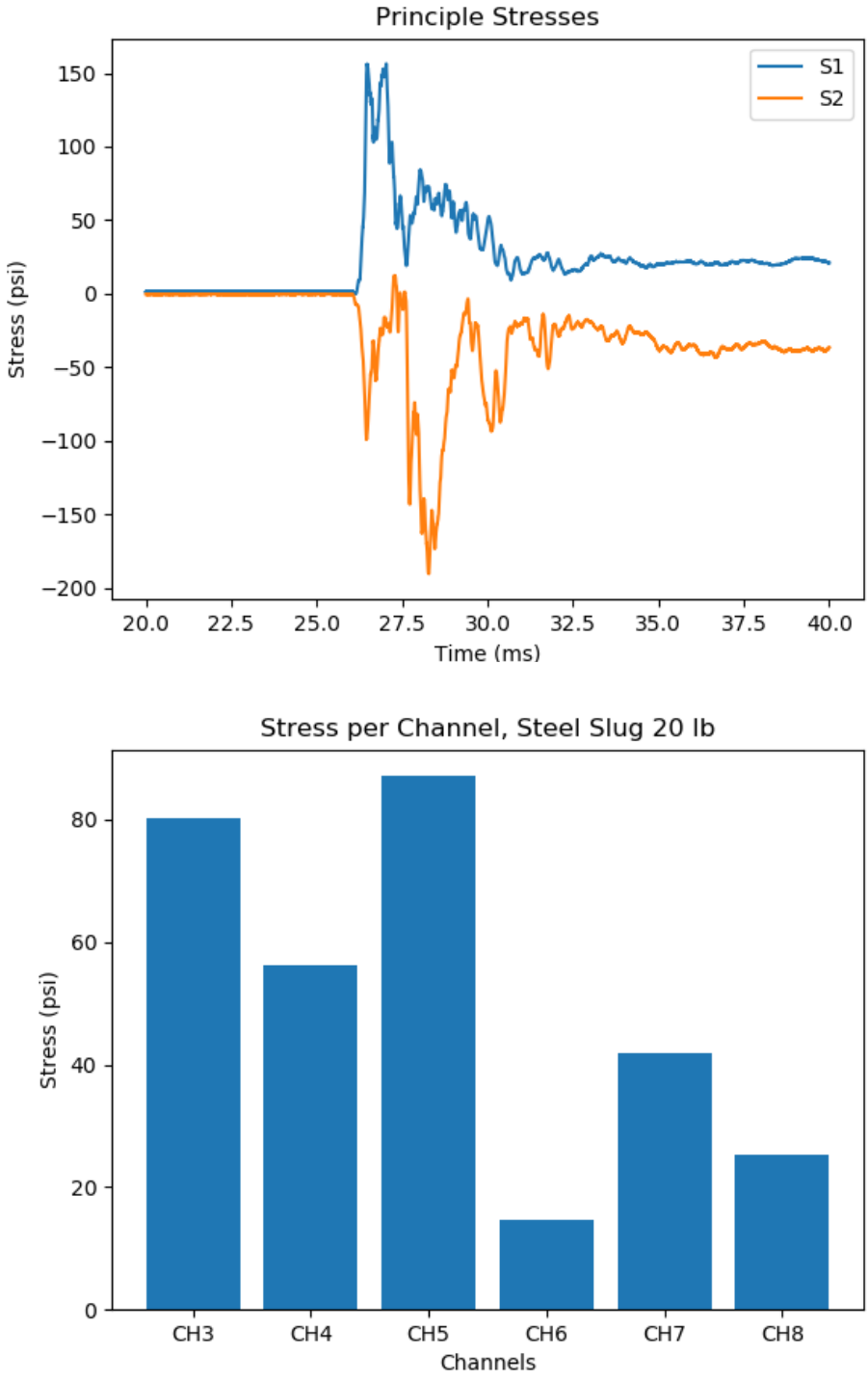

Figure B.11 Steel Slug 20 lb. Projectile Stresses

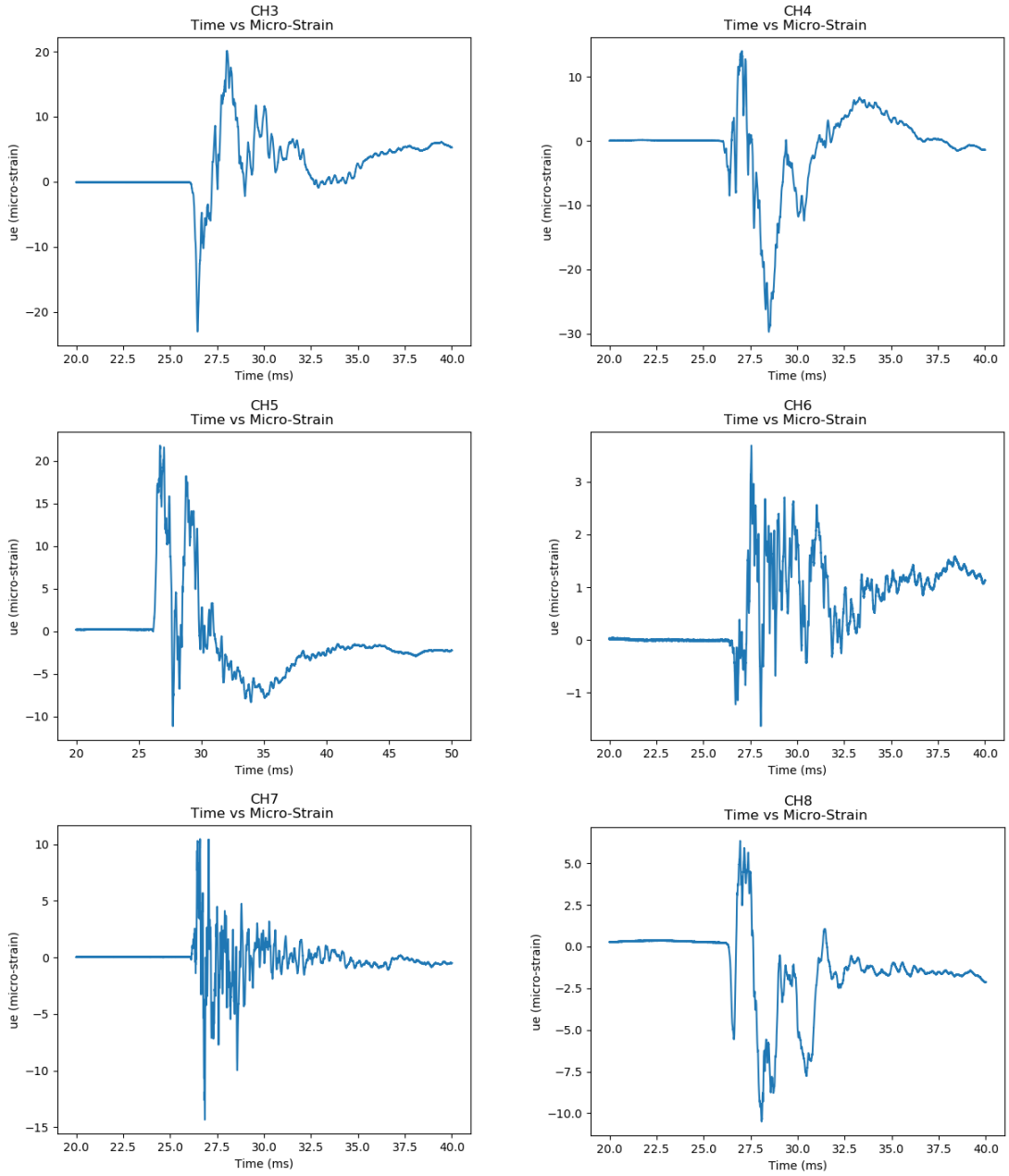

Figure B.12 Steel Slug 20 lb. Projectile Strains

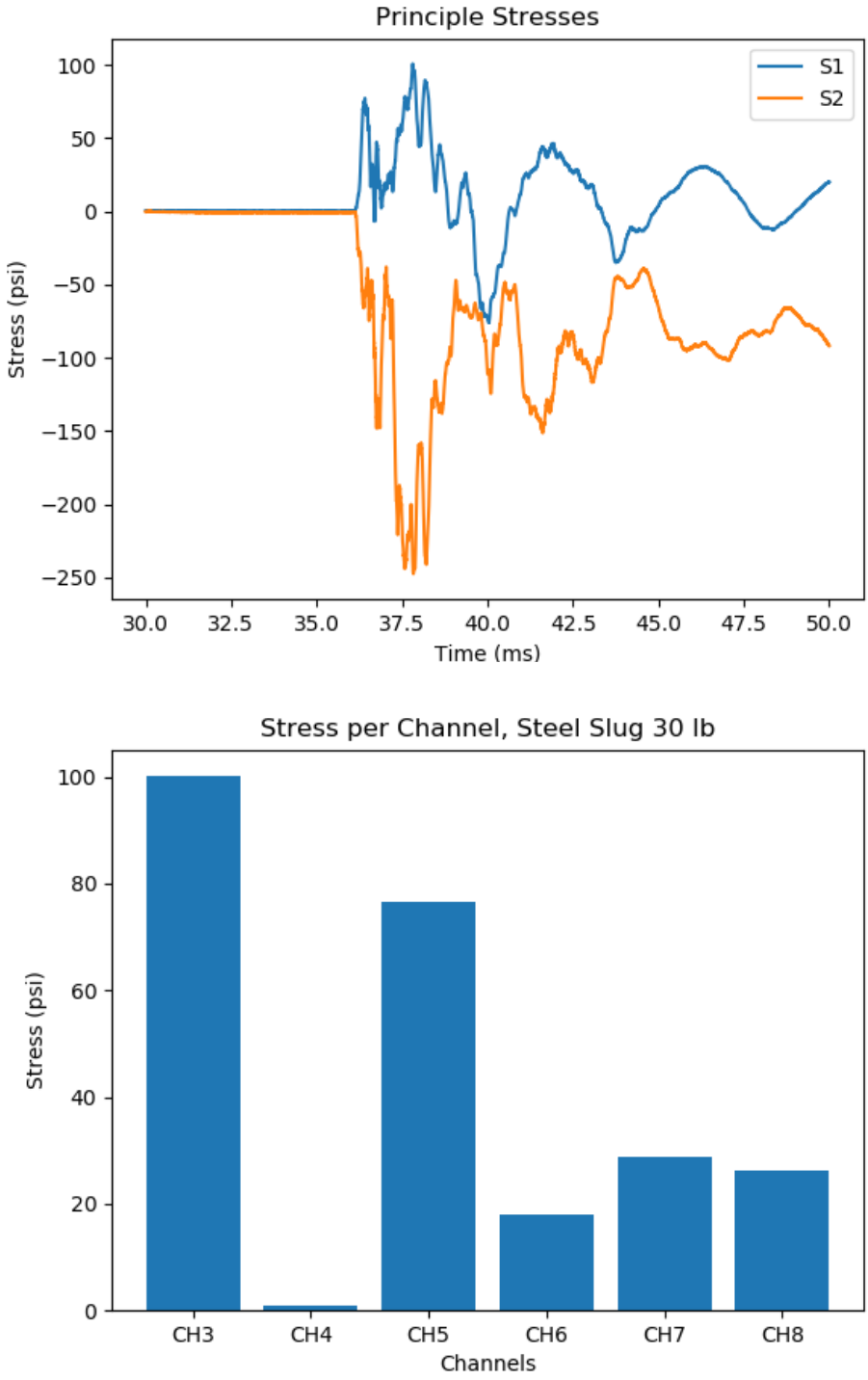

Figure B.13 Steel Slug 30 lb. Projectile Stresses

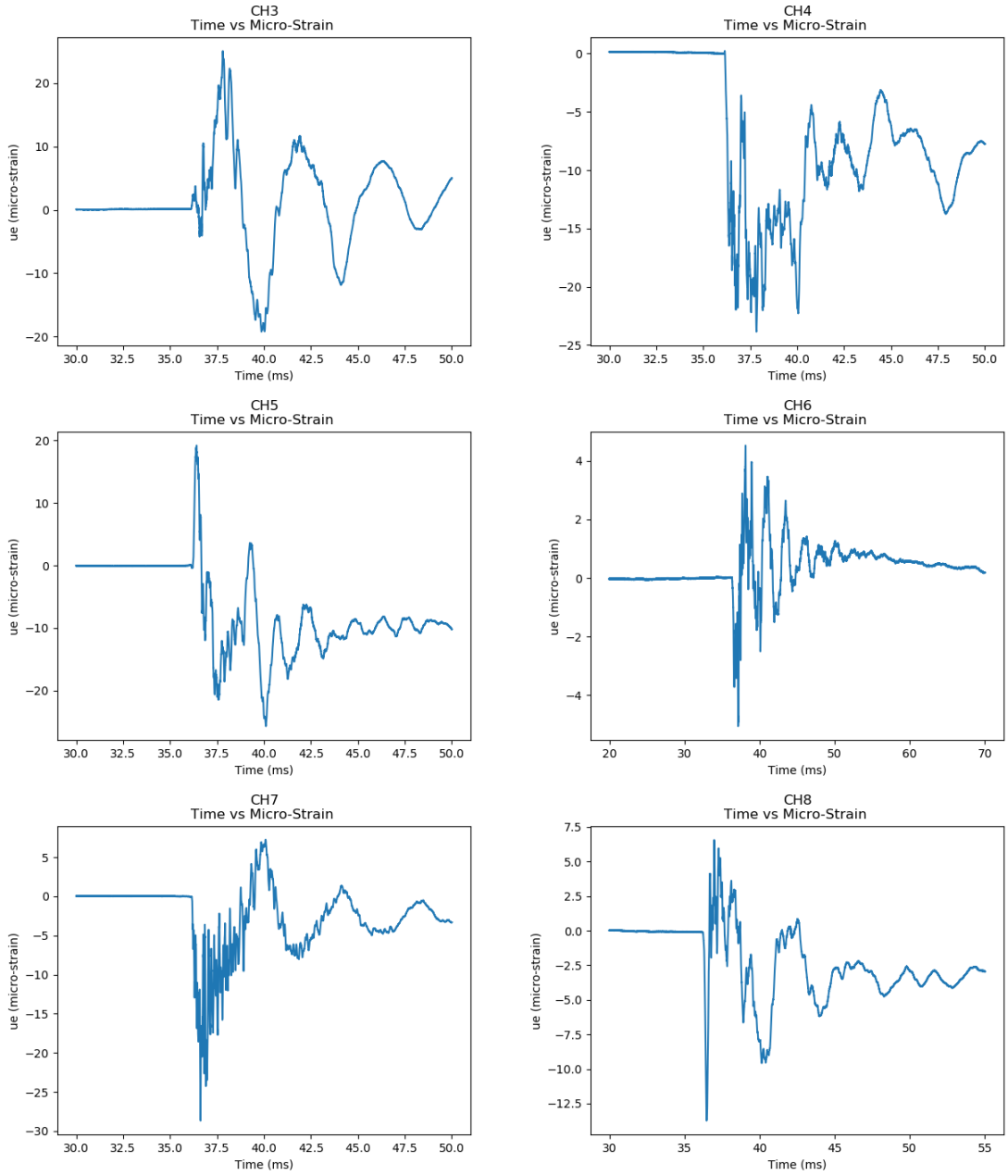

Figure B.14 Steel Slug 30 lb. Projectile Strains

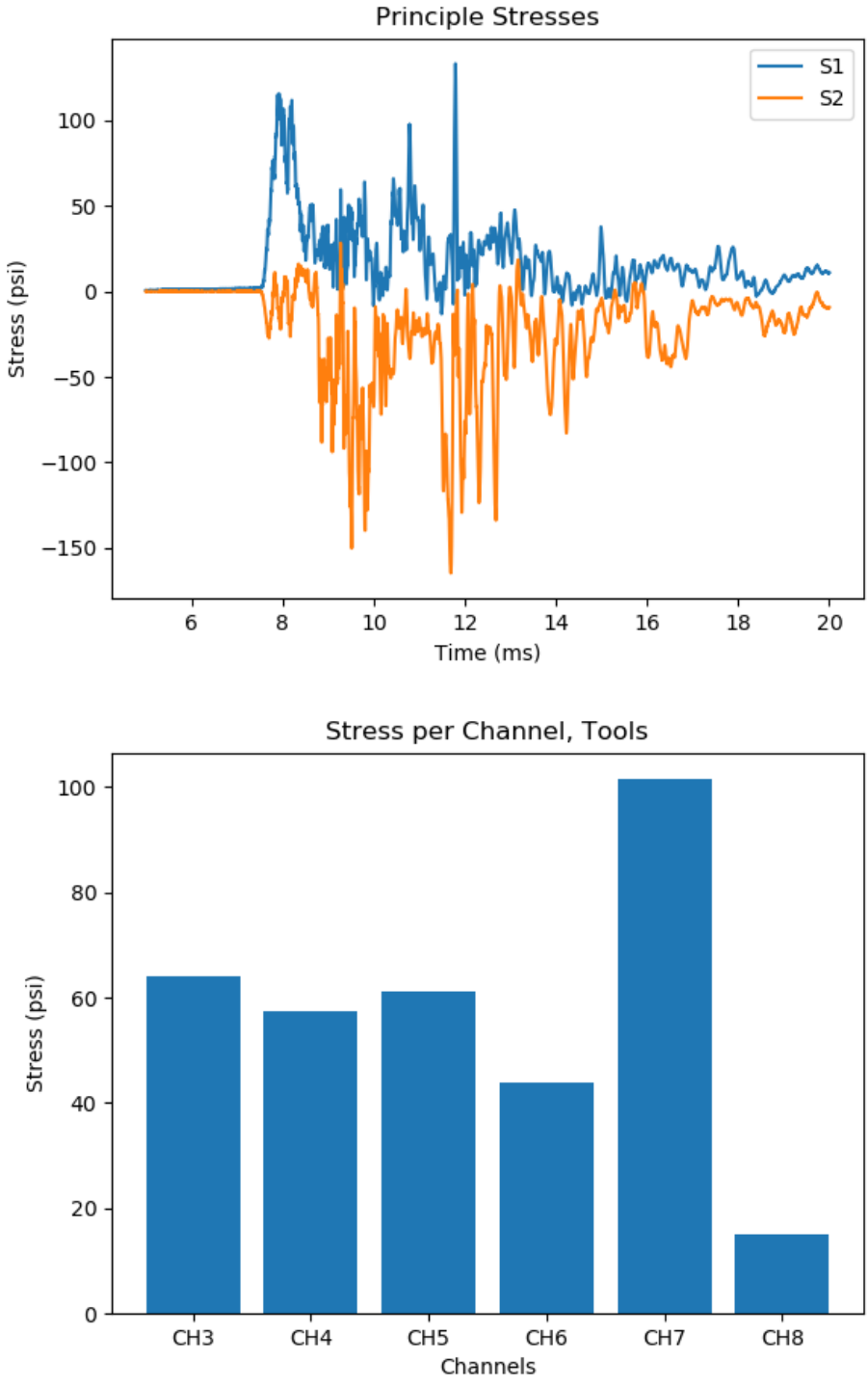

Figure B.15 Tool Projectile Stresses

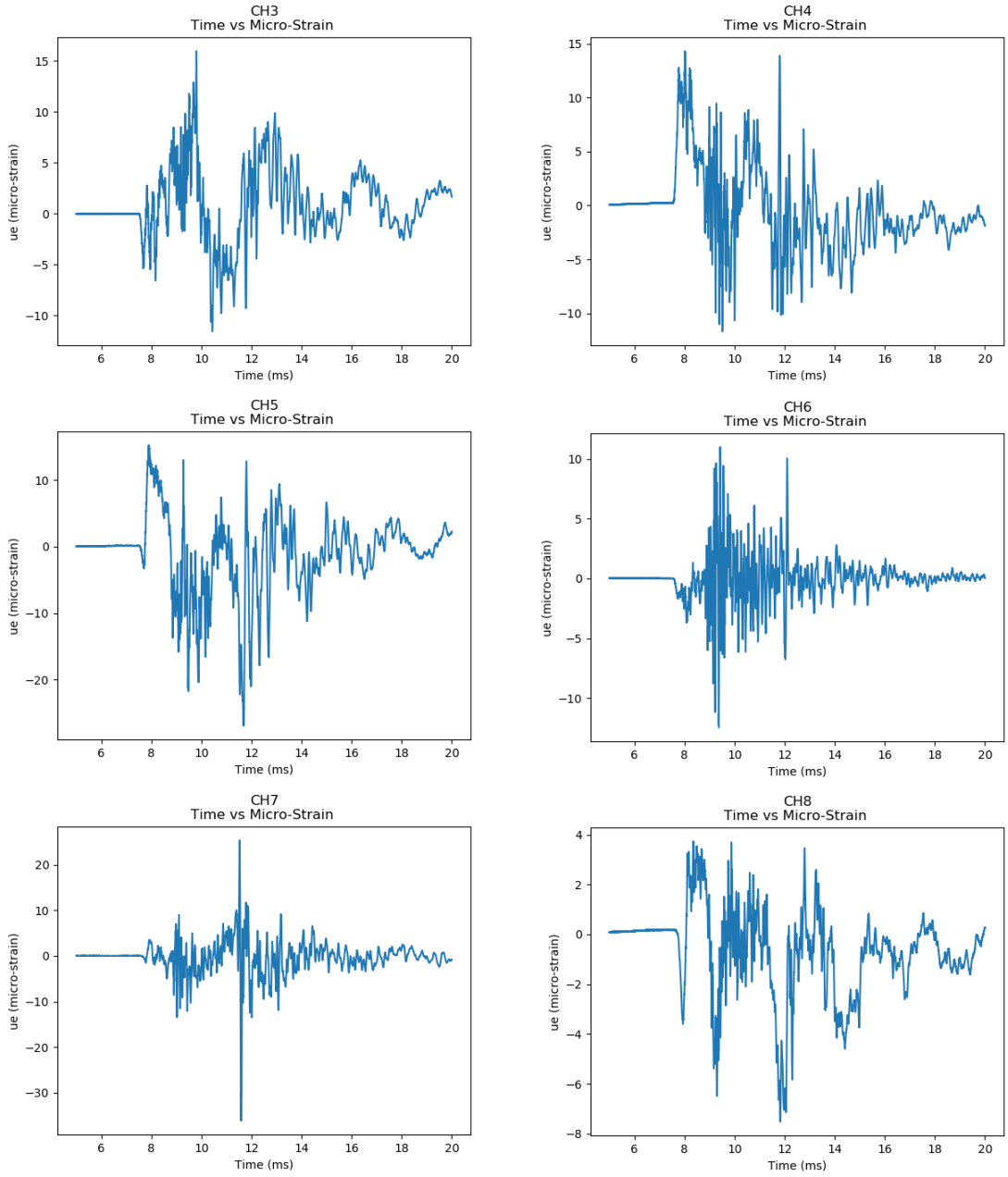

Figure B.16 Tool Projectile Strains

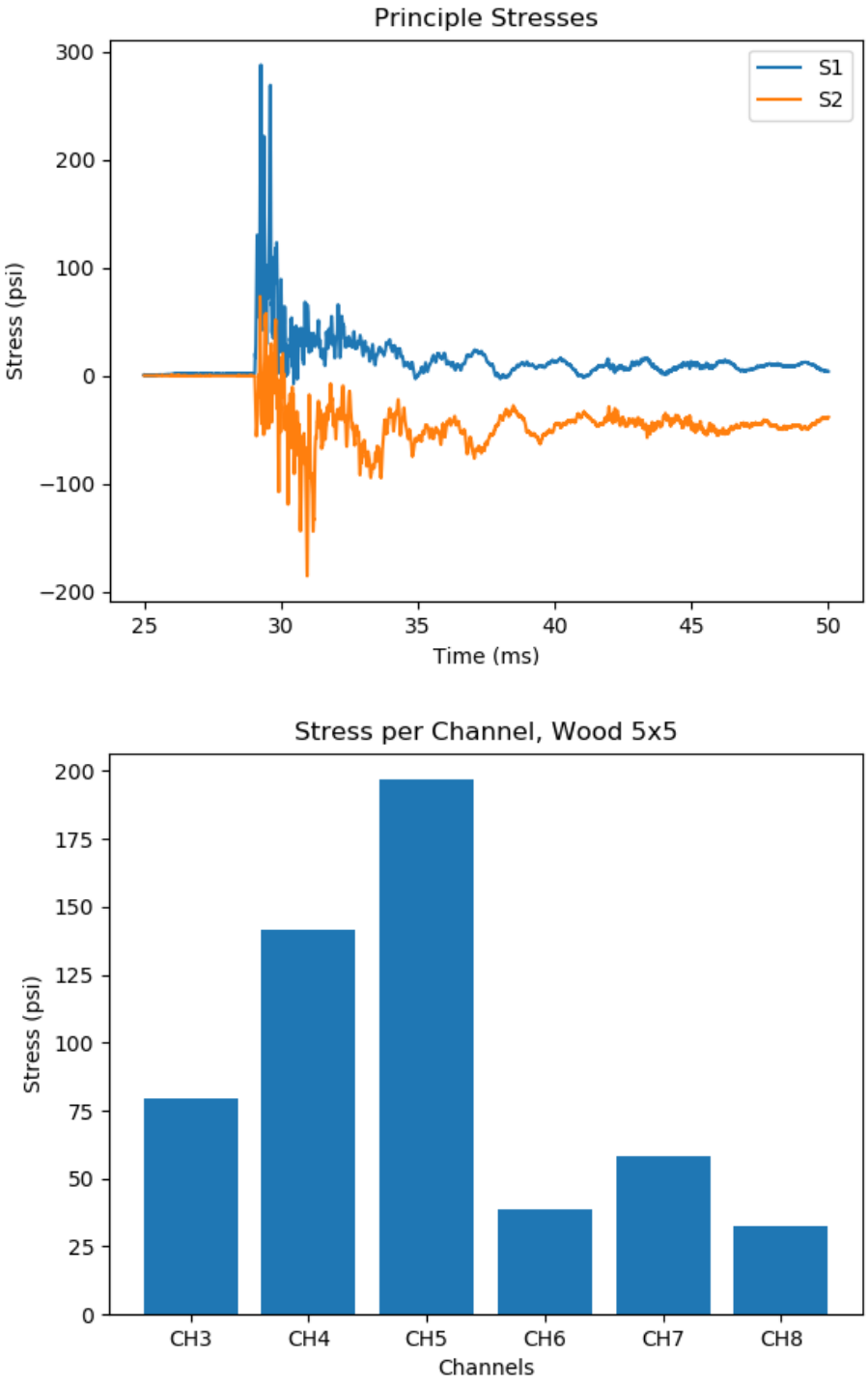

Figure B.17 Wood 5x5 Projectile Stresses

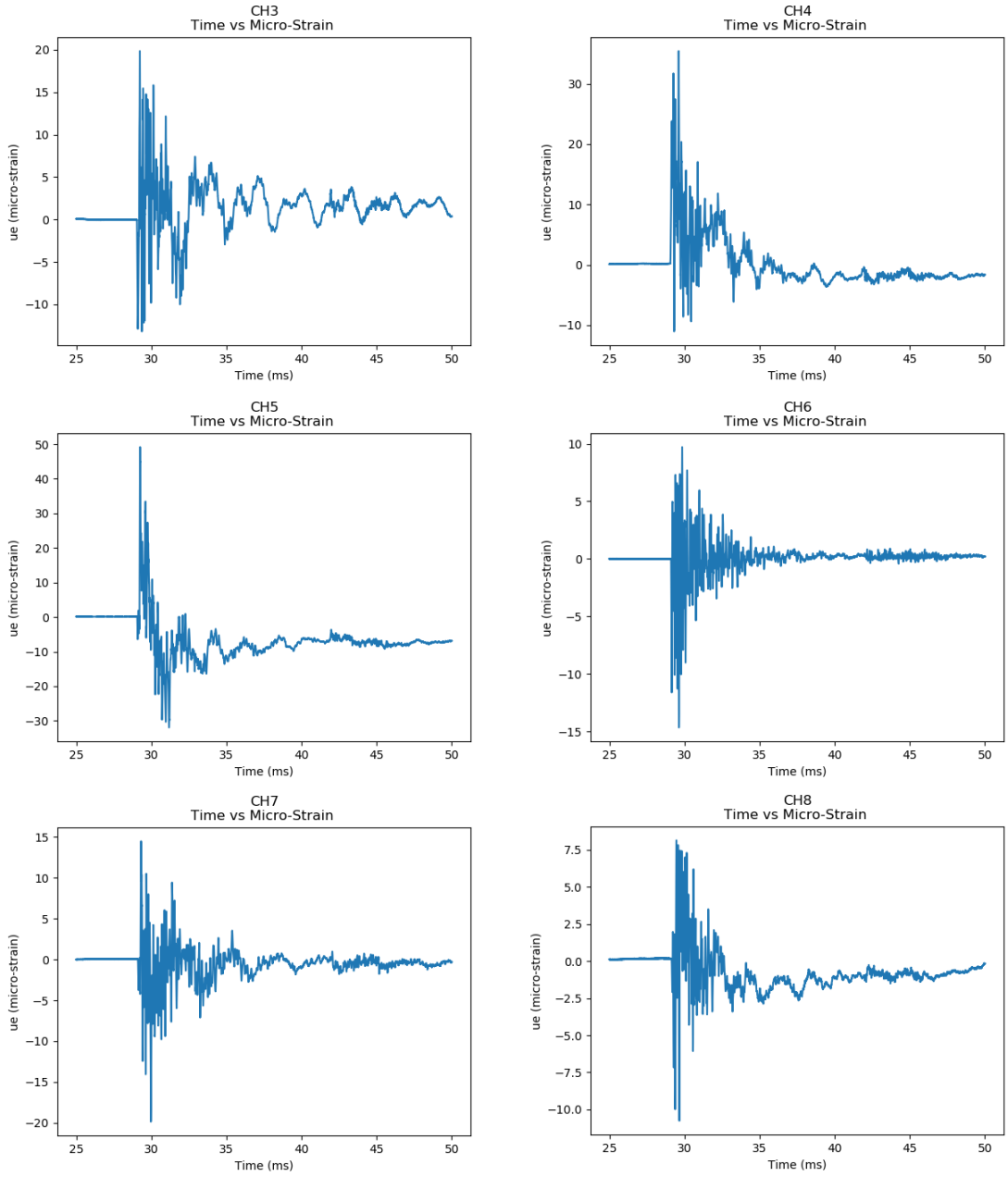

Figure B.18 Wood 5x5 Projectile Strains

Appendix C - Unreinforced Pumpable Cementitious Seal

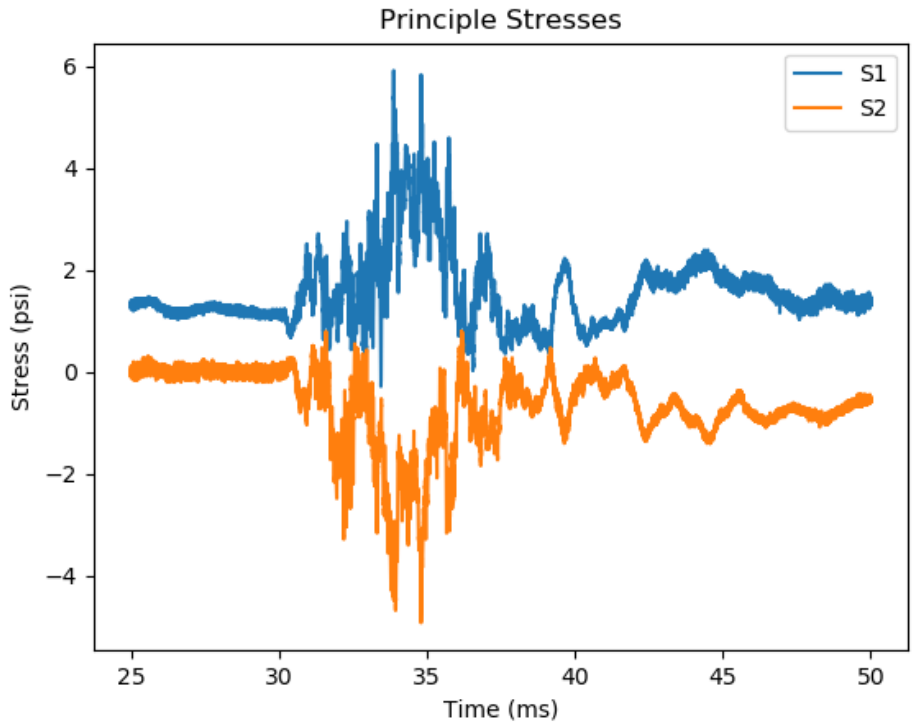

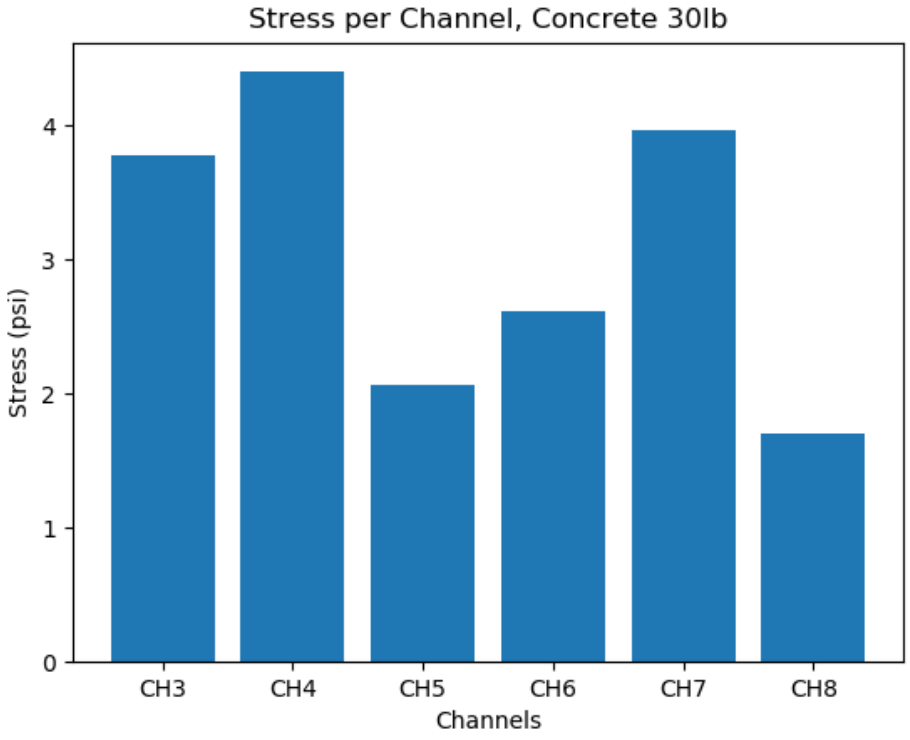

C.1 Concrete Projectile Stresses

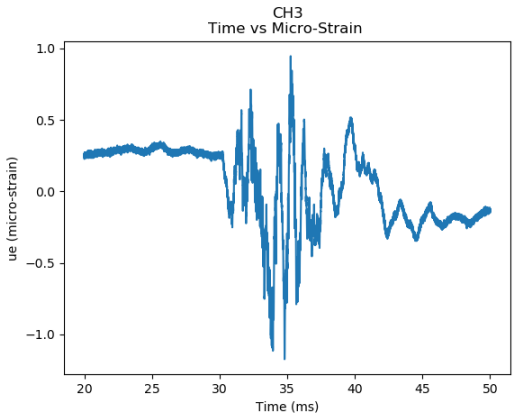

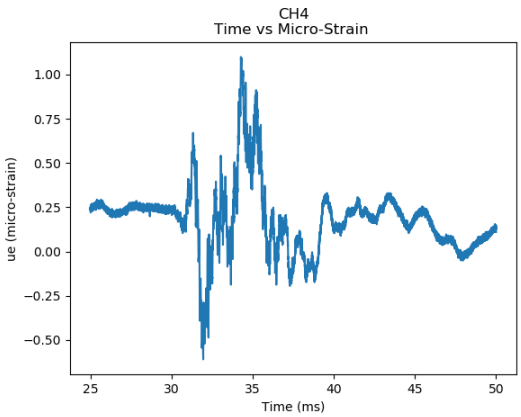

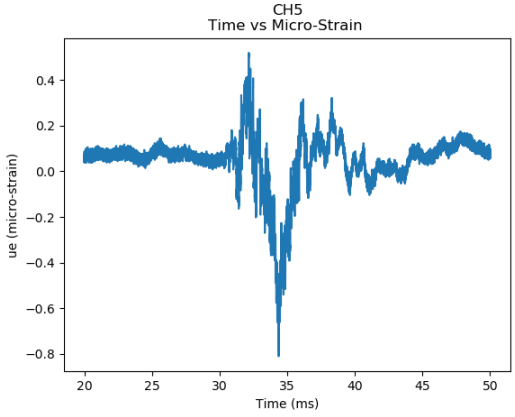

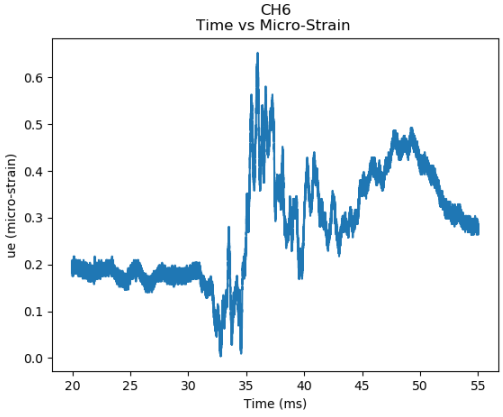

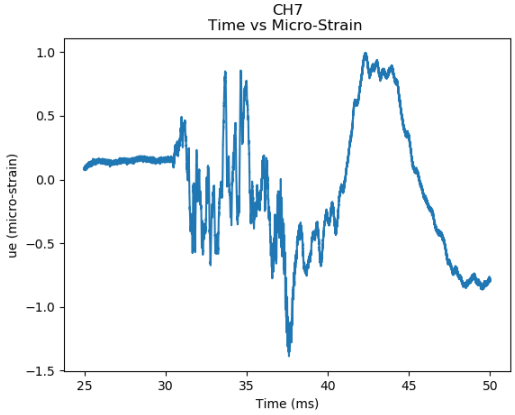

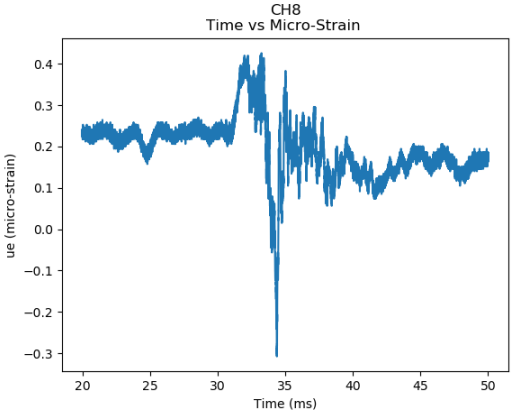

C.2 Concrete Projectile Strains

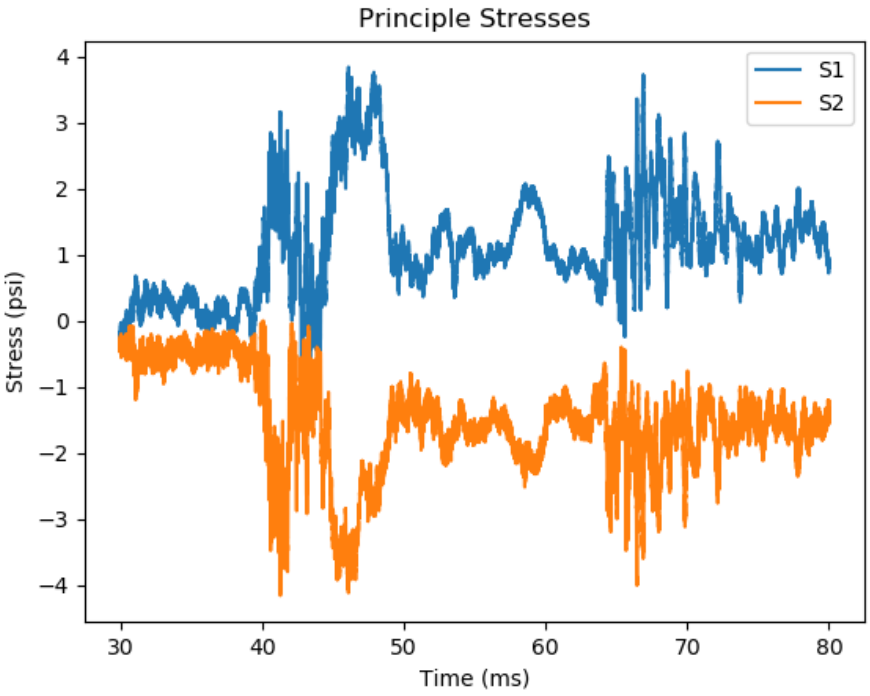

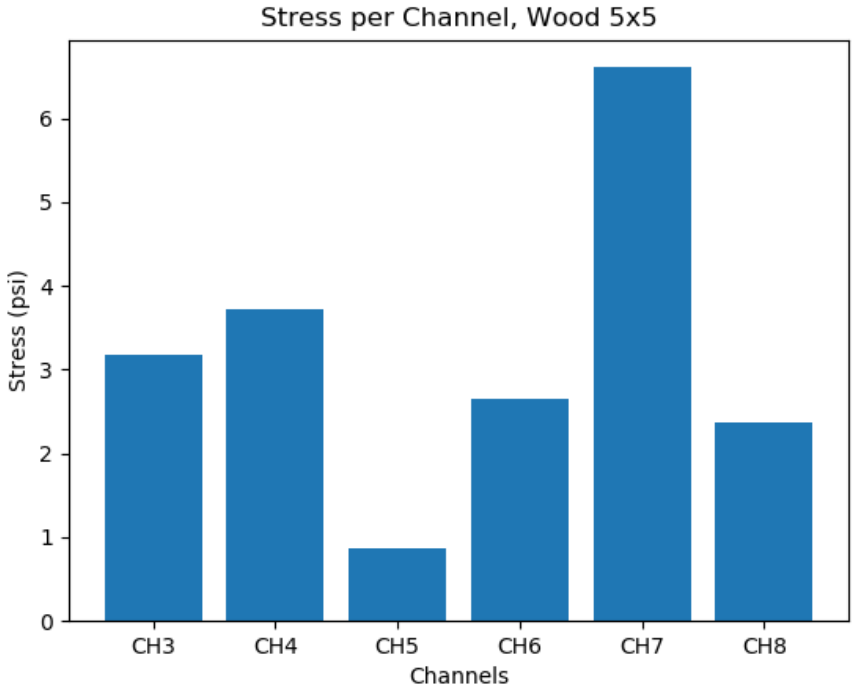

C.3 Wood Projectile Stresses

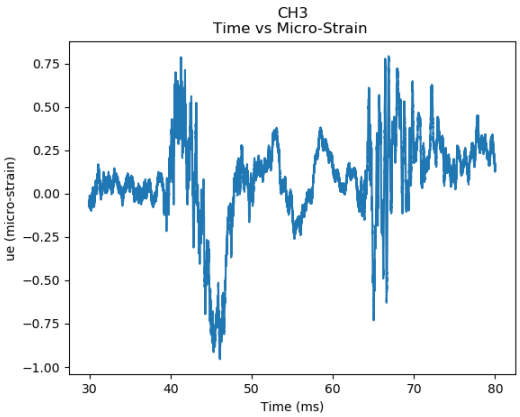

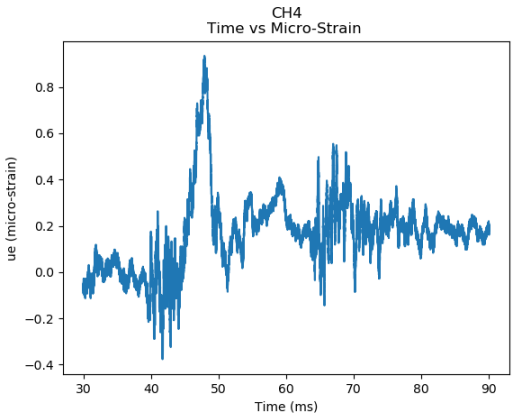

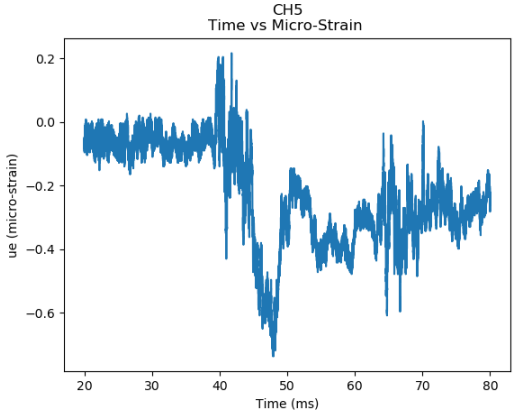

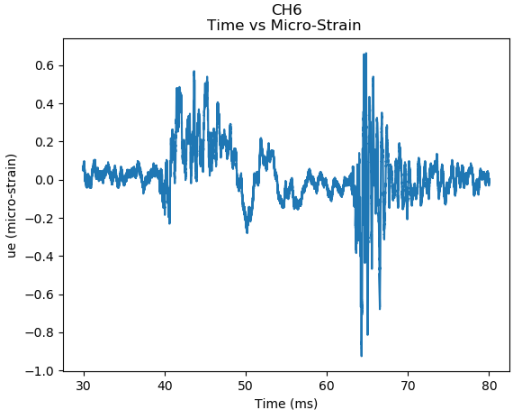

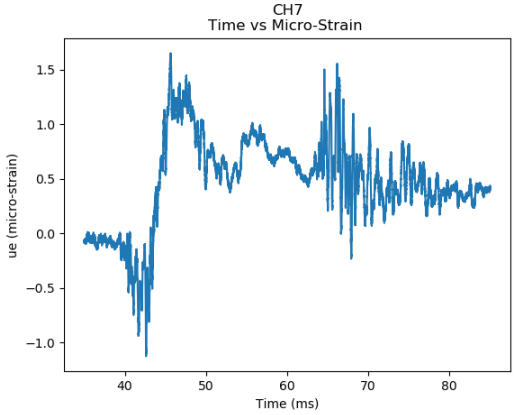

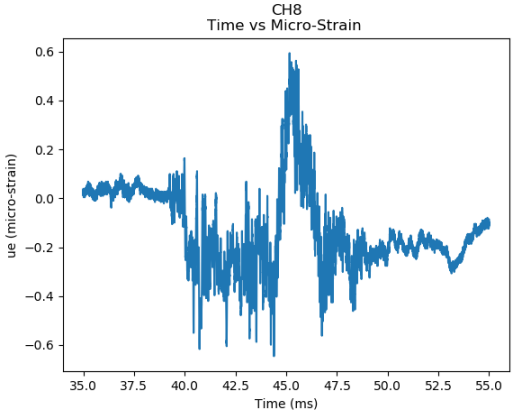

C.4 Wood Projectile Strains

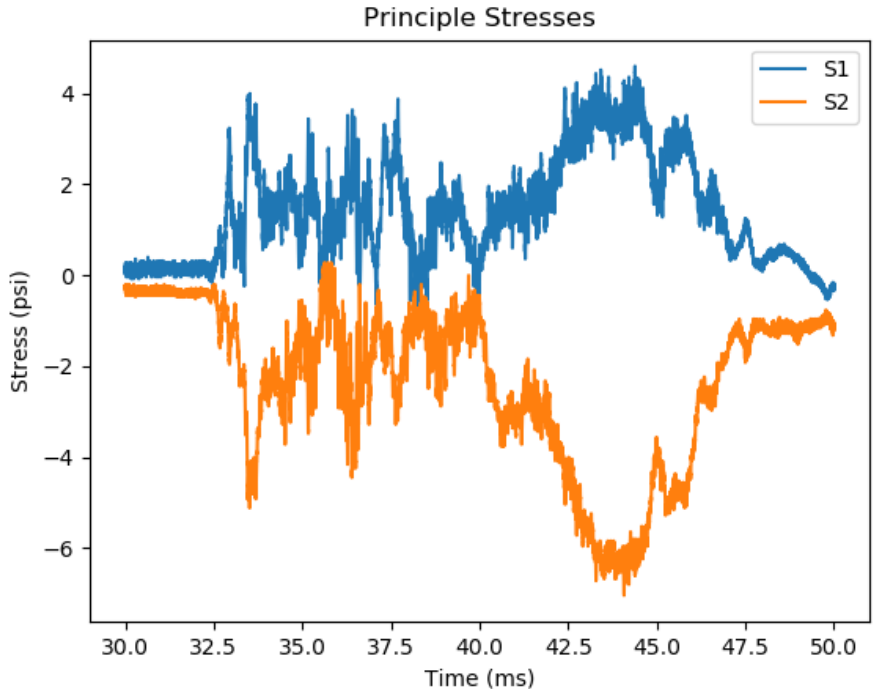

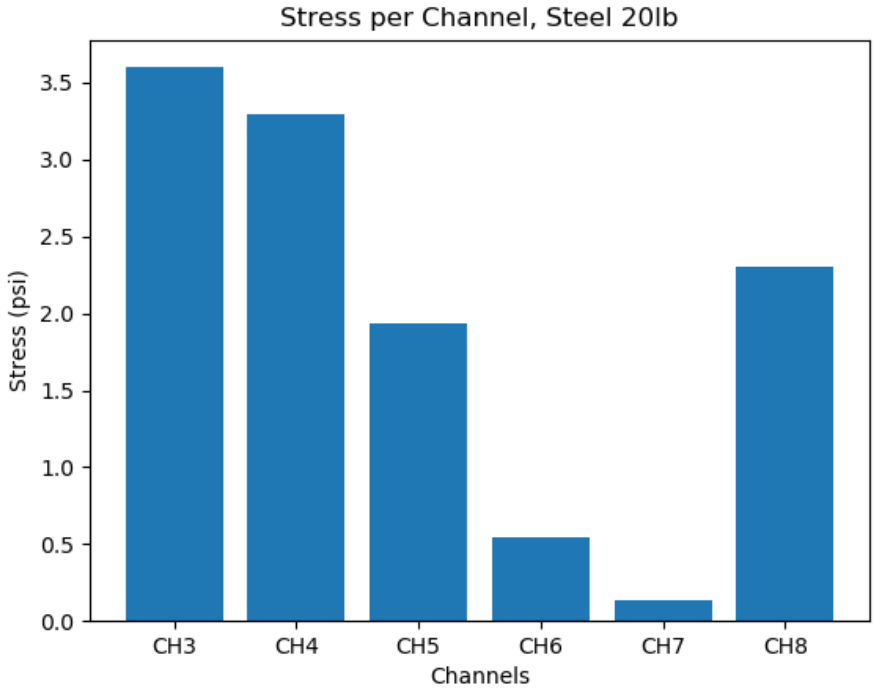

C.5 Steel Projectile 20 lb. Stresses

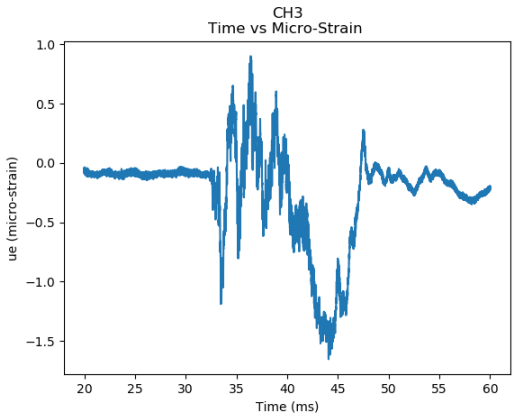

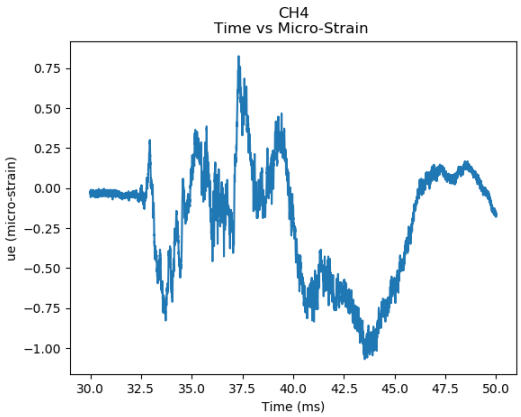

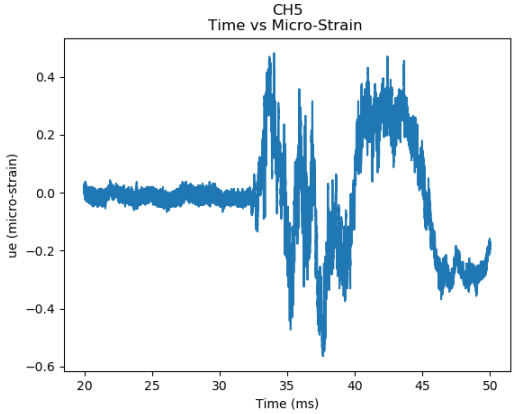

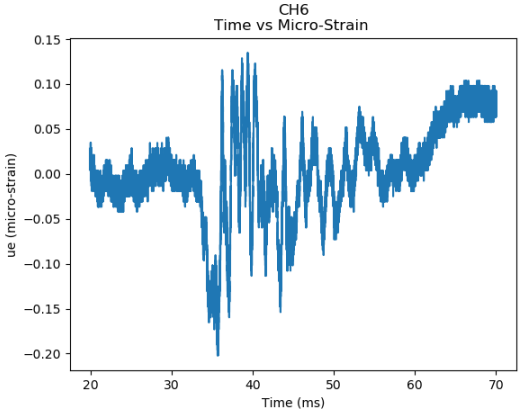

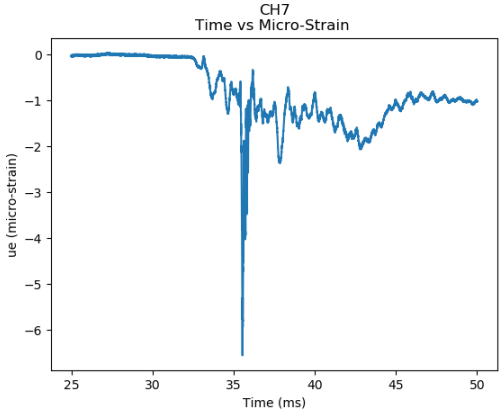

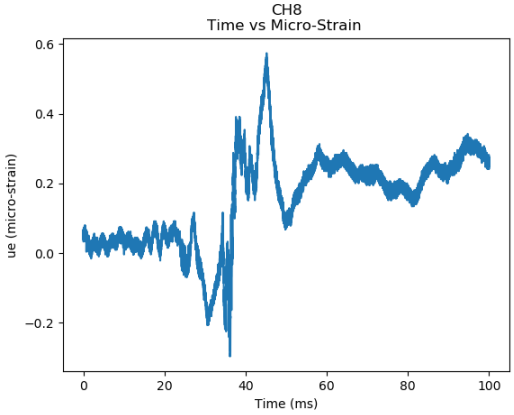

C.6 Steel Projectile 20 lb. Strains

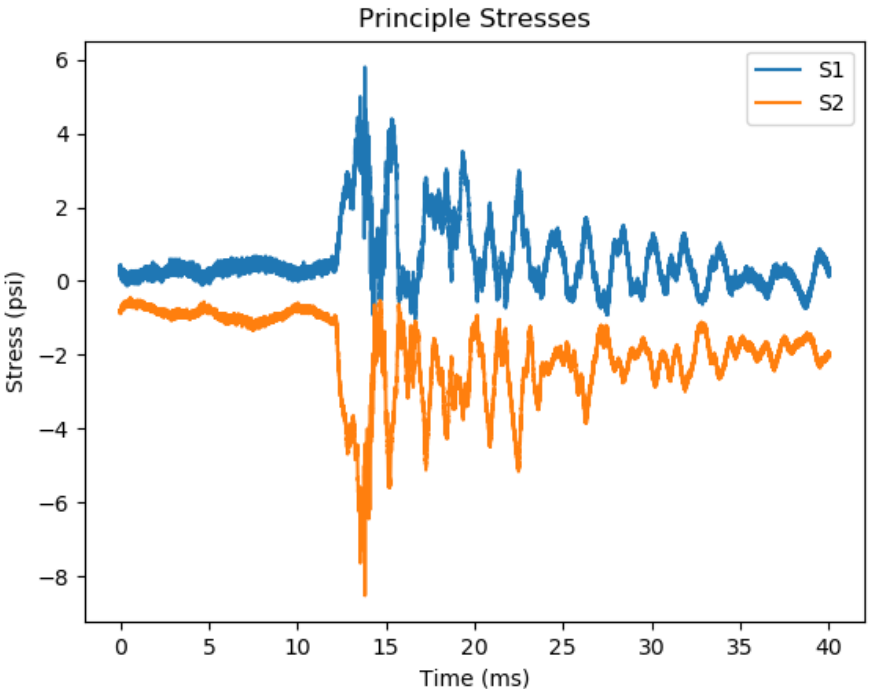

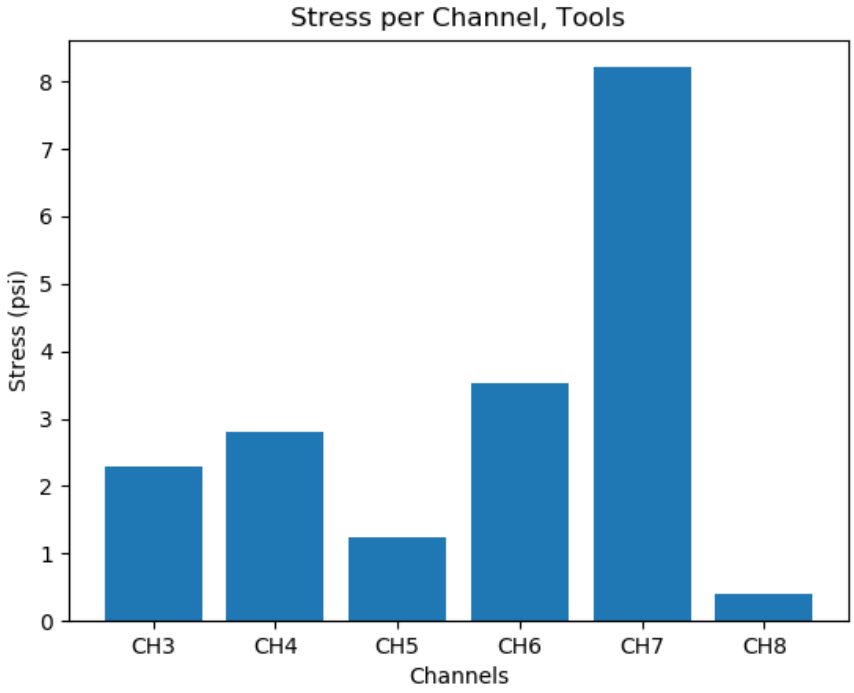

C.7 Tool Projectile Stresses

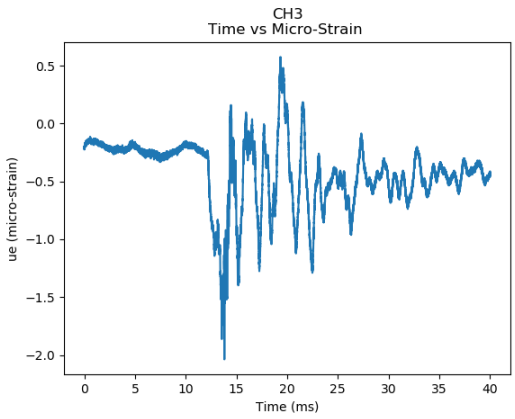

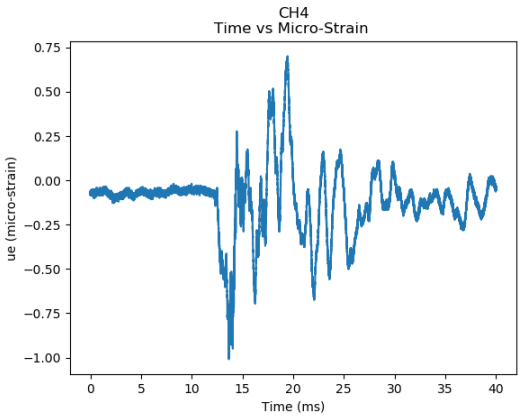

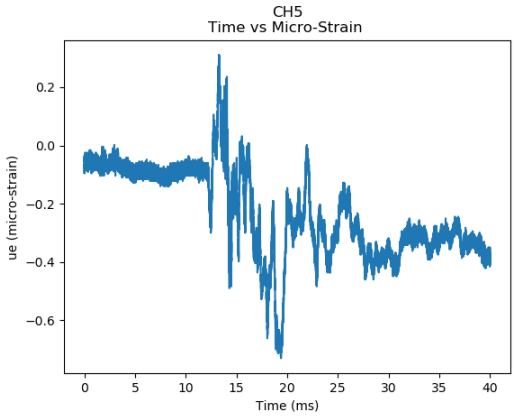

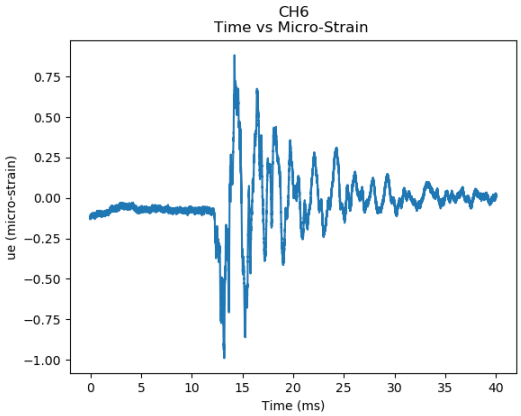

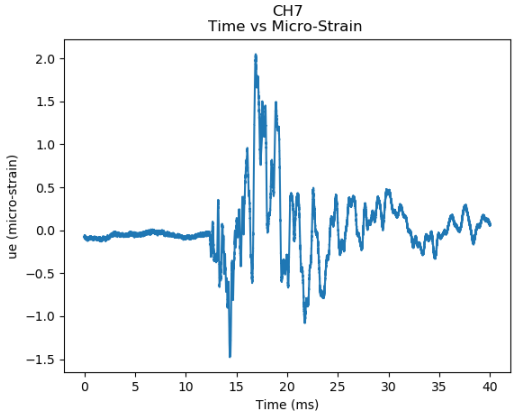

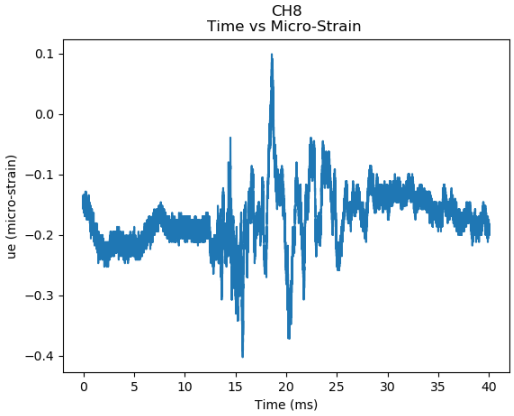

C.8 Tool Projectile Strains